Tin- and bismuth-based catalysts for electrochemical reduction of carbon dioxide to formic acid

Xiaowei An

Graduate School of Science and Technology

Hirosaki University

2020

ABSTRACT

In recent years, electrochemical reduction carbon dioxide (CO_2) to value-added chemicals has attracted widespread attention because of its efficiency, cleanliness and convenience to face the environmental and energy issues. Electroreduction of CO_2 to formic acid (HCOOH) is considered as one of economically feasible ways. Developing high-efficient electrocatalysts is key for this technology. The tin (Sn)- and bismuth (Bi)-based catalysts have been extensively studied due to their efficiency, low cost, and environmental friendliness. However, in order to meet large-scale industrial applications, more highly-efficient electrocatalysts based on them still should be developed. This study focused on Sn- and Bi-based catalysts prepared by different methods for electrochemical CO_2 reduction reaction (CO_2RR) to HCOOH. Besides, density functional theory (DFT) calculations were performed to help understand the catalytic mechanism.

Firstly, uniform Sn-based electrocatalysts with small particle size were coated on the carbon paper (CP) substrate by using unipolar pulse electrodeposition (UPED) method. It exhibited the maximum HCOOH faradaic efficiency of 89% at -1.7 V (vs. Ag/AgCl) with a current density of 6.0 mA cm^{-2} and long-term stability in the 0.1 M CO_2-saturated $KHCO_3$ solution. Moreover, the effects of surface oxides species on the performance of tin-based electrocatalysts were systematically investigated via DFT calculations. The calculation results indicated that both metal tin and tin oxides had excellent catalytic ability for the electrochemical reduction of CO_2 to HCOOH. Especially, the tetravalent tin (Sn^{4+}) and divalent tin (Sn^{2+}) species can reduce the overpotential and improve the HCOOH selectivity, respectively. In addition, it is found that the tin oxides/metal tin interface can suppress the evolution of H_2 but no obvious

effect on the formations of HCOOH and CO. Thusly, we propose that the actual CO_2 catalytic electroreduction process should be synergistically controlled by the complex surface oxide species on the tin-based electrocatalysts.

Secondly, to further increase the current density, the oxide catalysts were directly synthesized on the 3D porous Cu foam. Herein, a Bismuth (Bi)-doped SnO nanosheets were grown on copper foam (Bi-SnO/Cu foam) by a one-step hydrothermal reaction method and applied for the electrochemical reduction of CO_2 to HCOOH. The experimental results indicated that Bi doping stabilized the divalent tin (Sn^{2+}) existed on the surface of the electrocatalyst, making it difficult to be reduced to metallic tin (Sn^0) during the electrochemical reduction process. In addition, combining with the DFT calculations, it is found that Bi doping and the electron transfer from the catalyst to the Cu foam substrate could enhance the adsorption of *OOCH intermediates. As such, the Bi-doped SnO electrocatalyst exhibited a superior faradaic efficiency of 93% at -1.7 V (vs Ag/AgCl) for the reduction of CO_2 to HCOOH, together with a current density of 12 mA cm^{-2} and excellent stability in at least 30 h of operation.

Thirdly, to further reduce the overpotential of CO_2RR, Bi-based catalysts which usually have lower overpotential were prepared. In this section, we observed an interesting morphological transformation phenomenon accompanied by the formation of petal-shaped bismuth subcarbonate ($Bi_2O_2CO_3$) nanosheets in Bi-based catalyst. It was found that this transformation improved the electrocatalytic performance of CO_2 reduction to HCOOH. By using this catalyst, the faradaic efficiency of CO_2 to HCOOH reached 92% at -1.6 V (vs. Ag/AgCl) with a current density of 10 mA cm^{-2}. Also, this electrocatalyst exhibited good stability during the electrocatalysis operation for 20 h. DFT calculations revealed that *in-situ* formed $Bi_2O_2CO_3$ species can enhance the

catalytic activity by stabilizing *OOCH intermediate through the stronger orbital hybridization of Bi 6p of $Bi_2O_2CO_3$ with O 2p of *OOCH. As such, it can be considered that the rate-limiting step in the CO_2 electroreduction process should rely on the second-step electron transfer, which is consistent with the Tafel slope analysis result.

All in all, in this work, 3 kinds of Sn or Bi-based electrocatalysts were successfully developed for electrochemical CO_2RR to HCOOH. Their physicochemical properties and electrocatalytic performance have been characterized and tested in details, and the catalytic mechanisms have also been analyzed by DFT calculations. It is expected to give guidance for the design and application of electrocatalyst in the practical CO_2RR processes.

ACKNOWLEDGMENTS

First of all, I wish to thank my learned and respectable supervisor, Professor Dr. Guoqing Guan, who has instructed me academically since I am a postgraduate. His valuable instruction, suggestions, and encouragement supported my Ph.D study program.

I would like to thank Prof. Abuliti Abudula, Graduated School of Science and Technology, Hirosaki University, for all of his kind advice and help.

I would like to thank Professor Dr. Akihiro Yoshida in our group for his kind suggestions and helpful discussion on my research.

I would like to thank Dr. Xiaogang Hao, Department of Chemical Engineering, Taiyuan University of Technology, China, for recommending me to continue my study in this laboratory, and his help regarding the characterization of X-ray photoelectron spectroscopy, support for theoretical calculations and some helpful discussion.

I would like to thank all professors and staff at the Institute of Regional Innovation (IRI), and at Graduated School of Science and Technology, Hirosaki University, for all of their kind advices and supports of my study.

I would like to thanks all members in our research group for their helps and supports to my research and daily life.

I would like to thank my family for all their support, for their love, encouragement, and understanding during my Ph.D study.

Finally, I would like to deeply acknowledge the life supports by China Scholarship Council (CSC) and research support by ZiQoo Chemical Co. Ltd., Japan.

Thank you all very much.

Xiaowei An

TABLE OF CONTENTS

LIST OF TABLES

LIST OF FIGURES

Chapter 1 Introduction

1.1 General introduction

1.1.1 CO_2 excess emissions and hazards

Carbon dioxide (CO_2) is a ubiquitous gas in nature, accounting for about 0.03% of the air. Although its content is very low, its existence is indispensable for the evolution of the earth's ecological environment, which is used by plants through photosynthesis to transform into a variety of hydrocarbons. As a naturally occurring gas on earth, the low concentration of CO_2 is harmless. However, the concentration of CO_2 in the atmosphere has been increasing year by year due to the impact of energy consumption and human activities since the industrial revolution. So far the concentration of CO_2 in the atmosphere has risen from 320 ppm in 1960 to 414 ppm in February 2020, as shown in Figure 1.1a.[1]

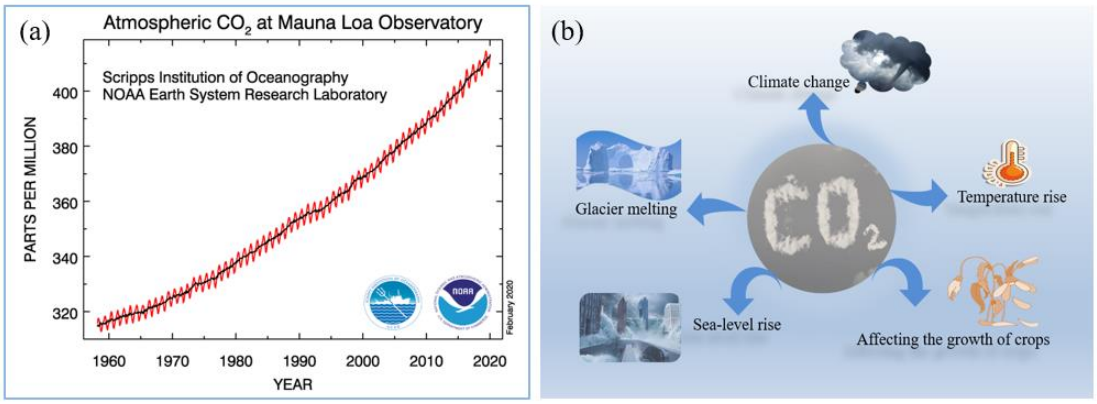

Figure 1.1 (a) Increase in CO_2 atmospheric concentration over the past 60 years. Reproduced with permission from Ref. [1]. (b) The harm caused by excessive emissions of CO_2.

With the increasing CO_2 concentration in the atmosphere, the harm it brings is becoming more and more obvious. As a kind of greenhouse gas, a high concentration of

CO_2 firstly increased the global temperature. Intergovernmental panel on climate change (IPCC) research indicates that human activities are estimated to have caused global warming to be approximately 1.0 °C above pre-industrial levels, with a possible range of 0.8 °C to 1.2 °C. If it continues to rise at the current rate, global warming may reach 1.5 °C between 2030 and 2052.[2] As shown in Figure 1.1b, the global warming will lead to a series of environmental problems, such as climate change, bipolar glacier melting and sea-level rise, which will seriously harm the survival of animals and humans on earth.[3] Besides, recent studies have shown that increased concentrations of CO_2 in the atmosphere can also affect plant growth, such as reducing crop yields and nutritional value.[4-5] To avoid this situation, many countries around the world joined the Paris Climate Agreement, aiming to limit global warming to 2 °C relative to the pre-industrial temperature, and try to control it at 1.5 °C.[6]

1.12 CO_2 capture and utilization

In order to reduce the increase rate of CO_2 concentration in the atmosphere, on the one hand, human society should reduce CO_2 emissions as much as possible. For example, to properly limit CO_2 emissions of factories, and actively develop new energy sources such as solar energy, wind energy, tidal energy and so on. On the other hand, researchers are also considering capturing and storing CO_2 in the atmosphere. CO_2 capture and storage (CCS) is an effective method to reduce CO_2 atmospheric concentration which has become one of the important research topics in the 21st century. As shown in Figure 1.2, the commonly used capture methods of CO_2 include solid material adsorption, liquid material absorption, and membrane separation and so on.

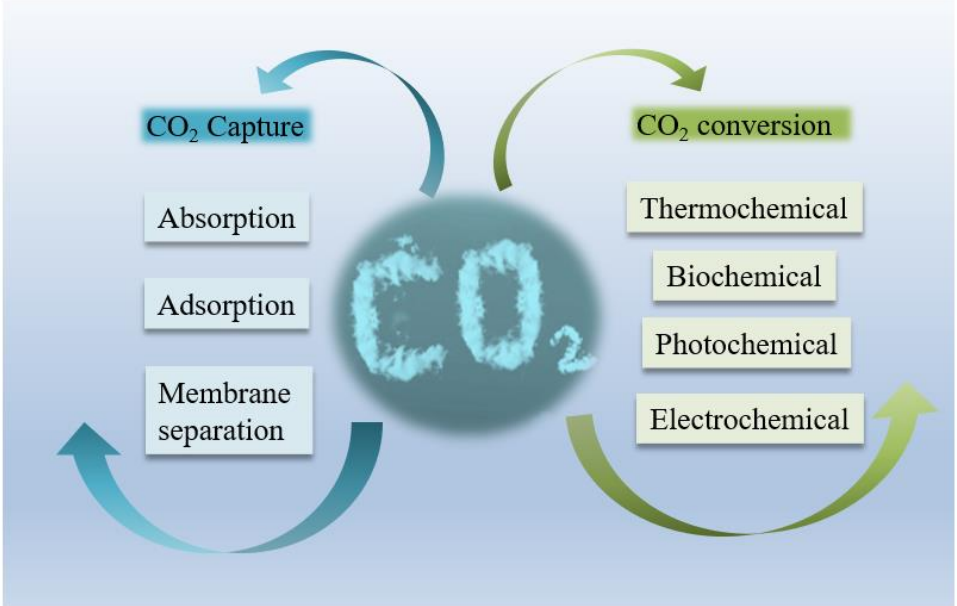

Figure 1.2 The common methods of CO_2 capture and conversion.

However, the above-mentioned CO_2 capture method has the problem of high energy consumption. For example, CO_2 usually needs to be desorbed for further storage at an elevated temperature after being captured by solid or liquid adsorbent materials. In addition, the current CO_2 storage technology also has the problem of the too high cost. Therefore, the development of low-cost CO_2 treatment methods has attracted more and more attention. From another perspective, CO_2 is an important carbon resource in nature. It can be converted into various organic substances by photosynthesis of plants. Therefore, the conversion and utilization of CO_2 is a more promising way. It can not only reduce the CO_2 concentration in the atmosphere but also convert it into other high value-added chemicals for producing economic benefits.

As shown in Figure 1.2, the currently common CO_2 conversion technologies include thermochemical, biochemical, photochemical, and electrochemical conversion methods. The thermochemical conversion usually requires high temperature and pressure, so the energy consumption is large. For example, the excellent Schiff-base-mediated gold

nanocatalyst reported by Liu *et al*. still needs to be performed at 90 ºC and 8.0 MPa for the thermal catalysis of CO_2 to formate.[7] The biochemical and photochemical conversion methods currently are still low efficiency. For example, the photosynthetic efficiency of photosynthesis that uses solar energy to convert water and CO_2 into carbohydrates is often less than 1%. Thus, the electrochemical CO_2 reduction reaction (CO_2RR) technology attracts more and more attention due to its unique advantages, which will be discussed further in the following sections.

1.2 Electrochemical reduction of CO_2

1.2.1 Overview of electrochemical reduction of CO_2

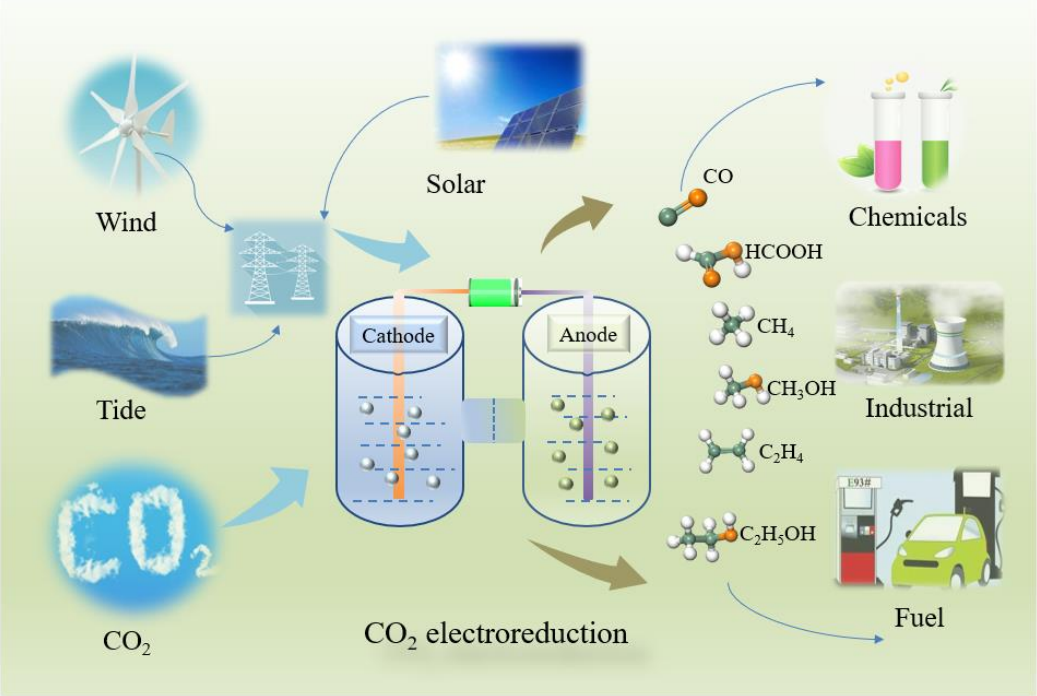

Figure 1.3 Schematic illustration of the electrochemical CO_2RR to value-added products powered by renewable energy sources such as wind, solar, and tide.

CO_2 electroreduction technology attracts rapidly growing attention recently due to its potential to meet both energy and environmental problems. It has become a research

hotspot in many research fields such as chemistry, energy, environment and material science. CO_2 is very stable at normal temperature, which makes its chemical fixation and conversion very difficult. The reduction of CO_2 by traditional chemical methods requires the provision of a large amount of hydrogen and also consumes huge amounts of energy. In contrast, the electrochemical CO_2RR is carried out at normal temperature and pressure, and the product selectivity and reaction rate can be easily adjusted by changing the electrolytic conditions. More importantly, as shown in Figure 1.3, the CO_2 electroreduction process can be combined with the use of renewable energy sources such as solar, wind and tidal energy to directly obtain high-value chemicals. These chemicals can be used directly as chemical reagents for scientific research, or as raw materials for industrial synthesis or as fuel for new energy vehicles, thereby achieving large-scale energy storage. In summary, compared to other CO_2 conversion technologies, the advantages of CO_2 electroreduction technology are: (i) the selective synthesis of products can be achieved by controlling the type of electrode and reaction conditions; (ii) the reaction conditions can be achieved at normal temperature and pressure, and (iii), the reaction device is simple, easy to operate and has a short reaction period. This technology shows a very promising application prospect, which is in line with the goal of human sustainable development.

1.2.2 Common products and catalysts

Although electrochemical reduction of CO_2 is considered as a CO_2 resource conversion method with great industrial production potential, it has not yet achieved industrial application. The main limitations are insufficient activity and selectivity of electrocatalysts, and low energy utilization efficiency. Due to the very high chemical stability of CO_2, electrocatalytic reactions usually require a high overpotential to occur in

order to overcome the reaction barrier. Besides, the existence of competitive electrocatalytic hydrogen (H_2) evolution reaction leads to the low energy conversion efficiency of the CO_2RR. Therefore, it is imminent to develop efficient CO_2 electroreduction catalysts.

$$CO_2 + H^+ + 2e^- \rightarrow HCOO^- \quad E^0 = -0.225\ V \tag{1}$$

$$CO_2 + 2H^+ + 2e^- \rightarrow CO + H_2O \quad E^0 = -0.103\ V \tag{2}$$

$$CO_2 + 8H^+ + 8e^- \rightarrow CH_4 + 2H_2O \quad E^0 = +0.169\ V \tag{3}$$

$$CO_2 + 6H^+ + 6e^- \rightarrow CH_3OH + H_2O \quad E^0 = +0.02\ V \tag{4}$$

$$2CO_2 + 12H^+ + 12e^- \rightarrow C_2H_4 + H_2O \quad E^0 = +0.079\ V \tag{5}$$

$$2CO_2 + 12H^+ + 12e^- \rightarrow C_2H_5OH + H_2O \quad E^0 = +0.09\ V \tag{6}$$

As shown in the above equations (1)-(6), CO_2 can be reduced to different products such as formic acid (HCOOH), carbon monoxide (CO), methane (CH_4), methanol (CH_3OH) ethylene (C_2H_4), ethanol (C_2H_5OH), *etc*. by applying different electrode potentials.[8] However, the potentials of these reaction processes are very close. Compared to reversible hydrogen electrodes (RHE), the standard electrode potentials of these CO_2RR are in the range of ~ 0.2 to - 0.3 V, which makes it difficult to control their selectivity resulting in a state where multiple products coexist. Therefore, the key to electrocatalytic CO_2RR is to develop highly active and selective electrocatalyst to improve energy utilization.

Currently, the catalysts used for the electrocatalytic CO_2RR include heterogeneous catalysts and homogeneous catalysts. Homogeneous catalysts have a large contact area because they are often mixed with the electrolyte, which makes them have higher utilization. However, from the perspective of catalyst recycling and product separation, heterogeneous catalysts are easier to be separated from the electrolyte for reuse which has more advantages. Therefore, this dissertation will focus on heterogeneous catalysts.

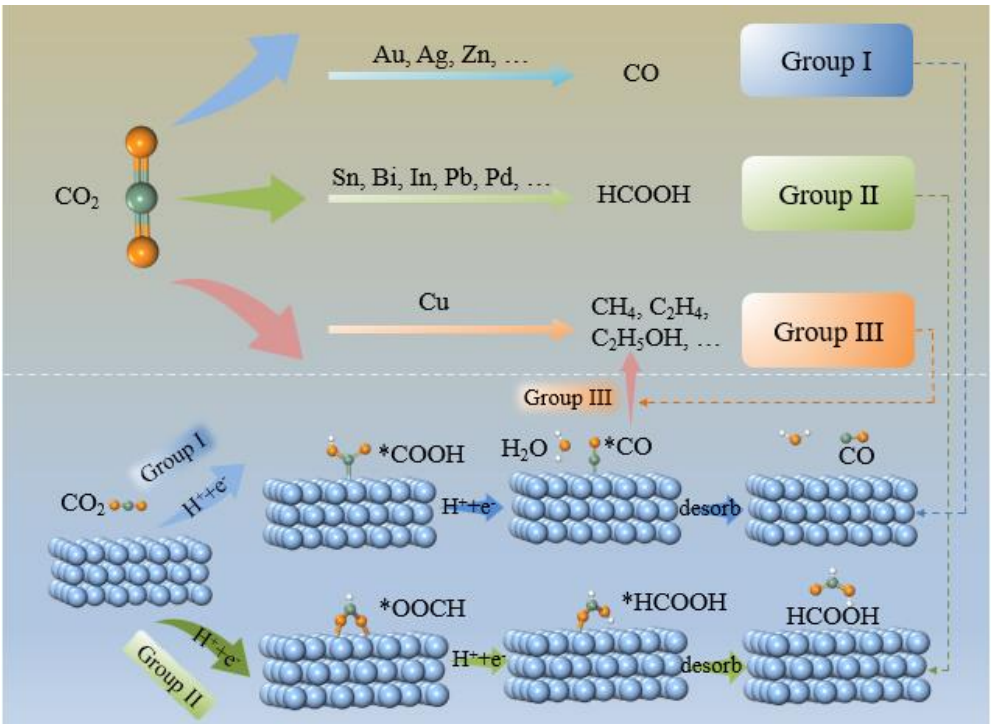

Figure 1.4 The common metal catalysts for electrocatalytic CO_2RR and their possible catalytic mechanism

The commonly used heterogeneous catalysts for CO_2RR can be divided into metal-based and metal-free-based catalysts. Among them, the metal catalysts are still the mainstream catalysts for the current CO_2RR due to their excellent conductivity and high selectivity. As shown in Figure 1.4, according to the main reduction products, the metal electrocatalysts are roughly divided into three categories: the first category is Au, Ag, Zn, *etc*., their main catalytic products are CO. The second category is Sn, Bi, In, Pb, *etc*., their main catalytic product is HCOOH. The third type is a Cu-based catalyst with unique electrocatalytic CO_2RR properties. It is the only catalyst that can produce a variety of considerable small molecule fuels such as CH_4, C_2H_4, C_2H_5OH *etc*.[9] Nørskov *et al*. used DFT calculations to analyze the reasons for the selectivity of products on different metal surfaces, and found that there are two possible intermediates in the initial process of CO_2

reduction, which are *COOH and *OOCH. Surfaces such as Ag and Zn have a strong binding ability to *COOH intermediates, which can be further reduced to CO. While, the surface of the second type of metal is more easily combined with *OOCH intermediates to form HCOOH. Copper has greater binding energy with CO, so it is beneficial to further hydrogenation of the adsorbed CO to produce hydrocarbon products.[10] The in-depth understanding of the catalytic mechanism helps to design high-performance catalysts.

1.2.3 Advantages of CO_2 reduction to HCOOH

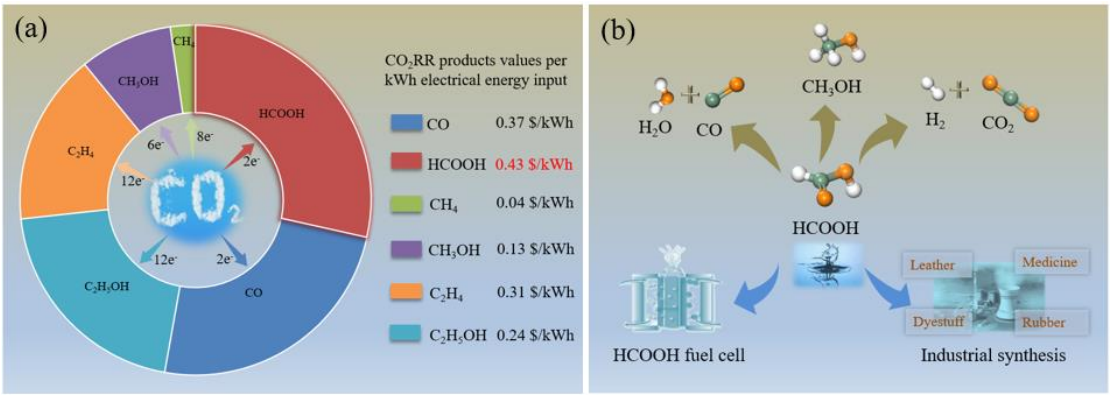

Figure 1.5 (a) Comparison of the values of different CO_2RR products in terms of per kWh electrical energy input ($/kWh) estimated based on ideal full cells from Ref. [11]. (b) Common conversions and application of HCOOH.

For CO_2 electroreduction to be fully developed, it will inevitably face commercialization issues, so its cost considerations are necessary. As shown in Figure 1.5a, researchers calculated the obtained value per kWh of electrical energy input under ideal conditions for different CO_2RR products (CO, HCOOH, CH_4, CH_3OH, C_2H_4, and C_2H_5OH). These calculation results show that HCOOH has the highest value of 0.43 $/kWh electricity input compared to other products (CO: 0.37 $/kWh, CH_4: 0.04 $/kWh, CH_3OH: 0.13 $/kWh, C_2H_4: 0.31 $/kWh and C_2H_5OH: 0.24 $/kWh).[11] Recent technical

and economic analysis also points out that the two-electron electrochemical conversion from CO_2RR to CO or HCOOH is the most economically feasible method.[12]

In addition, in terms of application, as shown in Figure 1.5b, HCOOH is an important substance, which can be directly used as a fuel for formic acid/formate fuel cell, and can also be conveniently converted into CO[13], H_2[14], and CH_3OH[15] through a simple catalytic reaction to meet different applications. Among them, since HCOOH can be easily decomposed into H_2, it has become a common hydrogen storage material. Besides, HCOOH is also a feedstock in many industrial processes such as leather, pesticide, pharmaceutical, and rubber industries.

Finally, compared to other C2-C3 products, the electroreduction of CO_2 to HCOOH currently has a maximum faradaic efficiency of nearly 100%, while other C2 or C3 products such as ethylene and propanol only reach 60% and 15% respectively.[11] Poor selectivity will not only lead to an additional input of electrical energy but also increase the cost of product separation. Therefore, from the current situation, the electroreduction of CO_2 to HCOOH seems to be the easiest option for large-scale industrialization.

1.2.4 The main electrocatalysts for CO_2RR to HCOOH

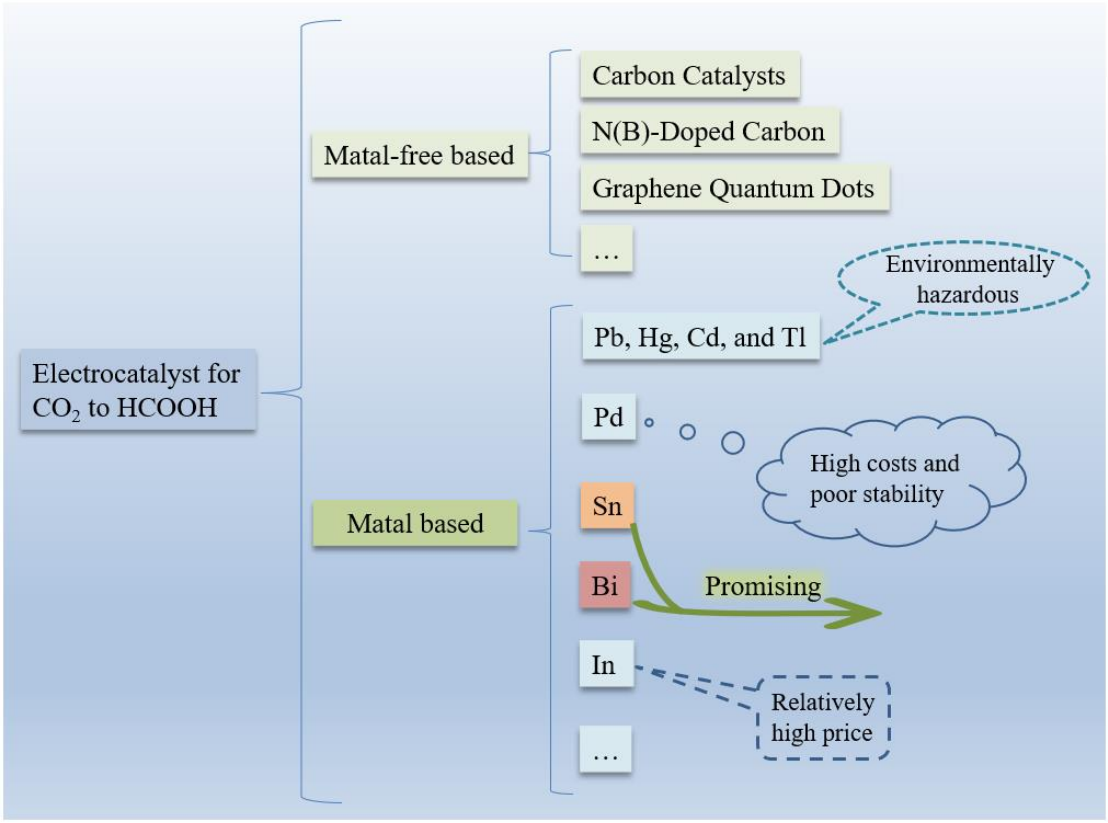

Figure 1.6 The classification of the electrocatalysts for CO_2RR to HCOOH.

At present, the electrocatalysts for CO_2RR to HCOOH can be divided into metal-based and metal-free-based categories. Among them, metal-free-based catalysts mainly contain some carbon materials, such as N(B)-doped Carbon and Graphene Quantum Dots and so on.[16] However, compared with metal-based catalysts, the poor electronic conductivity and selectivity limited their application in CO_2RR to HCOOH. Another is the metal-based catalysts that are more commonly used for CO_2RR. According to the reports published in recent years, it mainly includes Pb, Hg, Cd, Tl, Pd, Sn, Bi, and In. Among them, Pb, Hg, Cd, and Tl are not suitable for the green process of CO_2RR because of their toxicity and harm to the environment. Although Pd shows a low overpotential, its poor stability is a major problem, and moreover its high price makes it unsuitable for large-scale

applications. The remaining Sn, Bi, and In are the three materials that have been studied extensively at present since they have good selectivity and stability. In terms of price, compared with Sn and Bi, In has a relatively high price due to its less and scattered distribution in the crust. Therefore, among these metal-based materials shown in Figure 1.6, Sn and Bi-based electrocatalysts are the candidates most likely to realize the large-scale industrial production of CO_2RR to HCOOH. The following sections will mainly introduce some research progress of the application of Sn and Bi-based electrocatalysts in CO_2RR to HCOOH.

1.3 The common ways to improve the performances of Sn- and Bi-based catalysts

Sn- and Bi-based catalysts are the most widely studied catalysts in CO_2RR to HCOOH due to their high efficiency, low cost and environmental friendliness. Sn is the earliest batch of catalysts for CO_2RR. Its first research dates back to the work of Ito *et al*. in 1976.[17] Compared to metal Sn, Bi did not receive widespread attention in the early days, its electrochemical CO_2RR performance was first reported by Komatsu in 1995.[18] These early studies mainly uses bulk electrodes such as Sn plate, Bi particles, *etc*. These bulk electrodes have a certain selectivity but a relatively large overpotential and low current density. After entering the 21st century, the researchers found that the nano-effect of catalyst could greatly affect the catalytic performance. Subsequently, various methods such as controlling morphology, making defects, grain boundaries and dislocations, adjusting composition, *etc*. of the catalyst were carried out to obtain more and higher active sites. The following will introduce the different common methods for improving the performance of Sn- and Bi-based catalysts, and discuss their performances and mechanisms.

1.3.1 Controlling surface morphology

The actual catalytic reactions occur on the catalyst surface, so the surface morphology of the catalyst plays a vital role in the electrocatalytic process. The catalyst particle size scale can be roughly divided into three levels, one is above the nano-scale, usually at the micro-scale, the other is within the nano-scale range, and the last is directly prepared into a single atom catalyst. In the micrometer range, researchers often adjust performance by changing the shape of the particles such as regular tetrahedron, regular octahedron, and dendritic shapes. For example, Won *et al*. prepared a hierarchical tin dendrite electrode for CO_2RR to HCOOH, showing a highest HCOOH faradaic efficiency of 83.4% at -1.36 vs RHE and without any considerable catalytic degradation over 18 h of operation.[19] This method does not make the size of the catalyst nanometer-sized, but only changes its displayed shape, which may affect the specific surface area or the exposed crystal plane of the catalyst to a certain extent, and its performance improvement is often limited. Another way is the direct synthesis of nanoscale electrocatalysts, which is the most commonly used method to improve catalytic performance. Nanoscale catalysts usually have more catalytic sites because of their larger specific surface, thereby increasing the current density of the electrocatalytic reaction. On the other hand, the intrinsic activity of each catalytic site in nanocatalyst may increase due to the presence of more edge structures containing unsaturated sites. This strategy is widely used to improve the performance of Sn- and Bi-based electrocatalysts.

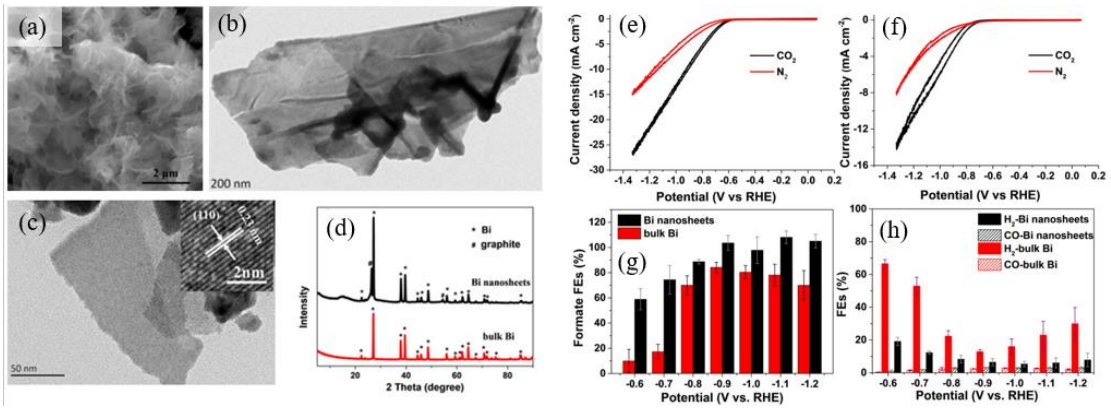

Figure 1.7 (a) SEM image, (b-c) HRTEM images with different magnifications of prepared Bi catalyst and (d) XRD patterns of synthesized Bi grown on carbon paper and commercial bulk Bi. Cyclic voltammograms curves of (e) ultrathin Bi nanosheets and (f) commercial bulk Bi in N_2 bubbled NaH_2PO_4/Na_2HPO_4 solution (0.5M, pH=7.2) and CO_2 bubbled $NaHCO_3$ (0.5M) aqueous solution with a scanning rate of 10 mV s^{-1}, faradaic efficiency (FE) of (g) formate, (h) CO and H_2 catalyzed by synthesized Bi nanosheets and Bi bulk. Reproduced with permission from Ref. [19].

At present, common nanomaterials include various morphologies such as one-dimensional nanowires, two-dimensional nanosheets, three-dimensional nanoparticles and so on. These catalysts have a larger specific surface area compared to bulk catalysts, thereby greatly increasing the electrocatalytic current density, that is, promoting the catalytic rate. For example, Su *et al*., synthesized ultrathin bismuth nanosheets with a thickness of ~10 nm, as shown in Figure 1.7a-d. When applied it to electrochemical CO_2RR, it exhibits much higher current and faradaic efficiency for formate generation than that of bulk Bi as shown in Figure 1.7 e-h. After careful characterization and analysis, they found that ultrathin Bi nanosheets have a large number of low-coordination sites. At the same time, by using DFT calculation, it is found that Bi nanosheets have a much

higher electron state density around Fermi level than the bulk counterpart, which favors the improvement of CO_2 reduction on Bi nanosheets.[20]

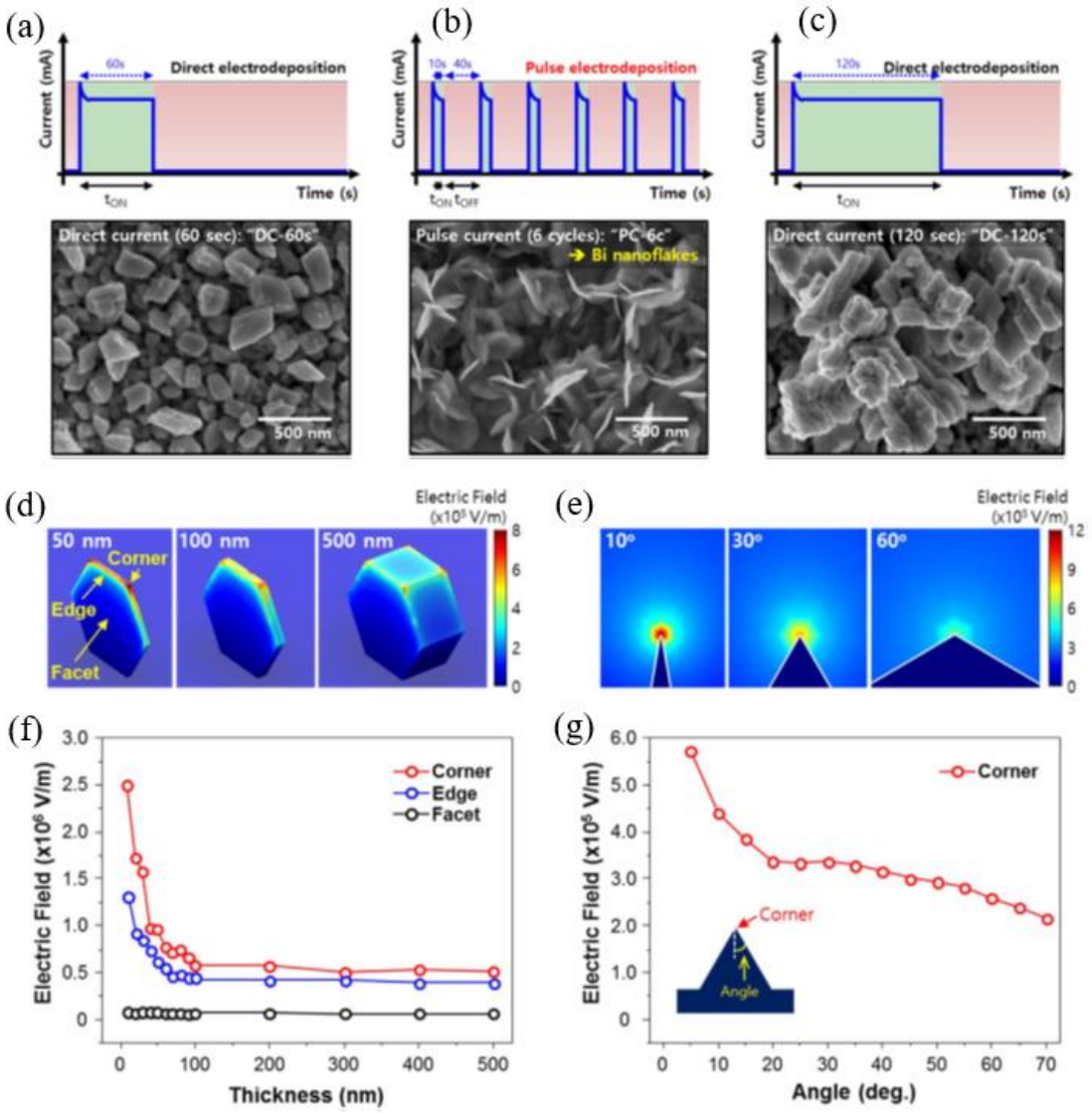

Figure 1.8 Transient current curves and SEM images of electrodeposited Bi films formed by (a) direct-current 60 s, (b) pulse-current 6 cycles, and (c) direct-current 120 s. Simulated electric field distribution in (d) three-dimensional and (e) two-dimensional Bi nanostructures; strong electric field is formed as the shape is thinner and sharper. Electric field intensity plotted as a function of (f) thickness and (g) corner angle of Bi nanostructure. Reproduced with permission from Ref. [20].

The common preparation methods of nanocatalyst include the hydrothermal method, roasting method, electrodeposition method, *etc*. Among them, the electrodeposition method is widely used due to its simple operation, low energy consumption and environmental friendliness. For example, Kim found that Bi catalysts with different morphologies can be obtained using different electrodeposition methods, as shown in Figure 1.8a-c. Compared with conventional bismuth film grown by direct-current electrodeposition, Bi nanoflakes obtained by a novel pulse electrodeposition method have a large number of edge and corner sites. Then they used numerical simulation to confirm that sharp edge or corner sites of the nanostructures have stronger local electric fields, which boost the catalytic activity for the electrochemical reduction of CO_2 in aqueous solution.[21]

Apart from these, there are numerous examples of using morphology control engineering to enhance Sn and Bi electrocatalysts to improve catalytic performance. For example, porous tin-based films developed by Lv *et al*.[22], nanocrystals tin catalysts by Zhang *et al*.[23], and hierarchical Bi dendrite catalysts obtained by electrodeposition from Koh *et al*.[24] A series of the size-tunable nano-Bi catalysts were synthesized by Qiu *et al* applied in CO_2 electrochemical conversion to formate. They found that the size effect greatly affects the electrochemically active surface area and current density, as well as faradaic efficiency. Therefore, we can conclude that compared with bulk catalysts, nanoscale electrocatalysts tend to have better performance due to larger specific surface area and more edge and corner sites.

1.3.2 Making defects, dislocations, grain boundaries

Defects

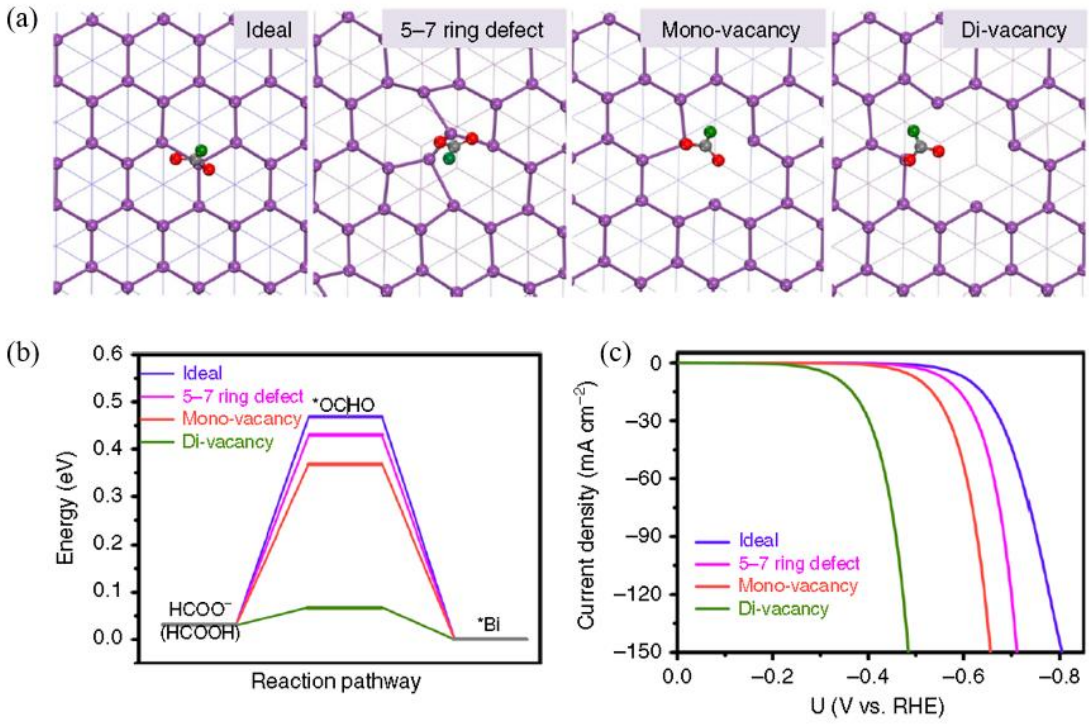

Figure 1.9 Theoretical calculations of reaction pathway on ideal and defective Bi(001) surfaces. (a) Optimized geometric structures of *OCHO adsorbed on ideal and three defective Bi(001) surfaces as indicated; the pink, gray, red, and green spheres represent Bi, C, O, and H atoms, respectively. (b) Free-energy profiles for HCOOH production on ideal and defective surfaces. (c) Corresponding simulated CO_2RR polarization curves. Reproduced with permission from Ref. [24].

In recent years, many crystallography researchers have found that defects, dislocation, grain boundaries and so on in crystals also have an important impact on the performance of catalysts. Crystal defects refer to the locations where the structural integrity of the crystal is damaged, and these locations often have some unique catalytic effects. For example, Gong *et al*. reported a defective bismuth nanotube prepared by electroreduction of Bismuth oxide double-walled nanotubes template with fragmented surface. This catalyst exhibited excellent activity, selectivity and stability. Most significantly, its

current density reached ~288 mA cm^{-2} at -0.61 V versus RHE within a flow cell reactor under ambient conditions. As shown in Figure 1.9, by using DFT calculations, they found that different defect structures could significantly reduce the formation of energy barrier of *OCHO intermediate, thus improving its catalytic performance.[25]

Dislocation

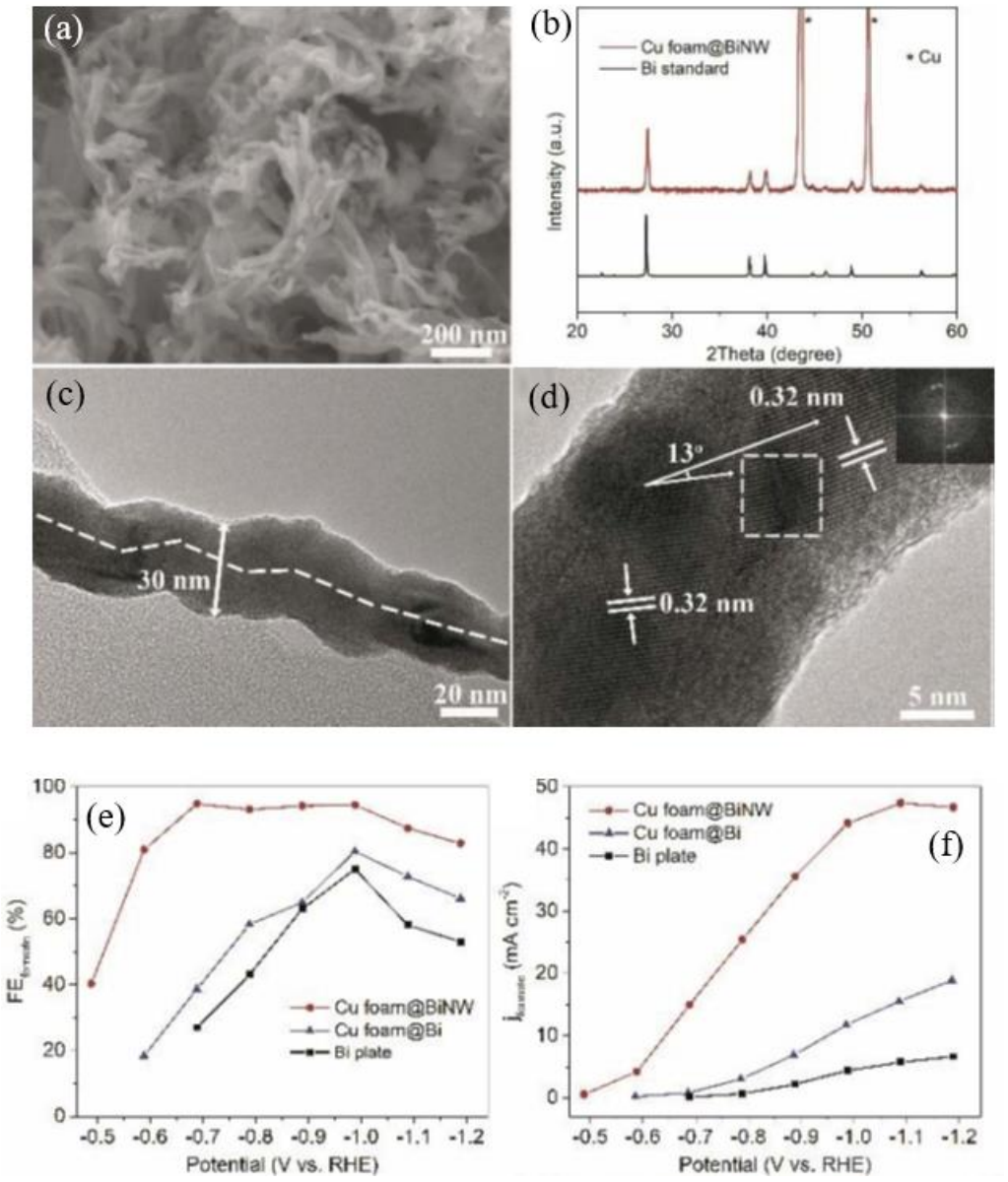

Figure 1.10 (a) SEM image and (b) XRD pattern of the Cu foam@BiNW electrode. (c) TEM image of a BiNW showing a twisted structure. (d) HRTEM image of the BiNW showing a grain boundary with crystal lattice dislocation (inset is an FFT image of the square area). A comparison of the potential-dependent (e) faradaic efficiencies and (f) partial current densities of formate on Cu foam@BiNW with Cu foam@Bi and Bi plate. Reproduced with permission from Ref. [25].

Lattice-dislocated refers to the local irregular arrangement of atoms. From the perspective of geometry, lattice-dislocated is a kind of line defect, which can be regarded as the boundary between the slipped part and the unslipped part in the crystal. In recent years, its role has been widely observed in the field of catalysis. For example, Zhang *et al*. developed a Bi nanowires catalyst with lattice-dislocated on copper foam (Cu foam@BiNW) and found it was a highly active electrocatalyst for CO_2RR to formate at a low overpotential, reaching a faradaic efficiency for formate of 95% and a partial current density of ~15 mA cm^{-2} at -0.69 V vs. RHE. Through characterization and analysis, they found the high CO_2 electroreduction activity of the Cu foam@BiNW electrode is attributed to the high intrinsic activity arising from the presence of crystal lattice dislocations on the twisted Bi nanowires and the large catalytic surface area associated with the porous structure.[26] This work demonstrates the use of lattice-dislocated engineering to improve the efficiency of electrocatalytic CO_2RR.

Grain boundary

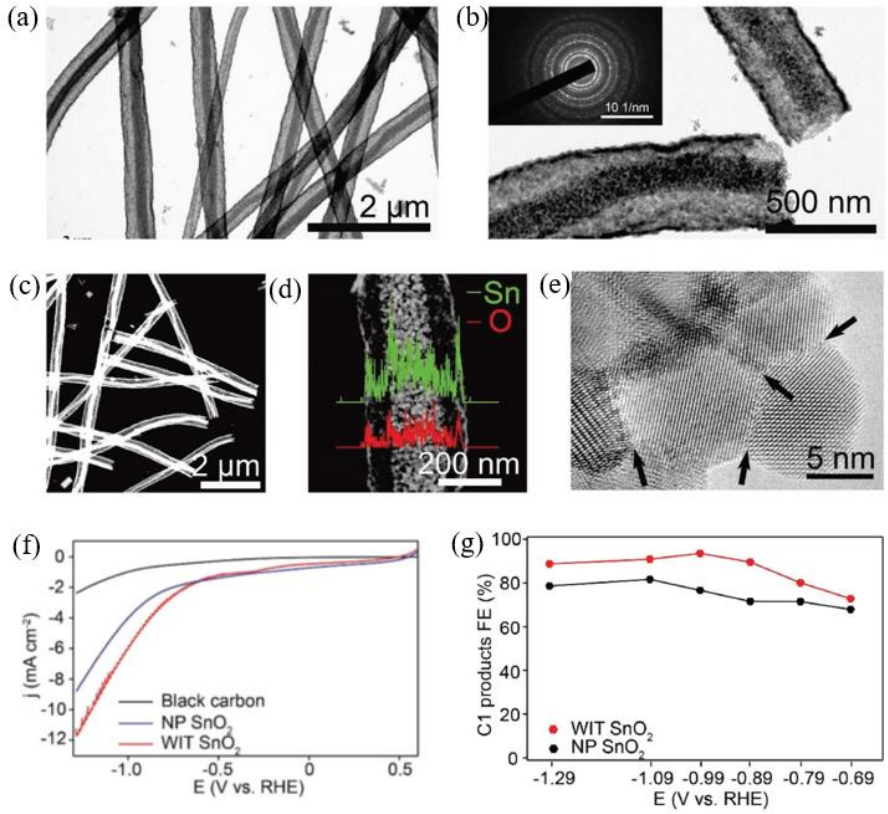

Figure 1.11 Characteristics of the WIT SnO_2 nanofibers. (a, b) HRTEM images of the WIT SnO_2 nanofibers. (c, d) Scanning TEM images of the WIT SnO_2 nanofibers. The inset in panel (d) is the line scan results, which show the distributions of Sn and O elements. (e) Magnified TEM image of the WIT SnO_2 nanofibers with a high density of grain boundaries. (f) LSVs of the NP SnO_2, blank carbon paper and the WIT SnO_2 electrode in CO_2 saturated $KHCO_3$. (g) Faradaic efficiency of C1 products (HCOOH, CO) for the WIT SnO_2 electrode and the NP SnO_2 electrode. Reproduced with permission from Ref. [26].

The grain boundary is an interface between grains with the same structure but different orientations. In particular, it refers to the position of the atoms in the transition state from one orientation to another on the grain boundary. The electrocatalytic properties of this

unique location have also been widely studied. For example, Fan *et al*. synthesized one 1D SnO_2 with wire-in-tube architectures for CO_2 reduction by using electrospinning and found that the structure contained a high density of grain boundaries (Figure 1.1a-e). As shown in Figure 1.1f-g, these large number of grain boundaries enhanced the faradaic efficiency of C1 products for the current density of electrocatalytic CO_2RR.[27]

Besides, the SnO_2 nanoparticles synthesized by Liang *et al*. also exposed a large number of grain boundary and corner/step sites via oxidization of the exfoliated SnS_2 sheets. The SnO_2 nanoparticles exhibited a high total faradaic efficiency of 97% towards electrochemical CO_2RR at -0.95 V vs RHE. They think that the distinctive grain boundary and exposed corner/step sites in the interconnected SnO_2 nanoparticles contribute to the high faradaic efficiency.[28]

In summarize, electrocatalysts containing lattice defects, dislocated, grain boundaries, *etc*., have been widely used in the electrocatalytic CO_2RR. However, it remains a challenge about how to clearly identify their respective roles of these different active sites and establish the corresponding structure-performance relationship.

1.3.3 Adjusting composition

Except for improving the catalytic performance by adjusting the structure of the catalyst, adjusting the composition of the catalyst is also an important method, which includes preparing metal alloys, oxide or sulfides, elemental doping, and compounding of multiple materials, which will be discussed in detail below.

Alloys

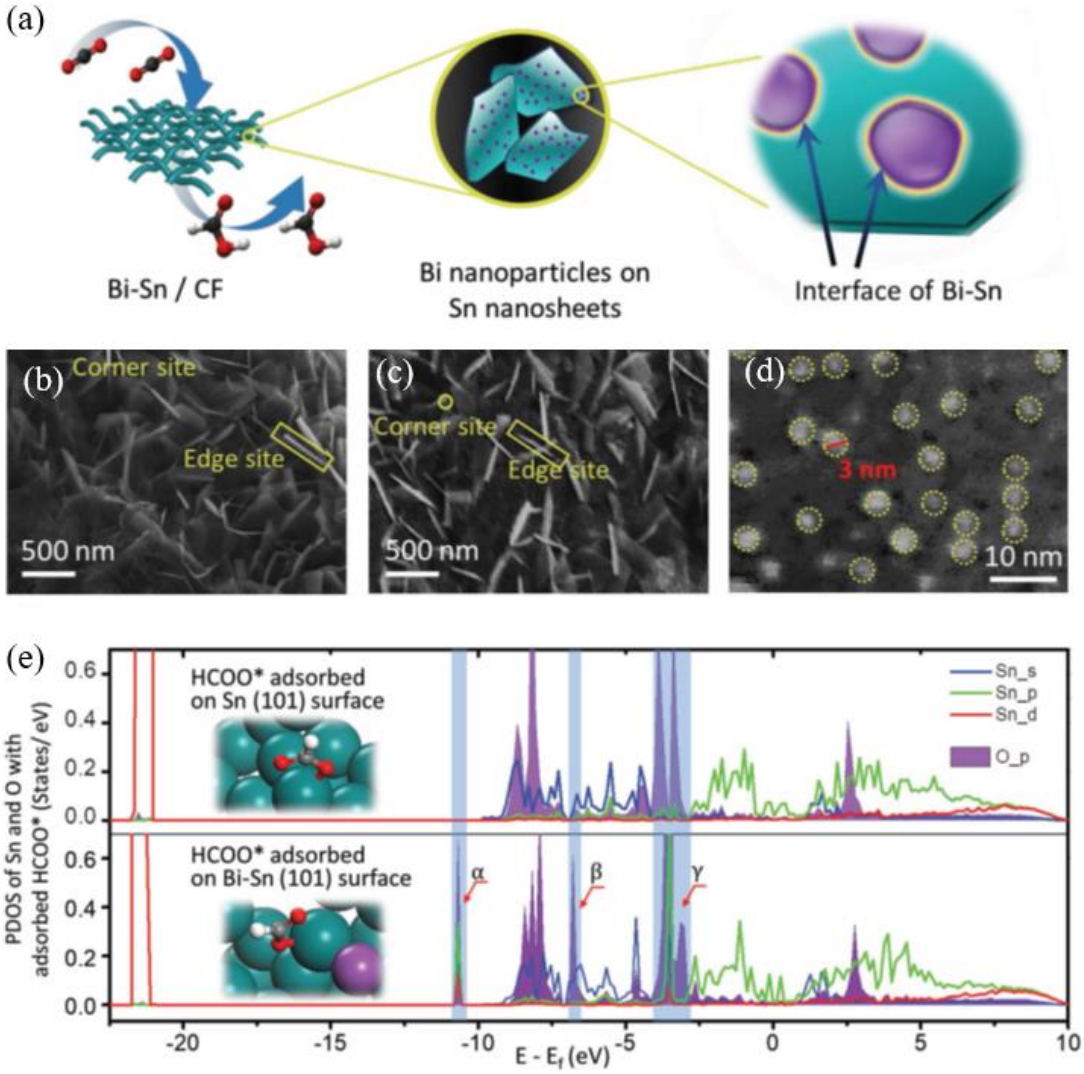

Figure 1.12 (a) A schematic illustration of the Bi-Sn catalyst structure grown on porous carbon fabric substrate and the active interface formed by Bi nanoparticle deposition on Sn nanosheets. SEM images of Bi-Sn/CF catalyst (b) before and (c) after the in situ pre-reduction step, respectively. (d) STEM image of the surface of a Bi-SnO_2 nanosheet. (e) Projected density of states (PDOS) of s, p, and d orbitals of Sn atom and p orbitals of O atom on Sn (101) and Bi-Sn (101) surfaces with adsorbed HCOO*. Reproduced with permission from Ref. [28].

The alloy usually refers to a substance with metallic properties synthesized from two

or more metals through a certain method. According to the number of constituent elements, it can be divided into binary alloys, ternary alloys and multiple alloys. After an extensive study on the electrocatalytic properties of single-element metals such as Sn, Bi, In, Pb, *etc*., it is natural to think about how the performance changes after a metal mixing with other metals. Therefore, various alloy catalysts were used in the study of electrocatalytic CO_2 reduction. For example, Wen *et al*. developed tin nanosheets decorated with bismuth nanoparticles by a three-step method of hydrothermal-electrodeposition-electroreduction. In detail, they first synthesized SnO_2 nanosheets directly on carbon paper by hydrothermal method, then loaded Bi nanoparticles on the SnO_2 nanosheets by electrodeposition method, and finally electrochemical reduced them to SnBi alloy containing a large amount of Bi-Sn interface (Figure 1.12a-b). This alloy exhibits remarkably high formate faradaic efficiency (96%) and production rate (0.74 mmol h^{-1} cm^{-2}) at -1.1 V versus RHE when used in CO_2RR to formate. Additionally, the catalyst maintains its initial efficiency over an unprecedented 100 h of operation. Then, they calculated by DFT calculation reveals that the addition of Bi nanoparticles increased new harmonic overlaps of α in addition to the α and γ areas as shown in Figure 1.12e, which indicates a stronger interaction between the O and Sn atoms for Bi-doped Sn (101) surface compared to a pure Sn surface.[29] Besides, Li *et al*. also prepared a series of BiSn, Bi_2Sn, Bi_3Sn, and Bi_4Sn catalysts for CO_2RR by using the electrodeposition method, which exhibited a faradaic formic acid efficiency of 90.4%.[30]

Apart from compounding Sn and Bi, some researchers have also compounded other metals with Sn or Bi. For example, Zheng *et al*. used co-electrodeposition to synthesize Sn/Cu alloy for CO_2RR to HCOOH. They first calculated the effect of alloying Cu and Sn on the activity and selectivity towards formate by DFT calculation and found that the

incorporation of Cu into Sn could suppress hydrogen evolution and CO production, thus favoring formate generation. Consistent with theoretical trends, the designed $CuSn_3$ catalysts exhibited a faradaic efficiency of 95% towards formate generation at -0.5 V versus RHE and no degradation over 50 h of operation. Also, by using in situ Sn L3-edge and Cu K-edge X-ray absorption spectroscopy characterization, they found electron transfer from Sn to Cu in Sn/Cu alloys, which led to positive oxidation states of Sn under operating conditions.[31] Besides, alloys such as Pd-Sn nanoparticles[32] and Ag_3Sn core-shell structure[33] developed by other researchers have also shown good electrocatalytic activity.

Oxides (sulfides) and other compounds of Sn (Bi)

The most common Sn or Bi compounds for CO_2RR to HCOOH are their oxides. In the previous studies, some researchers believed that the main active site of Sn or Bi-based catalysts was the metal site with 0 valent since the Sn and Bi oxide-based electrocatalysts would be reduced to metal during CO_2 reduction.[20, 34-35] However, with the deepening of research, many researchers have found that some metastable oxides exist in some metal-based catalysts even at a negative reduction potential during the electrochemical reduction of CO_2. For example, Chen *et al*. found that after the Sn-based catalyst was *etc*hed to expose fresh Sn^0 surface, its ability to catalyze the reduction of CO_2 to HCOOH dropped sharply to almost only H_2 evolution over the entire 0.5 V range of potentials examined. By using *in-situ* attenuated total reflectance infrared spectroscopy (ATR-IR), Bocarsly *et al.* confirmed such metastable oxides on the surface of Sn-based catalysts.[36] Nam *et al.* observed that 16.6% of Bi^{3+} was present on the BiO_x/C catalyst surface even at -1.51 V (vs Ag/AgCl) by using the *in-situ* X-ray absorption near edge structure (XANES) analysis.[37] Deng *et al.* found that the bismuth-oxygen structure of bismuth oxides should

be beneficial for the adsorption of CO_2 to generate intermediates with lower free energy in CO_2 electroreduction.[29] Therefore, more and more studies show that metal oxides play a more active role in the CO_2RR process.

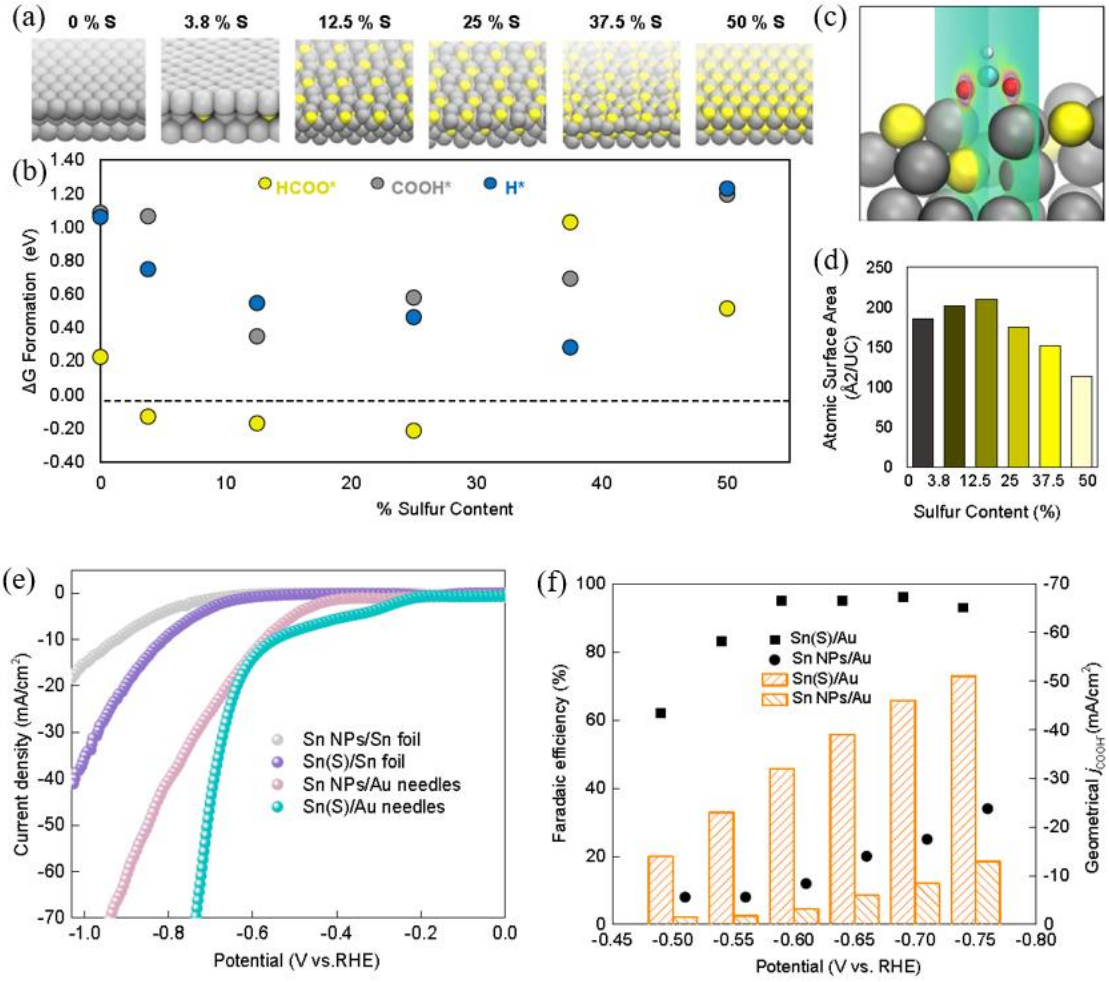

Figure 1.13 (a) Optimized surface slab structures of pure Sn, S-modulated Sn, and SnS. (b) Gibbs free energies of formation (ΔG formation) for HCOO* (yellow), COOH* (gray), and H* (blue) intermediates, which are the rate-limiting intermediates along the reaction pathway to produce HCOOH, CO, and H_2, respectively. (c) Volume slice of the charge densities through the middle of the oxygen atom of a bound HCOO* intermediate. (d) Atomic accessible surface area of the metal slab normalized to the number of tin atoms as a function of sulfur content. (e) The CO_2RR polarization curve and (f) faradaic efficiencies of catalysts loaded on Au needles and Sn foil in CO_2 saturated 0.1 M $KHCO_3$ aqueous electrolyte. Reproduced with permission from Ref. [37].

Due to the similarity properties of O and S, Sn or Bi sulfides are also widely used in CO_2RR. For example, Zheng *et al*. used atomic layer deposition to synthesize a sulfur-modulated tin (Sn(S)) catalysts for CO_2RR to HCOOH, showing faradaic efficiency of 93% and current densities of 55 mA cm^{-2} at 0.75 V vs. RHE. Also, this catalyst showed excellent stability without deactivation following more than 40 hours of operation. Through analysis and characterization, they found that the catalyst still has a certain amount of S atoms on its surface during the electrocatalytic process. Then they compared the effects of different amounts of S atoms on the catalytic activity of Sn by DFT calculations. At the same time, the in-situ X-ray absorption near-edge structure (XANES) characterization technology revealed the higher oxidation states of Sn in Sn (S) compared with that of tin in Sn nanoparticles.[38] Besides, Li *et al*. used a "one-pot" hydrothermal reaction to synthesize SnS_2 nanosheets, and then further reduced them to Sn/SnS_2 catalysts showing a maximum faradaic efficiency of 84.5% and the current density of 13.9 mA cm^{-2} at an overpotential of 0.68 V.[39] Similarly, the catalysts synthesized by Zhang *et al*. with Bi_2S_3 as precursors also showed similar performance.[40]

In addition to the oxides and sulfides of Sn (Bi), there are also some other compounds for electrochemical CO_2RR to HCOOH. Such as the p-orbital delocalization-Bi catalyst using BiOCl as a precursor developed by He *et al*,[34] and the ultrathin Bi nanosheets using BiOI as the precursor developed by Han *et al*.[41], all of which show an HCOOH faradaic efficiency higher than 90%. There is also an unusual class of electrocatalysts with $Bi_2O_2CO_3$ as the precursor, such as Lv *et al*. synthesized the $Bi_2O_2CO_3$ nanosheets by hydrothermal method and then coated them on a glassy carbon electrode for the CO_2RR and found that it exhibited excellent catalytic activity at low overpotentials.[42] Bond *et al.* used the electrochemical exfoliation method to prepare $Bi_2O_2CO_3$ nanosheets with few

layers and then coated them on a carbon paper for the electrochemical reduction of CO_2.[43] However, the research on such catalysts is still relatively less compared with Sn (Bi) oxides or sulfides. Among them, the influence of subcarbonate on catalytic performance and catalytic mechanism are still unclear, which needs more mechanism exploration.

With the development of *in-situ* characterization technology, some studies have found that these catalysts with Sn (Bi) compound as precursors often show positive oxidation states under catalytic conditions, which makes them show better performance.[37-38] However, there is still no definite conclusion as to how these sites in the oxidation state can enhance the electrocatalytic performance. One possible reason is that the Sn or Bi sites in the oxidation state have stronger adsorption ability to the electronegative O in the *OOCH intermediate, thus stabilizing the existence of the *OOCH intermediate. So far, there is no direct evidence to prove this point. Therefore, it is still a challenge to determine how Sn (Bi) in different valence states affects the intermediates adsorption and catalytic process, which should be investigated further by combining *in-situ* characterization technology and quantum chemical calculation.

Doping

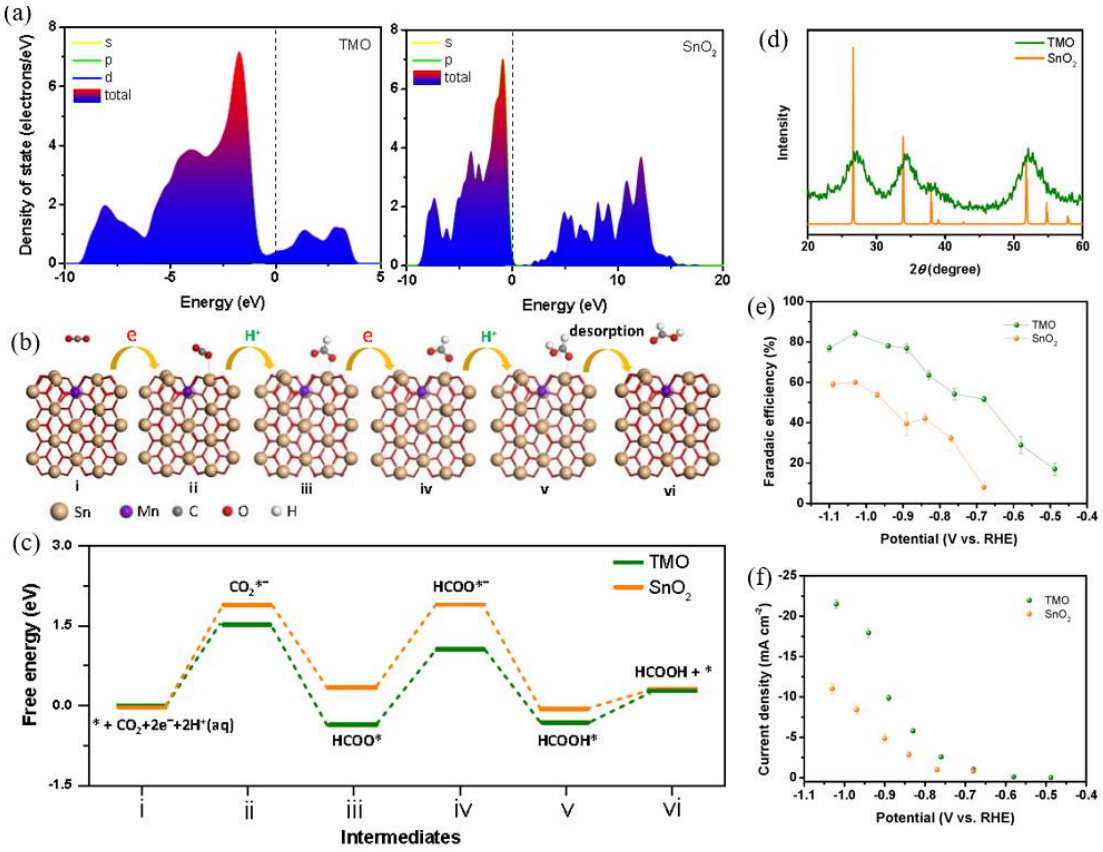

Figure 1.14 (a) DOS of TMO (left) and commercial SnO_2 (right). (b) Optimized structure of main intermediates. (c) The energy diagram of each step. * indicate active sites on the surface. (d) XRD patterns of TMO and commercial SnO_2. Comparison of HCOOH (e) faradaic efficiency and (f) j_{HCOOH} between TMO and commercial SnO_2. Reproduced with permission from Ref. [43].

Elemental doping has been widely used in semiconductor research as a method to change the electronic structure of materials. Such changes in electronic structure can generally affect the performance of semiconductors by affecting their band structures.[44] In the field of electrocatalysis, the influence of doping has also been observed. For example, Wei *et al*. reported a Mn-doped SnO_2 (TMO) with a thickness of 3-4 atomic layers synthesized by a facile *in-situ* gas induced growth strategy using for CO_2RR.

Through DFT calculation, they found that TMO has a continuous density of states (DOS) near Fermi level, the appearance of pseudo potential gap imparts a better electric conductivity and electrons transport ability of TMO as shown in Figure 1.14a. In addition, the calculation of electrocatalytic reaction path shows that Mn-doped SnO_2 has lower CO_2^- and *OOCH Forming energy barrier (Figure 1.14c). For these reasons, TMO exhibits enhanced performance with a larger current density (~21.2 mA cm^{-2}), higher faradaic efficiency (~85%) and lower overpotential (240 mV) for HCOOH formation.[45]

Besides, Zhang *et al.* found that adding 5 atm% Ni to SnS_2 nanosheets can significantly enhance the HCOOH faradaic efficiency and current density. Relevant DFT calculations show that the defect level caused by the Ni doping effectively narrowed the band gap from 2.3 eV to 1.9 eV. At the same time, Ni doping also makes the work function decreased from 4.1 eV to 3.7 eV, which improves the electron transfer process of electrocatalysts, and thus enhancing the performance of CO_2RR.[46] Besides the metal element doping, there are also some examples of non-metal doping such as N-doped SnO_2 nanostructured catalysts[47] and F-doped SnO_2 thin-film.[48]

Through the summary and analysis of these kinds of researches on improving catalytic performance through doping, it can be found that these doping materials are often Sn (Bi) oxides or sulfides because these materials are typical semiconductor materials. The semiconductor doping is simple and easy to implement, which usually leads to greater performance enhancement through fewer changes. Generally, elemental doping can improve electrocatalytic performance in two ways. One is to accelerate electron transfer by enhancing the electronic conductivity of semiconductor materials through doping, thus increasing current density. This change in performance can be confirmed by DFT calculating the band structure and work function of semiconductors. The other is to

improve the adsorption ability of active sites in semiconductors to *OOCH intermediates by doping, thus improving the selectivity to HCOOH. This change in performance can be confirmed by DFT calculating the adsorption energy or forming free-energy barrier of *OOCH on the surface of the catalyst. It should be pointed out that these two effects can coexist or exist alone to improve the electrocatalytic CO_2RR performance.

Other composite materials

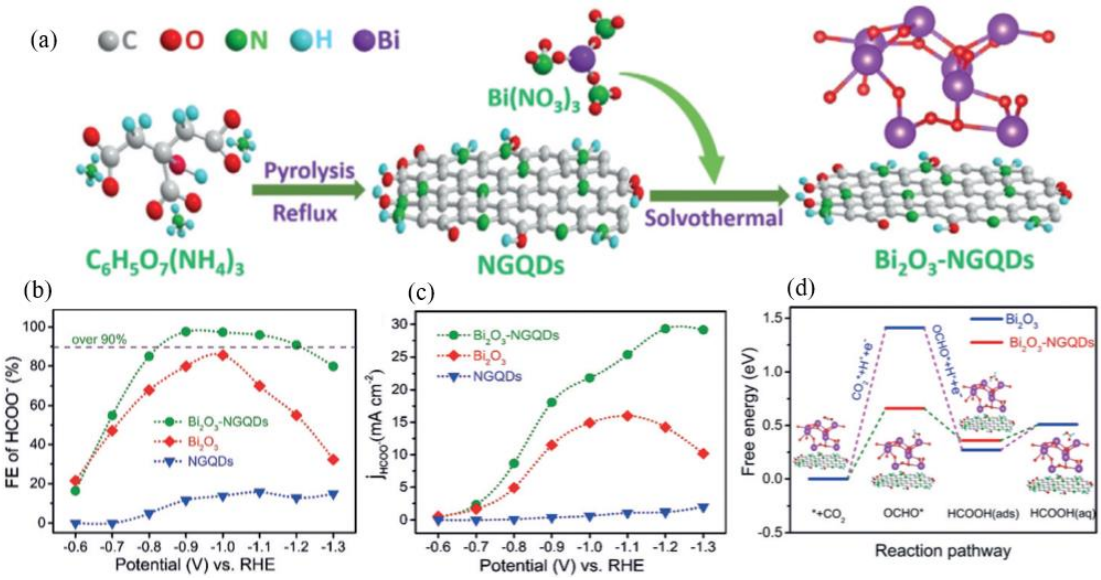

Figure 1.15 (a) Schematic of the synthesis process for Bi_2O_3-NGQDs. (b) Faradaic efficiency of formate and (c) partial current density of formate for Bi_2O_3-NGQDs, Bi_2O_3, and NGQDs at different electrolytic potentials. (d) Calculated the free-energy diagram of CO_2RR. Reproduced with permission from Ref. [48].

Apart from the metal-metal composite mentioned above, more and more researches have been made on the composite of various nonmetallic materials. One of the most commonly used nonmetallic material is carbon, which has not bad electrical conductivity, adjustable specific surface area and a wide range of sources. In particular, N-doped carbon is widely used because its strong electronegativity of N site can adsorb CO_2. For example,

Chen *et al*. composited bismuth oxide nanosheets and nitrogen-doped graphene quantum dots to prepare Bi_2O_3-NGQDs materials for electrochemical reduction of CO_2 to generate formate. This material exhibits nearly 100% formate faradaic efficiency at a potential of -0.9 vs. RHE and higher current density compared to Bi_2O_3 alone. In addition, DFT calculations showed that the composite material significantly reduces the energy barrier for OCHO * intermediate formation.[49] Similarly, Liu *et al*. prepared a Bi_2O_3 nanosheet grown on a conductive multiple channel carbon matrix, which also achieved excellent performance.[50] Besides, there are also composites of Sn and conductive polymers, such as Sn-Polyaniline film exhibited superior HCOOH faradaic efficiency of 94% at -1.7 V vs. Ag / AgCl.[51]

As introduced above, we have summarized some of the main methods such as controlling morphology, making defects, dislocations and grain boundaries, adjusting composition to improve the performances of Sn- and Bi-based electrocatalysis. So far, many studies have been made, however, the problems of low catalytic efficiency and unclear catalytic mechanism still exist. It is still a long way from large-scale industrial application. Therefore, more efficient catalysts should be developed and detailed catalytic mechanisms should be explored further.

1.4 Objectives of this study

As reviewed above, the electrochemical reduction of CO_2 is considered as a technology with great development potential in both the environment and energy fields. The electroreduction of CO_2 to HCOOH is considered economically feasible, and it is currently the most likely to achieve industrialization. The core of this technology is the development of catalysts. Among many candidate catalysts, Sn- and Bi-based catalysts have been the most widely studied due to their high efficiency, low price, and

environmental friendliness. Therefore, this study will develop a series of new and efficient the Sn- and Bi-based electrocatalysts for electrochemical CO_2RR. Besides, due to the complexity of the CO_2 electrocatalytic reactions, the catalysis mechanisms are still unclear, such as the effects of oxides (sulfide) and doping on the catalytic process. Thus, this study will also use DFT calculations to aid design synthesis and explain the catalytic mechanism, providing theoretical guidance for the development of efficient catalysts.

1.5 Scope of this dissertation

Chapter 1 introduces the background of electrochemical reduction of CO_2 and reviews the progress of Sn- and Bi-based catalysts for electrochemical CO_2RR to HCOOH. It summarizes several methods currently used to improve catalyst performance, such as controlling morphology, making defects, dislocations and grain boundaries, adjusting composition and so on.

Chapter 2 gives detailed descriptions about catalyst preparation, characterization and performance testing, and theoretical calculation details.

Chapter 3 focuses on Tin-based electrocatalysts, in which we prepared the electrocatalysts using unipolar pulse electrodeposition (UPED) method. It exhibited higher HCOOH faradaic efficiency compared to the electrocatalysts prepared by the potentiostatic and galvanostatic electrodeposition method. Moreover, the effects of surface oxides species on the performance of tin-based electrocatalysts were systematically investigated via DFT calculations.

Chapter 4 introduces a Bismuth (Bi)-doped SnO nanosheets grown on copper foam (Bi-SnO/Cu foam) by a one-step hydrothermal reaction method and applied for the electrochemical reduction of CO_2 to HCOOH, which exhibited a superior faradaic efficiency compared to the un-doped material. The effects of Bi doping were examined

in detail through physical and electrochemical characterization and DFT calculations.

Chapter 5 describes an interesting morphological transformation phenomenon accompanied by the formation of petal-shaped bismuth subcarbonate ($Bi_2O_2CO_3$) nanosheets in Bi-based catalyst. It was observed that this transformation improved the electrocatalytic performance of CO_2 reduction to HCOOH. The physical and electrochemical characterization and DFT calculations were performed to explain the reasons for performance improvement

Chapter 6 summarizes the general conclusions of this research and discusses the challenges and prospects for future work.

References

1. Ewald, J. Carbon dioxide at NOAA's Mauna Loa observatory reaches, new milestone, **2020**. https://www.esrl.noaa.gov/gmd/ccgg/trends/.
2. Intergovernmental panel on climate change (IPCC), Global warming of 1.5 °C. **2019**.
3. Hansen, J.; Sato, M.; Hearty, P.; Ruedy, R.; Kelley, M.; Masson-Delmotte, V.; Russell, G.; Tselioudis, G.; Cao, J.; Rignot, E., Ice melt, sea level rise and superstorms: evidence from paleoclimate data, climate modeling, and modern observations that 2 °C global warming is highly dangerous. *Atmos. Chem. Phys.* **2015,** *15* (14).
4. Váry, Z.; Mullins, E.; McElwain, J. C.; Doohan, F. M., The severity of wheat diseases increases when plants and pathogens are acclimatized to elevated carbon dioxide. *Global Change Biol.* **2015,** *21* (7), 2661-2669.
5. Li, X.; Ulfat, A.; Lv, Z.; Fang, L.; Jiang, D.; Liu, F., Effect of multigenerational exposure to elevated atmospheric CO_2 concentration on grain quality in wheat. *Environ. Exp. Bot.* **2019,** *157*, 310-319.
6. Lynsay, S.; Andrew Hugh, M., Quantifying the probability distribution function of the transient climate response to cumulative CO_2 emissions. *Environ. Res. Lett.* **2020**. *15(3)*, 034044.
7. Liu, Q.; Yang, X.; Li, L.; Miao, S.; Li, Y.; Li, Y.; Wang, X.; Huang, Y.; Zhang, T., Direct catalytic hydrogenation of CO_2 to formate over a schiff-base-mediated gold nanocatalyst. *Nat. commun.* **2017,** *8* (1), 1407.
8. Daiyan, R.; Lu, X.; Ng, Y. H.; Amal, R., Liquid hydrocarbon production from CO_2:

Recent development in metal-based electrocatalysis. *ChemSusChem* **2017,** *10* (22), 4342-4358.

9. Khezri, B.; Fisher, A. C.; Pumera, M., CO_2 reduction: the quest for electrocatalytic materials. *J. Mater. Chem. A* **2017,** *5* (18), 8230-8246.
10. Feaster, J. T.; Shi, C.; Cave, E. R.; Hatsukade, T.; Abram, D. N.; Kuhl, K. P.; Hahn, C.; Nørskov, J. K.; Jaramillo, T. F., Understanding selectivity for the electrochemical reduction of carbon dioxide to formic acid and carbon monoxide on metal electrodes. *ACS Catal.* **2017,** *7* (7), 4822-4827.
11. Han, N.; Ding, P.; He, L.; Li, Y.; Li, Y., Promises of main group metal-based nanostructured materials for electrochemical CO_2 reduction to formate. *Adv. Energy. Mater.* **2019**, 1902338.
12. Verma, S.; Kim, B.; Jhong, H. R. M.; Ma, S.; Kenis, P. J., A gross-margin model for defining technoeconomic benchmarks in the electroreduction of CO_2. *ChemSusChem* **2016,** *9* (15), 1972-1979.
13. Lee, H. J.; Kang, D. C.; Pyen, S. H.; Shin, M.; Suh, Y. W.; Han, H.; Shin, C. H., Production of H_2-free CO by decomposition of formic acid over ZrO_2 catalysts. *Appl. Catal. A-Gen.* **2017,** *531*, 13-20.
14. Koós, Á.; Solymosi, F., Production of CO-Free H_2 by formic acid decomposition over Mo_2C/carbon catalysts. *Catal. Lett.* **2010,** *138* (1), 23-27.
15. Savourey, S.; Lefèvre, G.; Berthet, J. C.; Thuéry, P.; Genre, C.; Cantat, T., Efficient disproportionation of formic acid to methanol using molecular ruthenium catalysts. *Angew. Chem. Int. Ed.* **2014,** *53* (39), 10466-10470.
16. Duan, X.; Xu, J.; Wei, Z.; Ma, J.; Guo, S.; Wang, S.; Liu, H.; Dou, S., Metal-free carbon materials for CO_2 electrochemical reduction. *Adv. Mater.* **2017,** *29* (41).
17. Ito, K.; Murata, T.; Ikeda, S., Electrochemical reduction of carbon dioxide to organic compounds. *Bulletin of Nagoya Institute of Technology* **1976,** *27*, 209-214.
18. Komatsu, S.; Yanagihara, T.; Hiraga, Y.; Tanaka, M.; Kunugi, A., Electrochemical reduction of CO_2 at Sb and Bi electrodes in $KHCO_3$ solution. *Denki Kagaku oyobi Kogyo Butsuri Kagaku* **1995,** *63* (3), 217-224.
19. Won da, H.; Choi, C. H.; Chung, J.; Chung, M. W.; Kim, E. H.; Woo, S. I., Rational design of a hierarchical tin dendrite electrode for efficient electrochemical reduction of CO_2. *ChemSusChem* **2015,** *8* (18), 3092-3098.
20. Su, P.; Xu, W.; Qiu, Y.; Zhang, T.; Li, X.; Zhang, H., Ultrathin bismuth nanosheets as highly efficient electrocatalyst for CO_2 reduction. *ChemSusChem* **2018,** *11* (5), 848-853.
21. Kim, S.; Dong, W. J.; Gim, S.; Sohn, W.; Park, J. Y.; Yoo, C. J.; Jang, H. W.; Lee, J.

L., Shape-controlled bismuth nanoflakes as highly selective catalysts for electrochemical carbon dioxide reduction to formate. *Nano Energy* **2017,** *39*, 44-52.

22. Lv, W.; Zhou, J.; Kong, F.; Fang, H.; Wang, W., Porous tin-based film deposited on copper foil for electrochemical reduction of carbon dioxide to formate. *Int. J. Hydrogen Energy* **2016,** *41* (3), 1585-1591.
23. Zhang, S.; Kang, P.; Meyer, T. J., Nanostructured tin catalysts for selective electrochemical reduction of carbon dioxide to formate. *J. Am. Chem. Soc.* **2014,** *136* (5), 1734-7.
24. Koh, J. H.; Won, D. H.; Eom, T.; Kim, N.-K.; Jung, K. D.; Kim, H.; Hwang, Y. J.; Min, B. K., Facile CO_2 Electro-reduction to formate via oxygen bidentate intermediate stabilized by high-index planes of bi dendrite catalyst. *ACS Catal.* **2017,** *7* (8), 5071-5077.
25. Gong, Q.; Ding, P.; Xu, M.; Zhu, X.; Wang, M.; Deng, J.; Ma, Q.; Han, N.; Zhu, Y.; Lu, J.; Feng, Z.; Li, Y.; Zhou, W.; Li, Y., Structural defects on converted bismuth oxide nanotubes enable highly active electrocatalysis of carbon dioxide reduction. *Nat. Commun.* **2019,** *10* (1), 2807.
26. Zhang, X.; Sun, X.; Guo, S.-X.; Bond, A. M.; Zhang, J., Formation of lattice-dislocated bismuth nanowires on copper foam for enhanced electrocatalytic CO_2 reduction at low overpotential. *Energy Environ. Sci.* **2019,** *12* (4), 1334-1340.
27. Fan, L.; Xia, Z.; Xu, M.; Lu, Y.; Li, Z., 1D SnO_2 with Wire-in-tube architectures for highly selective electrochemical reduction of CO_2 to C1 products. *Adv. Funct. Mater.* **2018,** *28* (17), 1706289.
28. Liang, C.; Kim, B.; Yang, S.; Liu, Y.; Woellner, C. F.; Li, Z.; Vajtai, R.; Yang, W.; Wu, J.; Kenis, P. J., High efficiency electrochemical reduction of CO_2 beyond the two-electron transfer pathway on grain boundary rich ultra-small SnO_2 nanoparticles. *J. Mater. Chem. A* **2018,** *6* (22), 10313-10319.
29. Wen, G.; Lee, D. U.; Ren, B.; Hassan, F. M.; Jiang, G.; Cano, Z. P.; Gostick, J.; Croiset, E.; Bai, Z.; Yang, L.; Chen, Z., Orbital Interactions in Bi-Sn bimetallic electrocatalysts for highly selective electrochemical CO_2 reduction toward formate production. *Adv. Energy. Mater.* **2018,** *8* (31), 1802427.
30. Li, Q.; Zhang, Y.; Zhang, X.; Wang, H.; Li, Q.; Sheng, J.; Yi, J.; Liu, Y.; Zhang, J., Novel Bi, BiSn, Bi_2Sn, Bi_3Sn, and Bi_4Sn catalysts for efficient electroreduction of CO_2 to formic acid. *Ind. Eng. Chem. Res.* **2019**.
31. Zheng, X.; Ji, Y.; Tang, J.; Wang, J.; Liu, B.; Steinrück, H.-G.; Lim, K.; Li, Y.; Toney, M. F.; Chan, K.; Cui, Y., Theory-guided Sn/Cu alloying for efficient CO_2 electroreduction at low overpotentials. *Nat. Catal.* **2019,** *5*, 55-61.

32. Bai, X.; Chen, W.; Zhao, C.; Li, S.; Song, Y.; Ge, R.; Wei, W.; Sun, Y., Exclusive formation of formic acid from CO_2 electroreduction by a tunable Pd-Sn alloy. *Angew. Chem.* **2017,** *129* (40), 12387-12391.
33. Luc, W.; Collins, C.; Wang, S.; Xin, H.; He, K.; Kang, Y.; Jiao, F., Ag-Sn bimetallic catalyst with a core-shell structure for CO_2 reduction. *J. Am. Chem. Soc.* **2017,** *139* (5), 1885-1893.
34. He, S.; Ni, F.; Ji, Y.; Wang, L.; Wen, Y.; Bai, H.; Liu, G.; Zhang, Y.; Li, Y.; Zhang, B.; Peng, H., The p-orbital delocalization of main-group metals to boost CO_2 electroreduction. *Angew. Chem. Int. Ed. Engl.* **2018,** *57* (49), 16114-16119.
35. Qiu, Y.; Du, J.; Dong, W.; Dai, C.; Tao, C., Selective conversion of CO_2 to formate on a size tunable nano-Bi electrocatalyst. *J. CO_2 Util.* **2017,** *20*, 328-335.
36. Baruch, M. F.; Pander, J. E.; White, J. L.; Bocarsly, A. B., Mechanistic insights into the reduction of CO_2 on tin electrodes using in situ ATR-IR spectroscopy. *ACS Catal.* **2015,** *5* (5), 3148-3156.
37. Lee, C. W.; Hong, J. S.; Yang, K. D.; Jin, K.; Lee, J. H.; Ahn, H.-Y.; Seo, H.; Sung, N.-E.; Nam, K. T., Selective electrochemical production of formate from carbon dioxide with bismuth-based catalysts in an aqueous electrolyte. *ACS Catal.* **2018,** *8* (2), 931-937.
38. Zheng, X.; De Luna, P.; García de Arquer, F. P.; Zhang, B.; Becknell, N.; Ross, M. B.; Li, Y.; Banis, M. N.; Li, Y.; Liu, M.; Voznyy, O.; Dinh, C. T.; Zhuang, T.; Stadler, P.; Cui, Y.; Du, X.; Yang, P.; Sargent, E. H., Sulfur-modulated tin sites enable highly selective electrochemical reduction of CO_2 to formate. *Joule* **2017,** *1* (4), 794-805.
39. Li, F.; Chen, L.; Xue, M.; Williams, T.; Zhang, Y.; MacFarlane, D. R.; Zhang, J., Towards a better Sn: Efficient electrocatalytic reduction of CO_2 to formate by Sn/SnS_2 derived from SnS_2 nanosheets. *Nano Energy* **2017,** *31*, 270-277.
40. Zhang, Y.; Li, F.; Zhang, X.; Williams, T.; Easton, C. D.; Bond, A. M.; Zhang, J., Electrochemical reduction of CO_2 on defect-rich Bi derived from Bi_2S_3 with enhanced formate selectivity. *J. Mater. Chem. A* **2018,** *6* (11), 4714-4720.
41. Han, N.; Wang, Y.; Yang, H.; Deng, J.; Wu, J.; Li, Y.; Li, Y., Ultrathin bismuth nanosheets from in situ topotactic transformation for selective electrocatalytic CO_2 reduction to formate. *Nat. Commun.* **2018,** *9* (1), 1320.
42. Lv, W.; Bei, J.; Zhang, R.; Wang, W.; Kong, F.; Wang, L.; Wang, W., $Bi_2O_2CO_3$ nanosheets as electrocatalysts for selective reduction of CO_2 to formate at low overpotential. *ACS Omega* **2017,** *2* (6), 2561-2567.
43. Zhang, Y.; Zhang, X.; Ling, Y.; Li, F.; Bond, A. M.; Zhang, J., Controllable synthesis of few-layer bismuth subcarbonate by electrochemical exfoliation for enhanced CO_2

reduction performance. *Angew. Chem. Int. Ed.* **2018,** *57* (40), 13283-13287.
44. Dvoranova, D.; Brezova, V.; Mazúr, M.; Malati, M. A., Investigations of metal-doped titanium dioxide photocatalysts. *Appl. Catal. B-Environ.* **2002,** *37* (2), 91-105.
45. Wei, Y.; Liu, J.; Cheng, F.; Chen, J., Mn-doped atomic SnO_2 layers for highly efficient CO_2 electrochemical reduction. *J. Mater. Chem. A* **2019,** *7* (34), 19651-19656.
46. Zhang, A.; He, R.; Li, H.; Chen, Y.; Kong, T.; Li, K.; Ju, H.; Zhu, J.; Zhu, W.; Zeng, J., Nickel doping in atomically thin tin disulfide nanosheets enables highly efficient CO_2 reduction. *Angew. Chem. Int. Ed. Engl.* **2018,** *57* (34), 10954-10958.
47. Li, Q.; Wang, Z.; Zhang, M.; Hou, P.; Kang, P., Nitrogen doped tin oxide nanostructured catalysts for selective electrochemical reduction of carbon dioxide to formate. *J. Energy Chem.* **2017,** *26* (5), 825-829.
48. Raghavachari, K., Reduction of CO_2 on fluorine-doped SnO_2 thin-film electrodes. J. Electrochem. Soc. **1992,** *139* (9), 2544-2549.
49. Chen, Z.; Mou, K.; Wang, X.; Liu, L., Nitrogen-doped graphene quantum dots enhance the activity of Bi_2O_3 nanosheets for electrochemical reduction of CO_2 in a wide negative potential region. *Angew. Chem. Int. Ed.* **2018,** *57* (39), 12790-12794.
50. Liu, S.; Lu, X. F.; Xiao, J.; Wang, X.; Lou, X. W., Bi_2O_3 nanosheets grown on multi-channel carbon matrix to catalyze efficient CO_2 electroreduction to HCOOH. *Angew. Chem. Int. Ed.* **2019,** *58* (39), 13828-13833.
51. Li, F., Efficient electrochemical reduction of CO_2 to formate using Sn-Polyaniline film on Ni foam. *Electrochim. Acta* **2020,** *332*, 135457.

Chapter 2 Methodology

2.1 Experimental part

2.1.1 Preparation of catalytic electrode

This thesis mainly involves two common materials preparation methods, namely the electrodeposition method and hydrothermal reaction method. The electrodeposition method refers to a method of directly growing a required material on a substrate by using an electrochemical oxidation or reduction method under the driving of electric energy. It has the advantages of being simple, fast and green. The hydrothermal method refers to a method for preparing materials in a sealed pressure vessel using water as a solvent, and the powder is dissolved and recrystallized. By controlling the reaction conditions, this method can often obtain some nanoscale catalysts with different morphologies, which have been widely used in materials preparation, chemical reactions and processing.

The electrodeposition method was used in chapters 3 and 5, and the hydrothermal method was used in chapter 4. To avoid repetition and easy reading, the detailed preparation methods of specific materials are shown in the corresponding sections.

2.1.2 Physical characterization

The physical characterization involved in this thesis include the following:

SEM

Scanning electron microscope (SEM) is a microscopic morphology observation method between transmission electron microscope and optical microscope. It uses secondary electron signal imaging to observe the surface morphology of the sample. The SEM instrument model is Hitachi SU8010.

EDS

Energy dispersive spectrometer (EDS) is a method for element type and content analysis based on the characteristics of various elements with their own X-ray characteristic wavelengths. In this thesis, it was used together with Hitachi SU8010 SEM instrument.

TEM

The principle of the transmission electron microscope (TEM) is to project the accelerated and concentrated electron beam onto a very thin sample. The electron collides with atoms in the sample and changes direction, resulting in phase formation after solid angle scattering. The nanostructures of the materials in this thesis were observed through the JEM-2100F TEM (JEOL, Japan).

XRD

X-ray diffraction (XRD) is a means to reflect the atomic distribution inside the crystal according to the different diffraction patterns produced by each crystal. The crystal structures of all samples in this thesis were determined by Rigaku SmartLab XRD using a Cu-Kα (λ = 1.5405 Å) radiation source.

XPS

X-ray photoelectron spectroscopy (XPS) is a method to determine the valence of the element by measuring the photoelectron energy of a sample after it is excited by X-ray radiation. The samples in this thesis were characterized by the Thermo ESCALAB 250XI XPS instrument.

2.1.3 Electrochemical characterization

All the electrochemical characterizations were measured by using a two-compartment electrochemical cell, in which the working and counter electrodes were separated by a Nafion 117 membrane (Chemours, Japan). The Ag/AgCl/saturated KCl electrode and

platinum wire (ALS, Japan) were applied as the reference and counter electrodes, respectively. All potentials and current densities present in this study were versus Ag/AgCl saturated KCl and geometric surface area (1×1 cm^2) of the working electrode immersed in the electrolyte respectively unless stated otherwise.

The specific electrochemical characterization methods used include the following.

Cyclic voltammetry

Cyclic Voltammetry (CV) is a commonly used method for electrochemical research. This method controls the electrode potential to scan one or more times at different rates and records the current-potential curve. Use the shape of the curve to determine what happens on the electrode. In this thesis, this method was used to judge the redox properties of the electrode and measure its electrochemical double-layer capacitance.

Linear sweep voltammetry

Linear sweep voltammetry (LSV) is a CV-like method, usually half the CV, sweeping from one applied potential to another and recording the current-potential curve. This thesis uses this method to preliminarily judge the activity of electrocatalysts.

Electrochemical impedance spectroscopy

Electrochemical impedance spectroscopy (EIS) refers to a method of determining the impedance by measuring the change in the ratio of the AC potential to the current signal through an electrochemical system. This paper uses this method to compare the charge transfer resistance of different electrodes.

2.1.4 Performance testing and product analysis

In this thesis, constant potential electrolysis was carried out for 1 h at various constant potentials in a CO_2-saturated 0.1 M $KHCO_3$ solution (pH 6.8). During this process, CO_2 was continuously purged into the reactor with a gas flow of 10 cm^3 min^{-1}. After finished,

the gas and liquid products were collected for analysis.

Gas products were analyzed with gas chromatography (GC, Agilent 7890A GC system, USA), by which CO and H_2 were detected with two thermal conductivity detectors (TCD), respectively. Liquid products were analyzed using a Shimadzu high performance liquid chromatography (HPLC) equipped with SPD-20AV and RID-10A detectors. Supelcogel C610-H (30 cm×7.8 mm, Sigma) and H_3PO_4 (0.05 %) solution were used as the column and mobile phase, respectively, and the temperature of the oven CTO-20A was set at 40 ºC. The faradaic efficiency of HCOOH, CO and H_2 were calculated as follows:

$$\text{Faradaic efficiency} = 2F \times n/Q \quad (2\text{-}1)$$

where F is the faraday constant, n the total amount of products (in moles), and Q the amount of total charge (in Coulomb).

2.2 Theoretical calculation part

2.2.1 Introduction of calculation theory

With the rapid development of computer technology, the use of computers to study chemical problems is becoming more and more common. Most materials, especially composite materials have complex internal structures. Only some macroscopic properties can be obtained through experimental means, and clear understanding cannot be obtained from the microscopic scale. Computer simulation technology shows unique advantages in studying such problems and provides powerful help for materials to predict the macroscopic properties of materials. The most fundamental problem of the quantum chemical calculation method is to solve the Schrodinger equation. The solution of the equation can be used to obtain the bond energy, geometric configuration, and charge distribution of the molecule. The theoretical method is an effective way to link experimental phenomena with the nature of molecules. It plays an irreplaceable role in

understanding the macroscopic properties of matter from the molecular level, which has become an indispensable research method in the field of science.

Quantum chemical calculations mainly include valence bond theory, molecular orbital theory, and density functional theory (DTF). Among them, DFT has become the most widely used method in quantum chemical calculations due to its fast calculation speed, high accuracy, and large number of countable atoms.[1] The calculation methods used in this thesis are based on DFT calculations. Its origin can be traced back to the famous Hohenberg-Kohn theorem proposed by Hohenberg and Kohn in 1964, which believed that the energy of systems such as molecules can be characterized as a function of electron density.[2] Subsequently, Kohn and Sham deduced the Kolm-Sham equation, which became the theoretical framework for the molecular system of DFT calculations, and also made it possible to apply DFT calculations to molecular systems. Kohn and John both won the 1998 Nobel Prize in Chemistry for their pioneering work in DFT.[3-4]

2.2.2 Introduction of Materials Studio

Materials Studio is a calculation software developed by Accelrys specifically for the field of materials science to help researchers solve many important problems encountered in the chemical and materials industry. It integrates many advanced algorithms, whether it is property prediction, polymer modeling or X-ray diffraction simulation, we can get some reliable data through some easy-to-learn operations. The content of the simulation includes the main topics in the field of materials science research such as catalysts, polymers, solid chemistry, crystallography, powder diffraction, and material properties.

In this thesis, we mainly apply the following modules in Material Studio software:

Visualizer

This module is mainly used to build molecular, crystal, interface, surface and

polymer material structure models. It can also operate, observe and analyze structural models before and after calculations, and process data in the form of diagrams, tables or text. It is the core module of the Materials Studio product line. The model construction in the thesis is mainly completed using this module.

DMol3

This module is a quantum mechanics calculation program based on DFT. It can simulate processes and properties such as gas phase, solution, surface, and solid. It is used in many fields such as chemistry, materials, chemical engineering, and solid physics. It can be used to study homogeneous catalysis, heterogeneous catalysis, semiconductors, molecular reactions, *etc*. It can also predict properties such as solubility, vapor pressure, partition function, heat of dissolution, and heat of mixing. The theoretical calculation part of the thesis is mainly completed by this module.

Reflex Plus

This module is mainly used to simulate X-ray, neutron and electron powder diffraction patterns of crystal materials. It can help researchers determine the crystal structure, analyze diffraction data and use it to verify calculations and experimental results. The simulated spectrum can be directly compared with the experimental data and can be updated instantly according to the structural change. The XRD simulation spectrum in the thesis is mainly completed using this module.

2.2.3 Parameter settings

All models were optimized by using the spin-polarized DFT computations with an all-electron method in the DMol3.[5-6] The electron exchange-correlation functions of generalized gradient approximation (GGA) and Perdew-Burke-Ernzerhof (PBE), and basis set of double numerical plus polarization (DNP) were used for these calculations.[7]

Specifically, the van der Waals correction was employed by using Grimme[8] method in DFT-D[9] to accurately describe the long-range electrostatic interactions. The solvent effects were also applied by using a conductor-like screening model (COSMO)[10] with the H_2O dielectric constant of 78.54.

Other specific parameters selected in this study were consistent with the data reported in the literature.[11] In detail, the convergence criterion was selected as 10^{-6} a.u. with the maximum force of 0.002 a.u. $Å^{-1}$ and the maximum displacement of 0.005 Å. The k points were set as $5 \times 5 \times 1$ by using the Monkhorst-Pack method.[12] The real-space global orbital cutoff radius was chosen as 4.7 Å in all the computations to ensure high quality.

The free energy of electrochemical reduction of CO_2 was calculated based on a computational hydrogen electrode (CHE) model,[13] in which the chemical potential of a proton/electron ($H^+ + e^-$) in solution is equal to the half chemical potential of a gas-phase H_2. The adsorption energy of adsorbate was defined as:

$$E_{ad} = E_{surface\text{-}adsorbate} - E_{surface} - E_{adsorbate} \quad (2\text{-}2)$$

where $E_{surface\text{-}adsorbate}$, $E_{surface}$, and $E_{adsorbate}$ are the DFT total energy for the adsorbate on the surface, surface, and adsorbate itself, respectively.

The change in Gibbs free energy (ΔG) was evaluated by the following equation:

$$\Delta G = \Delta E + \Delta E_{zpe} - T\Delta S \quad (2\text{-}3)$$

where the ΔE, ΔE_{zpe} and ΔS are the difference of DFT energy, zero point energy and entropy between products and reactants, respectively. T was set at 298.15 K in this work. E_{zpe} can be obtained by the vibrational frequency analysis over all normal modes ν ($E_{zpe} = 1/2\Sigma\hbar\nu$). The entropies of the free molecules (CO, CO_2, HCOOH, H_2, and H_2O) were obtained from the NIST database.[14] The configurational entropy in the adsorbed state was neglected by fixing the surfaces according to the way in most of the literatures.[13, 15-16]

Reference

1. Bickelhaupt, F. M.; Baerends, E. J., Kohn-Sham density functional theory: predicting and understanding chemistry. *Rev. Comput. Chem.* **2000,** *15*, 1-86.
2. Hohenberg, P.; Kohn, W., Density functional theory (DFT). *Phys. Rev* **1964,** *136*, B864.
3. Kohn, W.; And, A. D. B., †; Parr‡, R. G., Density functional theory of electronic structure. *J. Phys. Chem.* **1996,** *31* (31), 12974-12980.
4. Curtiss, L. A.; Redfern, P. C.; Raghavachari, K.; Pople, J. A., Assessment of Gaussian-2 and density functional theories for the computation of ionization potentials and electron affinities. *J. Chem. Phys.* **1998,** *109* (1), 42-55.
5. Delley, B., An all-electron numerical method for solving the local density functional for polyatomic molecules. *J. Chem. Phys* **1990,** *92* (1), 508-517.
6. Delley, B., From molecules to solids with the DMol3 approach. *J. Chem. Phys* **2000,** *113* (18), 7756-7764.
7. Perdew, J. P.; Burke, K.; Ernzerhof, M., Generalized gradient approximation made simple. *Phys. Rev. Lett.* **1996,** *77* (18), 3865.
8. Grimme, S., Semiempirical GGA-type density functional constructed with a long-range dispersion correction. *J. Comput. Chem.* **2006,** *27* (15), 1787-1799.
9. Harl, J.; Kresse, G., Accurate bulk properties from approximate many-body techniques. *Phys. Rev. Lett.* **2009,** *103* (5), 056401.
10. Klamt, A.; Schüürmann, G., COSMO: a new approach to dielectric screening in solvents with explicit expressions for the screening energy and its gradient. *J. Chem. Soc., Perkin Trans. 2* **1993,** 5, 799-805.
11. Liu, Y.; Zhao, J.; Cai, Q., Pyrrolic-nitrogen doped graphene: a metal-free electrocatalyst with high efficiency and selectivity for the reduction of carbon dioxide to formic acid: a computational study. *Phys. Chem. Chem. Phys.* **2016,** *18* (7), 5491-5498.
12. Monkhorst, H. J.; Pack, J. D., Special points for Brillouin-zone integrations. *Phys. Rev. B* **1976,** *13* (12), 5188-5192.
13. Peterson, A. A.; Abild-Pedersen, F.; Studt, F.; Rossmeisl, J.; Nørskov, J. K., How copper catalyzes the electroreduction of carbon dioxide into hydrocarbon fuels. *Energy Environ. Sci.* **2010,** *3* (9), 1311-1315.
14. Nørskov, J. K.; Rossmeisl, J.; Logadottir, A.; Lindqvist, L.; Kitchin, J. R.; Bligaard, T.; Jonsson, H., Origin of the overpotential for oxygen reduction at a fuel-cell cathode. *J. Phys. Chem. B* **2004,** *108* (46), 17886-17892.
15. Lim, D.-H.; Wilcox, J., Mechanisms of the oxygen reduction reaction on defective

graphene-supported Pt nanoparticles from first-principles. *J. Phys. Chem. C* **2012,** *116* (5), 3653-3660.

16. Kattel, S.; Atanassov, P.; Kiefer, B., Density functional theory study of Ni-N_x/C electrocatalyst for oxygen reduction in alkaline and acidic media. *J. Phys. Chem. C* **2012,** *116* (33), 17378-17383.

Chapter 3 Electrodeposition of tin-based electrocatalysts with different surface tin species distributions for electrochemical reduction of CO_2 to HCOOH

3.1 Introduction

Excessive carbon dioxide (CO_2) emission is considered as the main reason resulting in the global warming.[1] On the other hand, CO_2 is also an important carbon resource because it can be reduced to formic acid (HCOOH),[2-3] carbon monoxide (CO),[4-5] methane (CH_4),[6-7] methanol (CH_3OH),[8-9] ethanol (C_2H_5OH)[10-11] and other valuable liquid fuels. Among them, HCOOH is an important basic organic chemical which can be used as a fuel, a means of H_2 storage, or a feedstock in the synthesis of other fine chemicals.[2] Electroreduction of CO_2 to HCOOH is considered as an economically feasible way to utilize CO_2 resource.[12] Electrochemical reduction of CO_2 can be realized in mild and controllable reaction conditions in a simple reaction device with a short reaction time.[13] More importantly, it is driven by electric power, which can be attained with renewable energy sources such as solar power, wind power, and so on without any additional CO_2 generation.[14] However, developing electrocatalysts with high activity, selectivity and stability is the key for this process.

In recent years, various electrocatalysts such as Sn,[15] Bi,[16] Pb[17] and Pd[18] based ones have been developed for the reduction of CO_2 to HCOOH. Among them, tin-based catalysts are the most widely studied ones because of their high activity, high selectivity and economical and environmentally friendly feature. To date, various preparation

methods such as hydrothermal,[19] electrodeposition,[20] and atomic layer deposition[2] have been applied to fabricate different tin-based electrocatalysts coated electrodes. Direct electrodeposition of catalysts on the substrate can not only avoid the using of a binder (e.g., Nafion), which always causes a complex electrode preparation process and unstable electrode interface,[21] but also obtain various microstructures by tuning the electrodeposition conditions. In our group, a unipolar pulse electro-deposition (UPED) method was developed for the preparation of various functional electrodes with excellent performance in electrochemically switched ion exchange (ESIX) process,[22] supercapacitor,[23] and water electrolysis.[24] It is found that the microstructure of materials prepared by the UPED method are different from those by other common methods such as potentiostatic, galvanostatic and cyclic voltammetry (CV), and in general, the different resulting microstructures or surface morphologies often lead to different catalytic properties. To date, Tin-based electrocatalysts were usually prepared by a galvanostatic deposition method,[20, 25-26] and the obtained tin particles usually had large and non-uniform sizes, which tended to exhibit unsatisfactory catalytic performance or stability.

Moreover, the tin-based catalysts always have different compositions, such as Sn,[27] SnO,[28] SnO_2[15] and SnS_2,[29] which also exhibit different activity and selectivity. Kanan *et al.* compared the performances of the clean tin surface and the SnO_x/Sn thin-film catalyst for the electrochemical reduction of CO_2, and found that the SnO_x/Sn electrode exhibited highly enhanced activity.[30] Qiao *et al.* developed a hybrid electrode composed of SnO and SnO_2, which showed a much higher selectivity towards formate than the pure SnO_2 based one.[19] Since the reduction potential of tin oxide is more positive than the CO_2 reduction potential to HCOOH, partial tin oxides (or sulfide) will be inevitably reduced to metal tin during the electrochemical process, resulting in the formation of metal oxide

and metal interfaces.[31] Moreover, in these interfaces, different valence states of tin (Sn^0, Sn^{2+}, and Sn^{4+}) may exist together so that it is particularly difficult to study the mechanism from an experimental perspective. To the best of our knowledge, the specific impact mechanism of these coexisting species still remains unclear, especially for the different surface tin valence states or the metal oxide/metal composite interfaces.

Herein, three electrodeposition methods, i.e., potentiostatic deposition, galvanostatic deposition and UPED methods, were used to prepare tin-based electrocatalysts for the selective reduction of CO_2 to HCOOH. The experimental results showed that all the electrocatalysts prepared by these different methods resulted in different surface oxide species distributions, which made them exhibit different catalytic properties. To understand the mechanism, the density functional theory (DFT) calculation was used to systematically study the effect of different surface oxide species on the catalytic performance.

3.2 Methods

3.2.1 Preparation of Sn electrodes

As the substrate, carbon paper (CP, 1×1 cm^2) was pretreated by ultrasonic bath with sulfuric acid, water and ethanol for 20 minutes to improve its hydrophilicity.[32] The electrolyte for the preparation of the Sn-based electrocatalysts was 0.018 mol L^{-1} $SnCl_2$ dissolved in 0.05 mol L^{-1} sodium citrate ($Na_3C_6H_5O_7$) solution (pH was adjusted to 6 with H_2SO_4). All electrodes prepared in this study used a three-electrode system controlled by an electrochemical workstation (Princeton, Versa STAT 4 USA) with VersaStudio software. Platinum wire (ALS, Japan), Ag/AgCl/saturated KCl reference (ALS, Japan) and CP (Toray Industries Inc., Japan) were applied as the counter electrode, reference electrode and working electrode, respectively. After the electrodeposition, the electrode

obtained was washed completely by distilled water and then dried in a 40 ºC oven for 12 hours. For the UPED method, the pulse current with an applied potential of -1.0 V, on-time and off-time of 1.0 s was applied to the CP support immersed in the electrolyte. For comparison, the potentiostatic and galvanostatic deposition methods were also used for the preparation of electrodes. Moreover, in order to control the tin deposition amount for comparison, the deposition charge of 1 C was controlled for all three methods, and the final mass loading amount determined by weighing was about 0.6 mg, which is consistent with theoretical electrodeposition mass amount calculated by the reaction equation ($Sn^{2+}+2e^{-} = Sn$).

3.2.2 Physical characterizations

The morphology and microstructure of the obtained Sn/CP were detected by a scanning electron microscope (SEM, Hitachi SU8010), and the nanostructure was analyzed with a JEM-2100F transmission electron microscope (TEM, JEOL, Japan). The crystal structures of various electrodes before and after electrocatalysis were determined by X-ray diffraction (XRD, Rigaku SmartLab X-Ray Diffractometer) using a Cu-Kα (λ=1.5405 Å) radiation source. The surface compositions and valence states of catalyst before and after the electrocatalysis were characterized by using X-ray photoelectron spectroscopy (XPS) (Thermo ESCALAB 250XI).

3.2.3 Electrochemical characterizations

Electrochemical performance was characterized by the linear sweep voltammetry (LSV), cyclic voltammetry (CV), electrochemical impedance spectroscopy (EIS) and constant potential electrolysis. All the electrochemical characterizations were measured by using a two-compartment electrochemical cell, in which the working and counter

electrodes were separated by a Nafion 117 membrane (Chemours, Japan). The obtained Sn/CP electrode with the geometric area of 1 cm^2 was used as the working electrode, and Ag/AgCl/saturated KCl and platinum wire (ALS, Japan) were applied as the reference and counter electrodes, respectively. All potentials and current densities present in this study were versus Ag/AgCl saturated KCl and geometric surface area (1×1 cm^2) of the CP immersed in the electrolyte respectively unless stated otherwise. All the working electrodes were pre-reduced before the electrochemical measurements at -1.6 V in 0.1 M CO_2-saturated $KHCO_3$ solution for 1 h, which is consistent with the method reported in the literatures.[33-35]

LSV was carried out in a potential range of 0 to -2 V at a scan rate of 10 mV s^{-1} in N_2 or CO_2-saturated 0.1 M $KHCO_3$ solution. CV was performed at 20, 40, 60 mV s^{-1} with a potential range from 0 to -2 V also in the N_2-saturated 0.1 M $KHCO_3$ solution. Electric double layer capacitance was determined by CV measurement at various scan rates (40, 80, 120, 160, 200 mV s^{-1}) from -0.81 to -0.71 V.

Constant potential EIS was performed within a frequency range of 0.01 Hz-0.1 MHz in a CO_2-saturated 0.1 M $KHCO_3$ solution at -1.1 V. Constant potential electrolysis was carried out for 1 h at various constant potentials (-1.5, -1.6, -1.7, -1.8, -1.9, -2.0 V) also in a CO_2-saturated 0.1 M $KHCO_3$ solution (pH 6.8). During this process, CO_2 was continuously purged into the reactor with a gas flow of 10 cm^3 min^{-1}. After finished, the gas and liquid products were collected for analysis.

3.2.4 DFT computational details

Table 3.1 Surface energies for various facets of Sn, SnO, and SnO_2 slab models.

Facet	Lattice spacing d(A)	Energy (Ha)	Surface energy (Ha)	Relative surface energy (Ha)
Bulk Sn		-144600.331		
2 0 0	2.915	-144600.060	0.135	0.000
1 0 1	2.792	-144599.952	0.189	0.054
2 2 0	2.061	-144599.875	0.228	0.093
2 1 1	2.016	-144599.707	0.312	0.177
3 0 1	1.658	-144599.573	0.379	0.244
Bulk SnO		-97603.414		
0 0 1	4.850	-97603.344	0.035	0.000
1 0 1	2.989	-97603.174	0.120	0.085
1 1 0	2.688	-97602.831	0.292	0.257
0 0 2	2.418	-97603.344	0.035	0.000
1 0 2	2.039	-97603.200	0.107	0.072
Bulk SnO2		-49403.696		
1 1 0	3.347	-49403.193	0.252	0.000
1 0 1	2.642	-49402.852	0.422	0.170
2 0 0	2.369	-49402.761	0.468	0.216
1 1 1	2.309	-49403.089	0.304	0.052
2 1 0	2.118	-49403.110	0.293	0.041

To understand the effect of tin oxide species on electrochemically catalytic reduction of CO_2, the Sn, SnO, and SnO_2 crystals were selected as the calculation model species in this study. In the calculations, the crystal surface of each species was artificially exposed by cleaving the basic crystal and building a vacuum slab of 15 Å. By comparing the surface energy of the first five low index crystal facets, it is found that the Sn (200), SnO (001), and SnO_2 (110) crystal facets had the lowest surface energy, which should be the most stable crystal facets and were selected for the further study (Table 3.1). For SnO_2, the (110) facet is the most stable surface, which has been also proved by many researchers.[36-38]. In addition, in order to study the metal oxide/metal interface, half of the

tin atoms on the Sn (200) facet were replaced by oxygen atoms according to the reported method.[31]

3.3 Results and discussion

3.3.1 Preparation and characterization of Sn/CP electrodes

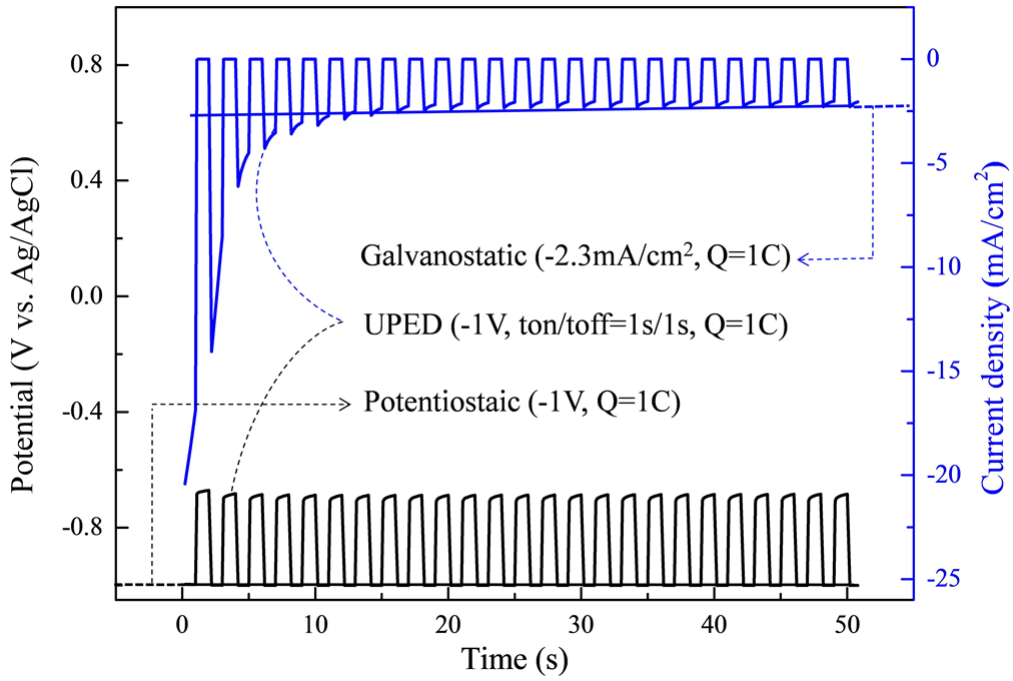

Figure 3.1 Potential-time (left) and current-time (right) transient curves in the initial 50 s during the UPED, potentiostatic and galvanostatic electrodoposition processes.

Figure 3.1 shows the curves of potential or current density versus time in three different electrodeposition methods. As a pulse method, UPED has the parameters of the on-time and off-time during the electrodeposition process. During the on-time period, the potential maintains a constant high potential, and the current increases sharply in a short time so that the crystal nucleus can be formed on the surface of the substrate. Then, the system is turned to the off-time period, the circuit becomes the open circuit state with the current density of 0 mA cm^{-2}, and the potential begins to decrease. In this case, Sn^{2+} near

the working electrode will be supplemented via ion diffusion, and the ion concentration around the electrode remains stable, which is benefit to the formation of uniform particles on the substrate. As comparison, in the potentiostatic method, the same potential (-1 V) as that in the UPED process was applied, and in the galvanostatic method, the same current density (-2.3 mA cm^{-2}) as the stabilized current in the UPED process. To control the amount of tin deposited on the CP, the deposition charge amount of 1 C was controllably adjusted for the three electrodeposition processes. As such, the electrodes were prepared and used for characterizations and performance testing.

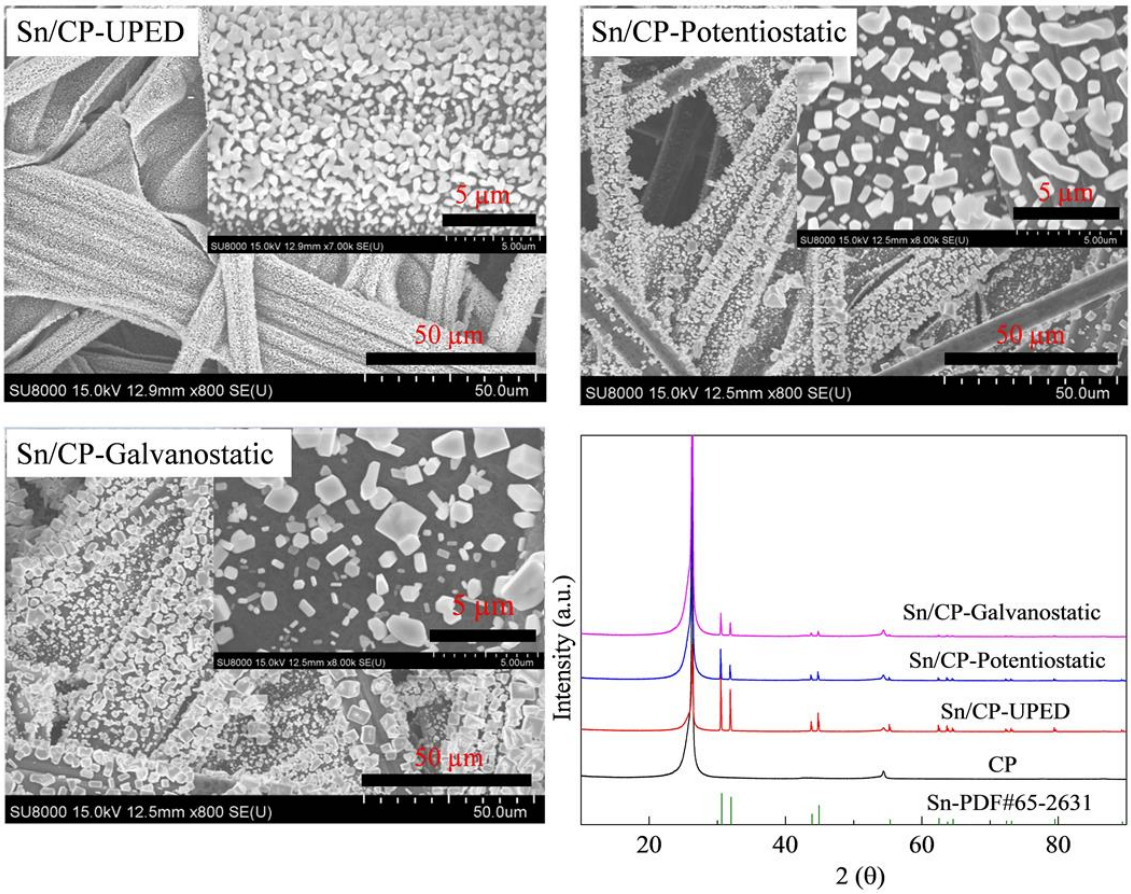

Figure 3.2 SEM images and XRD patterns of Sn/CP electrodes prepared using the three different electrodeposition methods.

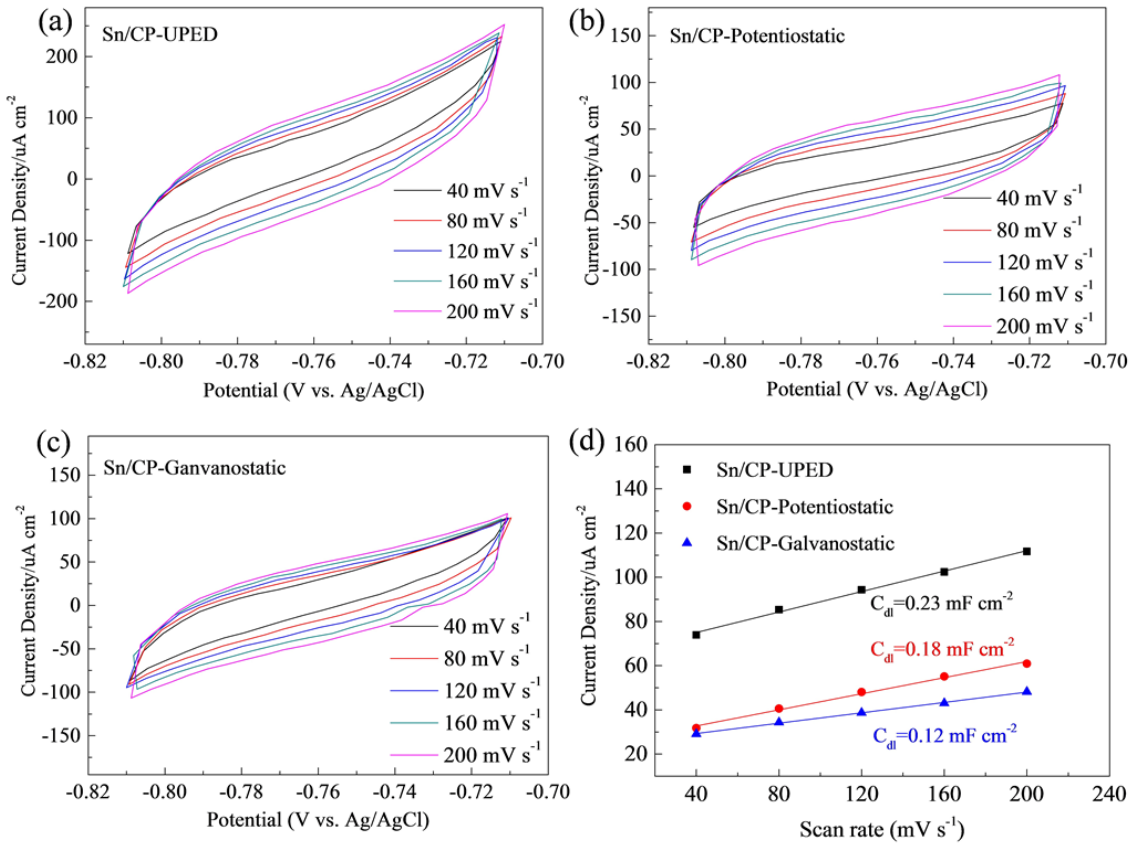

Figure 3.3 Determination of double layer capacitance over a range of scan rates from 40-200 mV s^{-1} for the three kinds of electrodes.

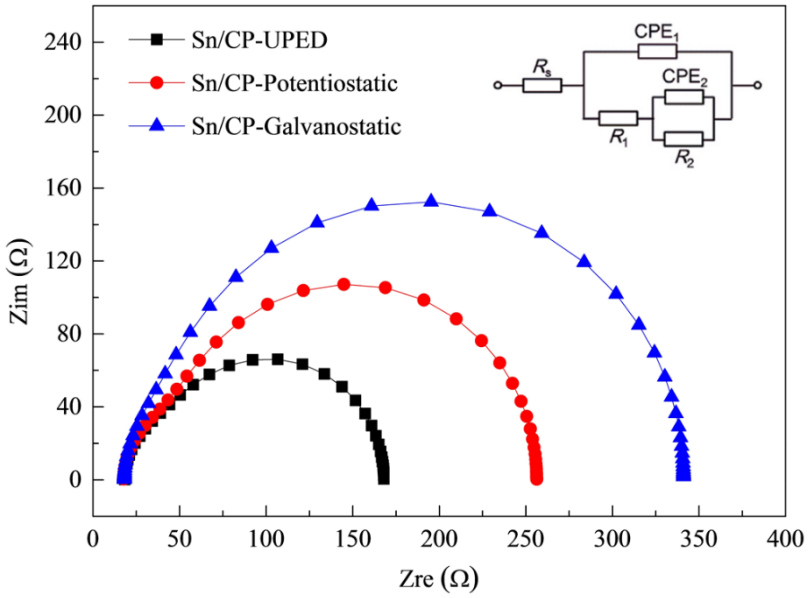

Figure 3.4 EIS on the three kinds of electrodes in CO_2 saturated 0.1 mol L^{-1} $KHCO_3$ solution.

As shown in Figure 3.2, comparing with other two electrodeposition methods, smaller and more uniform particles were well distributed on carbon fiber in CP when the UPED method was used. The electric double layer capacitance results (Figure 3.3) also identified that the obtained electrode by this method exposed larger electrochemically active surface area. In addition, the tight and uniform particle arrangement could be also conducive to the charge transfer, which was further confirmed by electrochemical impedance spectroscopy analysis test (Figure 3.4). It indicates that the UPED method is a better way to prepare tin-based electrocatalysts on the substrate. XRD results indicated that the main component in all the obtained tin-based electrocatalysts using different electrodeposition methods were the metal tin.

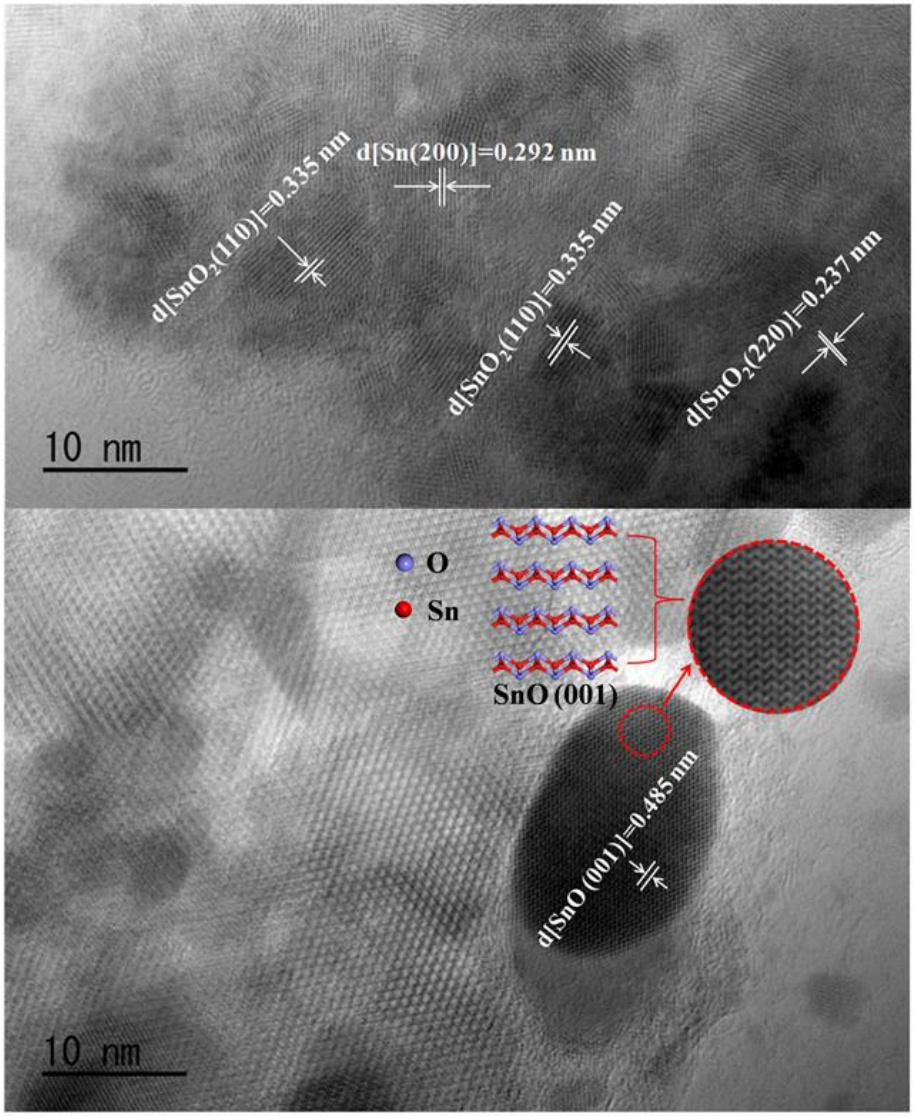

Figure 3.5 TEM images of Sn/CP-UPED electrode.

However, it is difficult to know the surface compositions in details by the XRD analysis. In general, a native tin oxide layer can be formed rapidly when the metal tin electrode is exposed to air.[31] Moreover, this tin oxide layer can maintain on the surface even after electrochemical reduction of CO_2 for a long time, which could affect the electrocatalytic process.[30, 34] In order to get more information on the surface composition, TEM images were obtained for the Sn/CP-UPED (Figure 3.5). A large number of lattice stripes were

observed, in which the maximum lattice spacing is 0.292 nm, belonging to the metal Sn (200) lattice plane (Table 3.1). Meanwhile, a large number of crystal lattice spacing larger than 0.292 nm, which are not belong to the metal tin, were also found in the TEM image. The lattice spacings of 0.237 and 0.335 nm correspond to the (220) and (110) plane of SnO_2, and that of 0.485 nm corresponds to the (001) plane of SnO (see Tables 3.1). Especially, the lattice shape of SnO (001) was M-shape, which is consistent with the shape of the SnO (001) surface obtained by the model used in the latter calculation. Therefore, there were abundant oxides species in fact existed on the surface of the tin electrode, which could have a significant influence on the CO_2 electrochemical reduction.

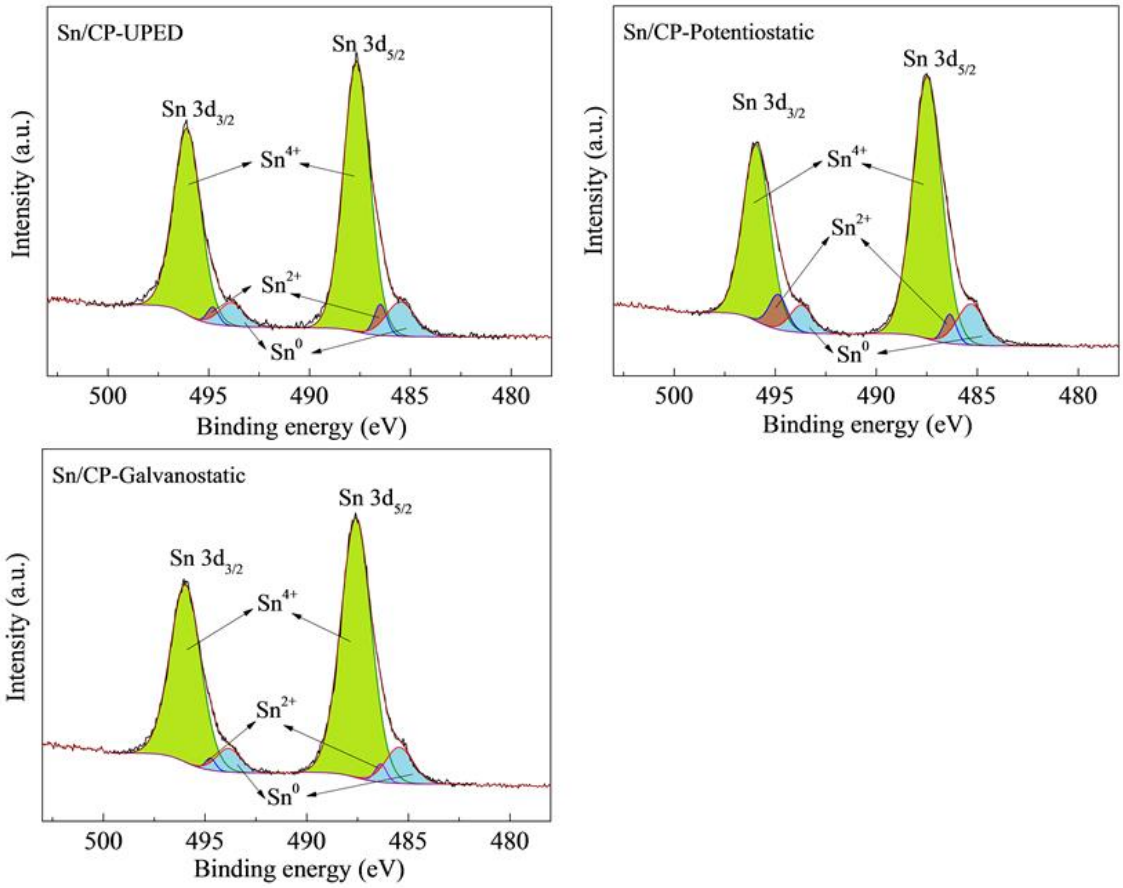

Figure 3.6 High-resolution Sn 3d XPS spectra of the three kinds of Sn/CP electrodes.

XPS analysis was also applied to obtain more information on the surface chemical compositions and the valence states for the Sn/CP electrodes. Figure 3.6 shows the Sn 3d XPS spectra for the three kinds of Sn/CP electrodes. It can be seen that the Sn $3d_{5/2}$ and Sn $3d_{3/2}$ spectra can be deconvoluted to three peak groups, which correspond to Sn^{4+}, Sn^{2+}, and Sn^{0}. As an example, the Sn 3d XPS spectrum of Sn/CP-UPED can be deconvoluted into speaks at 487.7, 496.1 (Sn^{4+}), 486.5, 494.8 (Sn^{2+}), 485.5 and 493.9 eV (Sn^{0}). For other two electrodes, a similar tendency was observed except for some negligible binding energy shifts. These observations are consistent with those reported elsewhere.[29] It is considered that the valence state of tin and content of different surface oxides species could affect the performance of electrochemical reduction of CO_2.

3.3.2 Electrochemical reduction of CO_2

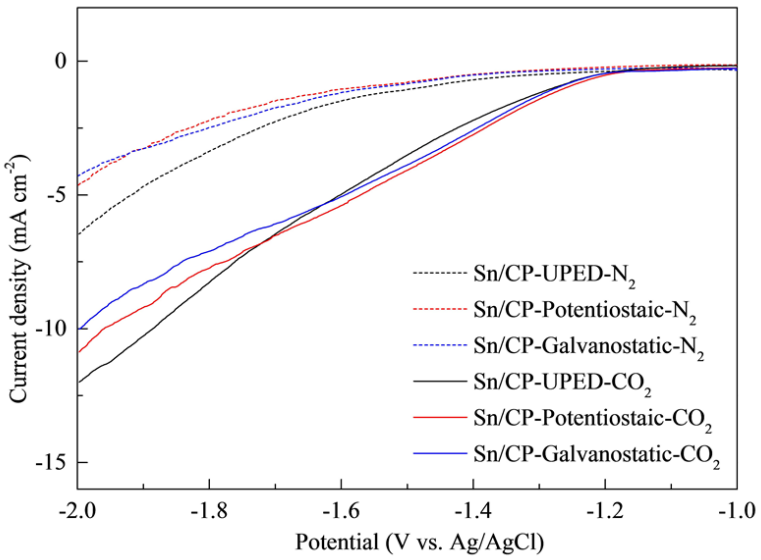

Figure 3.7 LSV curves of the three kinds of electrodes in the N_2-saturated (dash) or CO_2-saturated (solid) 0.1M $KHCO_3$ solutions at a scan rate of 5 mV s^{-1}.

In order to investigate the electrocatalytic performance of three kinds of electrodes,

LSVs were tested in the N_2-saturated and CO_2-saturated 0.1 M $KHCO_3$ solutions at first. As shown in Figure 3.7, Sn/CP electrodes exhibited more negative current density under the CO_2-saturated 0.1M $KHCO_3$ solution than that under the N_2-saturated one since the reductions of H_2O and CO_2 can occur simultaneously in the former condition but only H_2O can be reduced under the latter one. Moreover, comparing the performances of these three electrodes, the current density of the Sn/CP-UPED was slightly higher than those of the other two electrodes, which could be attributed to the larger electrochemically active surface area and smaller charge transfer resistance of this electrode (Figures 3.3 and 3.4).

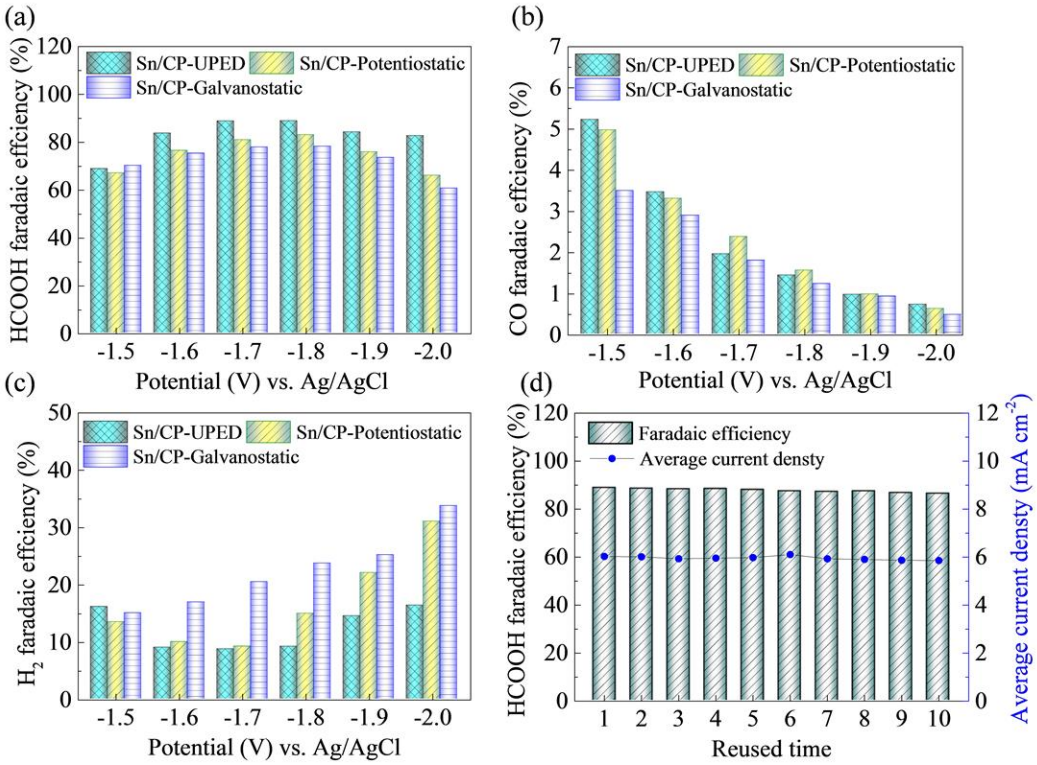

Figure 3.8 Variations of the faradaic efficiency for producing HCOOH (a), CO (b), H_2 (c) with the electrolysis potential on the three Sn/CP electrodes. (d) The stability test for Sn/CP-UPED electrode.

To further explore the selectivity of the three electrodes for the CO_2 reduction, the constant potential electrolysis was performed for 1 h at different potentials. The gas and liquid products were collected for analysis to calculate the faradaic efficiency. It is found that the total faradaic efficiency of HCOOH, CO and H_2 was close to 100%, indicating that almost no other byproducts were formed. Obviously, the Sn/CP-UPED electrode exhibited the best selectivity for the HCOOH formation, and the highest faraday efficiency reached 88.8% at the potentials of -1.7 V or -1.8 V. Generally, the Sn-based catalysts reported in the literature had the highest HCOOH faraday efficiency at -1.8 V.[25-27] However, in this work, the HCOOH faraday efficiency at -1.7 V was identical with that at -1.8 V for the Sn/CP-UPED electrode. Namely, the optimal reduction potential was reduced to some extent, which is favorable for the energy saving in a practical operation. Furthermore, the stability test indicated that the electrode prepared by the UPED method had no obvious performance degradation in 10 reused cycles, and the faraday efficiency still reached 86.4% (Figure 3.8d) at the last cycle testing.

3.3.3 Mechanism analysis

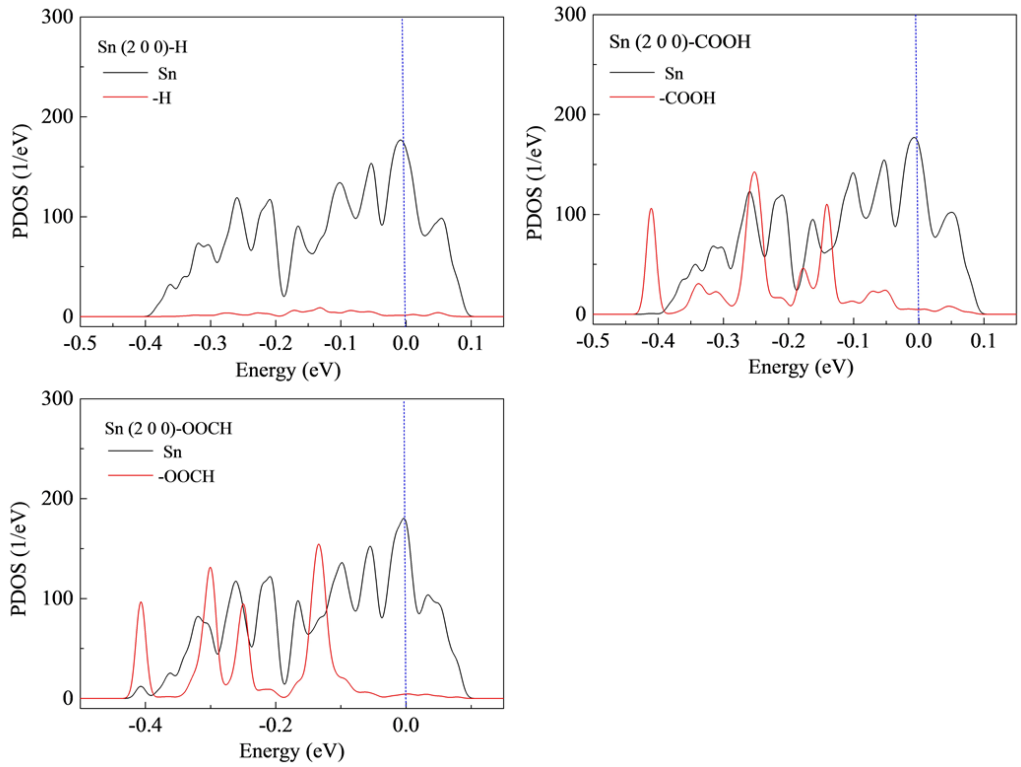

Figure 3.9 Calculated projected density of states of *H, *COOH, *OOCH species on Sn (200) facet.

Numerous experimental studies have already indicated that the surface oxides species could affect the catalytic performance of any tin-based electrocatalysts.[27, 30, 39] However, the specific mechanism still remains unclear.[31] In order to gain a clearer understanding, four special crystal facets were separately established to study their catalytic activity by the DFT calculation. For the tin-based electrocatalysts, the following reaction steps for the reduction CO_2 to HCOOH and CO have been widely accepted.[2, 40]

HCOOH formation:

$$CO_2 + H^+ + e^- + * \rightarrow *OOCH \quad (3\text{-}1)$$

$$*OOCH + H^+ + e^- \rightarrow * + HCOOH \quad (3\text{-}2)$$

$$CO_2 + H^+ + e^- + * \rightarrow *COOH \quad (3\text{-}4)$$

$$*COOH + H^+ + e^- \rightarrow * + HCOOH \quad (3\text{-}4)$$

CO formation:

$$CO_2 + H^+ + e^- + * \rightarrow *COOH \quad (3\text{-}5)$$

$$*COOH + H^+ + e^- \rightarrow * + CO + H_2O \quad (3\text{-}6)$$

H_2 formation (side reactions)

$$H^+ + e^- + * \rightarrow *H \quad (3\text{-}7)$$

$$*H + H^+ + e^- \rightarrow * + H_2 \quad (3\text{-}8)$$

Essentially, a highly selective catalyst requires strong intermediate binding but a weak product adsorption, ensuring that it possesses the capability of immobilizing intermediate but loosening products at the same time.[34] Thus, we firstly examined the adsorption energy of OOCH, COOH, HCOOH CO and H_2O on the Sn (200) facet. As a result, the metal tin exhibited strong bindings to OOCH and COOH intermediates (-2.84, -1.72 eV, respectively) but weak bindings to HCOOH, CO and H_2O (-0.21, -0.15, -0.15 eV, respectively). This makes it easier to bond with the OOCH and COOH intermediates but loose HCOOH and CO at the same time, thereby exhibiting excellent catalytic activity and selectivity for the reduction of CO_2 to HCOOH and CO. The projected density of states (PDOS) calculation results indicate that the tin atoms can strongly hybridize with the adsorbed *COOH and *OOCH species below the Fermi level (Figure 3.9). Meanwhile, we compared the adsorption energies of different tin oxides species when binding with different intermediates, it is found that the SnO_2 (110) facet had the strongest binding ability to OOCH with the adsorption energy of -3.12 eV. Liu's work[19] also indicated that SnO_x with a valence of +4 can play an essential role in the CO_2 electroreduction process.

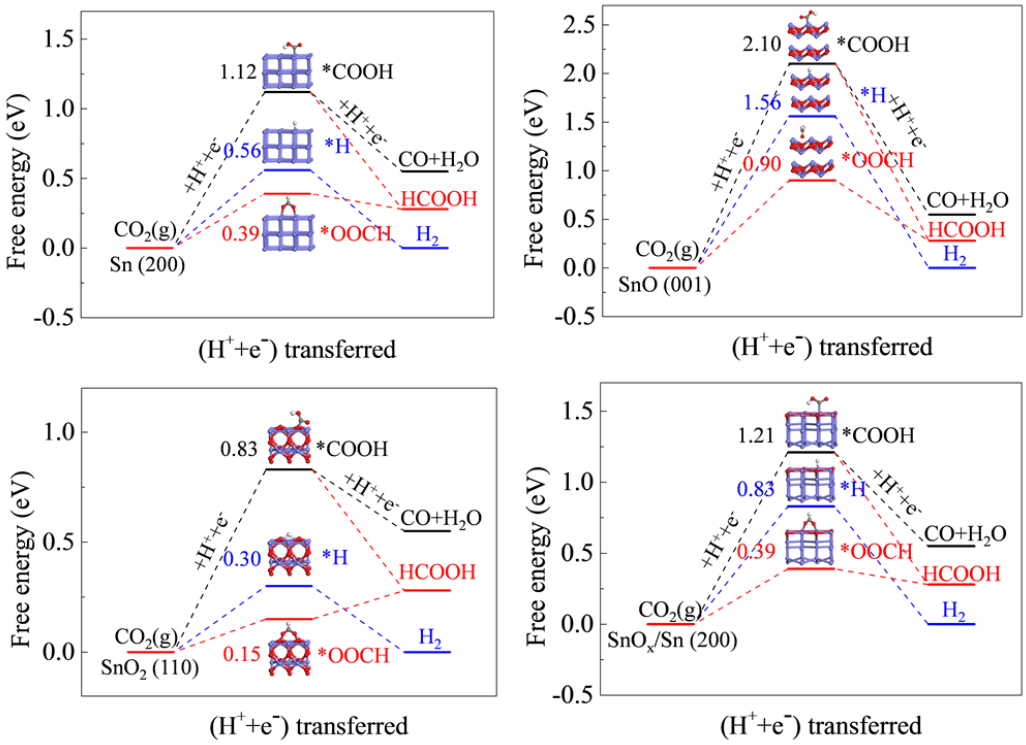

Figure 3.10 Calculated free energy diagram for electroreduction of CO_2 to HCOOH, CO and H_2 on the different facets of the tin species: (a) Sn (200), (b) SnO (001), (c) SnO_2 (110) and (d) SnO_x/Sn (200).

In order to get a clearer understanding of the free energy changes in each step of the catalytic process, free energies for CO_2 electroreduction to HCOOH, CO and H_2 on the different tin oxide species facets were calculated. The calculated free energies of CO + H_2O and HCOOH relative to the initial state were 0.55 eV and 0.28 eV, respectively, which were similar to the results reported in the literature.[45] As shown in Figure 3.10, all four facets showed lower free energy barriers in the formation of HCOOH. In this study, it is found that the order of free energy barrier was consistent with the product selectivity order. A similar order was also found in the DFT calculations for the Sn (100) surface in the literature.[2] Compared with the pure metal tin, the energy barriers of intermediates for

the formations of three products on the SnO (001) facet were significantly increased, which are corresponding to the increases of overpotentials in CO_2 electroreduction processes. Therefore, the presence of divalent tin may lead to the increase of the overpotential of CO_2 reduction. However, as can be seen from the degree of increase, the energy barriers for H_2 and CO generations were increased by nearly 1.0 eV, which are much higher than the 0.5 eV for HCOOH on the Sn (200) facet. Usually, the distribution of different products can be estimated by their free energy differences according to the thermodynamic formula of exp[- ($\Delta G/RT$)].[41] Therefore, the presence of divalent tin (Sn^{2+}) on the surfaces of tin-based electrocatalysts could increase the HCOOH faraday efficiency. For the SnO_2 (110) facet, the energy barriers for the three products were reduced, and the decrease degree had no much different. Therefore, the presence of tetravalent tin (Sn^{4+}) on the surface could reduce the overpotential of CO_2 reduction to HCOOH.

In the actual CO_2 electrochemical reduction process, because the reduction potential of tin oxide is more positive than the CO_2 reduction potential, the tin-based catalyst cannot be maintained in the form of pure SnO or SnO_2. That is to say, a part of tin oxide could be reduced to metal tin so that only the remained part of divalent or tetravalent tin will exist on the surface to form the metal oxide/metal interfaces.[31, 42] For the sake of investigation of the interface effect on the catalytic performance, an interface model was established based the method reported in the literature.[31] The calculation results for the SnO_x/Sn (200) interface showed that the existence of the interface mainly increased the energy barrier for H_2 generation but had only a little effect on the formations of CO and HCOOH. Thusly, such metal oxide/metal interfaces can increase the HCOOH faraday efficiency by suppressing H_2 generation.

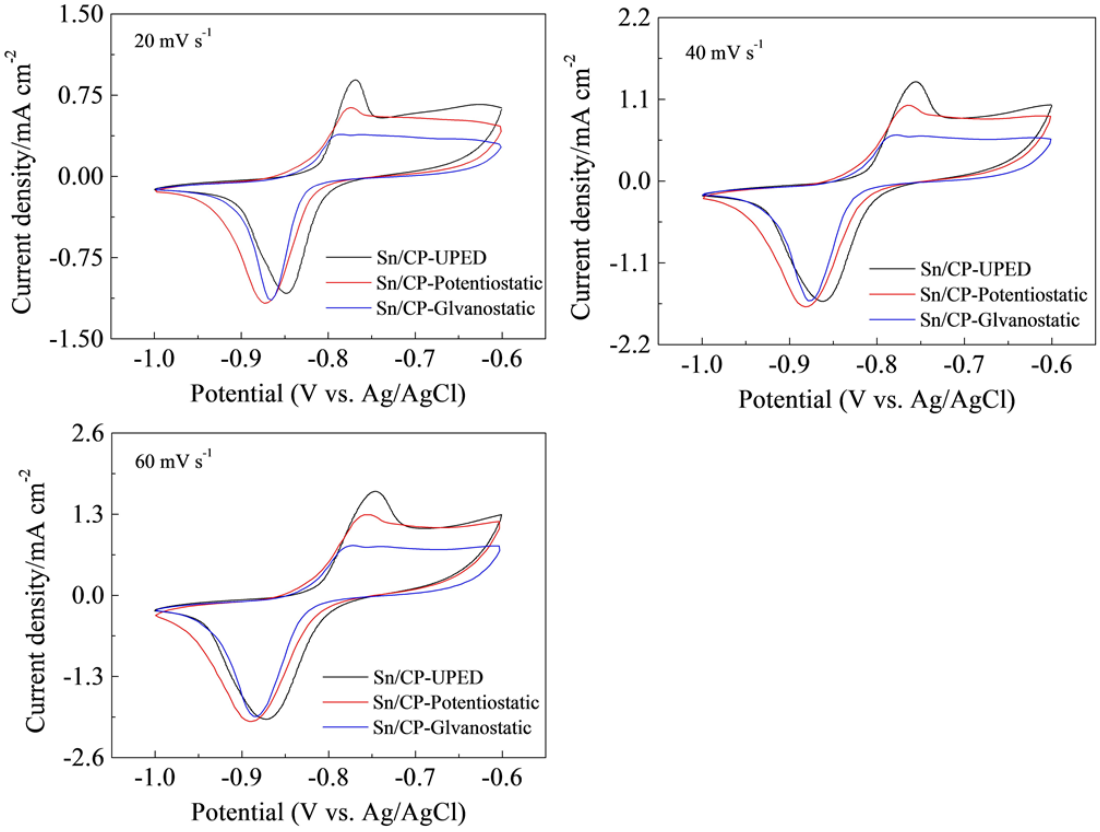

Figure 3.11 CV curves of the three kinds of Sn/CP electrodes in the N_2-saturated 0.1 M $KHCO_3$ solution at 20, 40 and 60 mV s^{-1}.

In this study, the Sn/CP-UPED electrode showed the best catalytic performance for HCOOH generation. It is also possible that different tin oxide species distributed on the surface. Based on the above calculation results, the Sn^{4+} may lead to an increase of the overpotential but with an improvement of the HCOOH faradaic efficiency and meanwhile, the Sn^{2+} can reduce the overpotential. Herein, it is considered that a suitable ratio of Sn^0 : Sn^{2+} : Sn^{4+} on the surface of the electrode could result in a synergy effect among them, especially between the Sn^{2+} and Sn^{4+} species since the interface of tin oxides/tin could suppress the evolution of H_2 but no obvious effects on the formations of HCOOH and CO. In the actual CO_2 catalytic electroreduction process, the oxide species on the

electrode surface will be reconstituted. Therefore, CV was performed between -0.6 and -1 V to analyze the surface oxide species in the $KHCO_3$ solution. It is found that a larger oxidation peak current but almost the same reduction current appeared for the Sn/CP-UPED electrode worked under the same conditions (20, 40 and 60 mV s^{-1} shown in Figure 3.11). It identifies that some metal tin on its surface was more easily oxidized to tin oxides, resulting in the formation of more tin oxide/metal tin interfaces, which should be beneficial for the increase of HCOOH faraday efficiency for the tin-based catalyst.

3.4 Conclusions

In this work, tin-based catalysts coated electrodes were fabricated using three different electrodeposition methods for the electrochemical reduction of CO_2 to HCOOH. It is found that the electrode prepared with the UPED method exhibited better catalytic performance than the other two. Physical and electrochemical characterizations indicated that the Sn/CP-UPED electrocatalyst composed of smaller and more uniform particles with larger electrochemically active surface area, smaller charge transfer resistance and proper ratio of surface oxides species. Furthermore, the effects of different surface oxides species on the catalytic performance were investigated by DFT calculations. It is found that the presence of Sn^{4+} can effectively reduce the overpotential of CO_2 reduction while the presence of Sn^{2+} can improve the selectivity towards HCOOH formation. In addition, the formation of SnO_x/Sn interface can suppress the side reactions (i.e., generation of H_2), thereby improving the catalytic efficiency in the CO_2 reduction. Based on our experimental and DFT calculation results, it can be concluded that the actual CO_2 reduction catalytic process is synergistically controlled by the complex surface oxides species, which plays a key role in the electroreduction of CO_2 process.

References

1. Hansen J.; Johnson D.; Lacis A.; Lebedeff S.; Lee P.; Rind D.; Russell G. Climate impact of increasing atmospheric carbon dioxide. *Science* **1981,** *213* (4511), 957-966.
2. Zheng, X.; De Luna, P.; García de Arquer, F. P.; Zhang, B.; Becknell, N.; Ross, M. B.; Li, Y.; Banis, M. N.; Li, Y.; Liu, M.; Voznyy, O.; Dinh, C. T.; Zhuang, T.; Stadler, P.; Cui, Y.; Du, X.; Yang, P.; Sargent, E. H., Sulfur-modulated tin sites enable highly selective electrochemical reduction of CO_2 to formate. *Joule* **2017,** *1* (4), 794-805.
3. Gao, S.; Sun, Z.; Liu, W.; Jiao, X.; Zu, X.; Hu, Q.; Sun, Y.; Yao, T.; Zhang, W.; Wei, S.; Xie, Y., Atomic layer confined vacancies for atomic-level insights into carbon dioxide electroreduction. Nat. Commun. **2017**, *8*, 14503.
4. Han, N.; Wang, Y.; Ma, L.; Wen, J.; Li, J.; Zheng, H.; Nie, K.; Wang, X.; Zhao, F.; Li, Y.; Fan, J.; Zhong, J.; Wu, T.; Miller, D. J.; Lu, J.; Lee, S.-T.; Li, Y., Supported cobalt polyphthalocyanine for high-performance electrocatalytic CO_2 reduction. Chem **2017**, *3* (4), 652-664.
5. Li, J.; Chen, G.; Zhu, Y.; Liang, Z.; Pei, A.; Wu, C. L.; Wang, H.; Lee, H. R.; Liu, K.; Chu, S.; Cui, Y., Efficient electrocatalytic CO_2 reduction on a three-phase interface. Nat. Catal. **2018**, *1* (8), 592-600.
6. Liu, X.; Yang, H.; He, J.; Liu, H.; Song, L.; Li, L.; Luo, J., Highly active, durable ultrathin $MoTe_2$ layers for the electroreduction of CO_2 to CH_4. Small **2018**, *14* (16), 1704049.
7. Sun, X.; Kang, X.; Zhu, Q.; Ma, J.; Yang, G.; Liu, Z.; Han, B., Very highly efficient reduction of CO_2 to CH_4 using metal-free N-doped carbon electrodes. *Chem. Sci.* **2016,** *7* (4), 2883-2887.
8. Sun, X.; Zhu, Q.; Kang, X.; Liu, H.; Qian, Q.; Zhang, Z.; Han, B., Molybdenum-bismuth bimetallic chalcogenide nanosheets for highly efficient electrocatalytic reduction of carbon dioxide to methanol. *Angew. Chem. Int. Ed.* **2016,** *55* (23), 6771-6775.
9. Lu, L.; Sun, X. F.; Ma, J.; Yang, D. X.; Wu, H. H.; Zhang, B. X.; Zhang, J. L.; Han, B. X., Highly efficient electroreduction of CO_2 to methanol on palladium-copper bimetallic aerogels. *Angew. Chem. Int. Ed.* **2018,** *57* (43), 14149-14153.
10. Liu, Y.; Zhang, Y.; Cheng, K.; Quan, X.; Fan, X.; Su, Y.; Chen, S.; Zhao, H.; Zhang, Y.; Yu, H.; Hoffmann, M. R., Selective Electrochemical reduction of carbon dioxide to ethanol on a boron- and nitrogen-Co-doped nanodiamond. *Angew. Chem. Int. Ed. Engl.* **2017,** *56* (49), 15607-15611.
11. Song, Y.; Peng, R.; Hensley, D. K.; Bonnesen, P. V.; Liang, L.; Wu, Z.; Meyer, H. M.; Chi, M.; Ma, C.; Sumpter, B. G.; Rondinone, A. J., High-selectivity

electrochemical conversion of CO_2 to ethanol using a copper nanoparticle/N-doped graphene electrode. *ChemistrySelect* **2016,** *1* (19), 6055-6061.

12. Verma, S.; Kim, B.; Jhong, H. R. M.; Ma, S.; Kenis, P. J., A gross-margin model for defining technoeconomic benchmarks in the electroreduction of CO_2. *ChemSusChem* **2016,** *9* (15), 1972-1979.
13. Costentin, C.; Robert, M.; Savéant, J.-M., Catalysis of the electrochemical reduction of carbon dioxide. *Chem. Soc. Rev.* **2013,** *42* (6), 2423-2436.
14. Zhang, W.; Hu, Y.; Ma, L.; Zhu, G.; Wang, Y.; Xue, X.; Chen, R.; Yang, S.; Jin, Z., Progress and perspective of electrocatalytic CO_2 reduction for renewable carbonaceous fuels and chemicals. *Adv. Sci.* **2018,** *5* (1), 1700275.
15. Fan, L.; Xia, Z.; Xu, M.; Lu, Y.; Li, Z., 1D SnO2 with wire-in-tube architectures for highly selective electrochemical reduction of CO_2 to C1 products. *Adv. Funct. Mater.* **2018,** *28* (17), 1706289.
16. Su, P.; Xu, W.; Qiu, Y.; Zhang, T.; Li, X.; Zhang, H., Ultrathin bismuth nanosheets as highly efficient electrocatalyst for CO_2 reduction. *ChemSusChem* **2018,** *11* (5), 848-853.
17. Yadav, V. S. K.; Purkait, M. K., Synthesis of Pb_2O electrocatalyst and its application in the electrochemical reduction of CO_2 to HCOOH in various electrolytes. *RSC Adv.* **2015,** *5* (50), 40414-40421.
18. Jiang, B.; Zhang, X. G.; Jiang, K.; Wu, D. Y.; Cai, W. B., Boosting formate production in electrocatalytic CO_2 reduction over wide potential window on Pd Surfaces. *J. Am. Chem. Soc.* **2018,** *140* (8), 2880-2889.
19. Li, Y.; Qiao, J.; Zhang, X.; Lei, T.; Girma, A.; Liu, Y.; Zhang, J., Rational design and synthesis of SnO_x electrocatalysts with coralline structure for highly improved aqueous CO_2 reduction to formate. *ChemElectroChem* **2016,** *3* (10), 1618-1628.
20. Zhao, C.; Wang, J., Electrochemical reduction of CO_2 to formate in aqueous solution using electro-deposited Sn catalysts. *Chem. Eng. J.* **2016,** *293*, 161-170.
21. Li, S.; Sirisomboonchai, S.; Yoshida, A.; An, X.; Hao, X.; Abudula, A.; Guan, G., Bifunctional CoNi/$CoFe_2O_4$/Ni foam electrodes for efficient overall water splitting at a high current density. *J. Mater. Chem. A* **2018,** *6* (39), 19221-19230.
22. Du, X.; Guan, G.; Li, X.; Jagadale, A. D.; Ma, X.; Wang, Z.; Hao, X.; Abudula, A., A novel electroactive λ-MnO_2/PPy/PSS core-shell nanorod coated electrode for selective recovery of lithium ions at low concentration. *J. Mater. Chem. A* **2016,** *4* (36), 13989-13996.
23. Wang, X.; Li, X.; Du, X.; Ma, X.; Hao, X.; Xue, C.; Zhu, H.; Li, S., Controllable synthesis of NiCo LDH nanosheets for fabrication of high-performance

supercapacitor electrodes. *Electroanalysis* **2017,** *29* (5), 1286-1293.

24. Li, X.; Li, C.; Yoshida, A.; Hao, X.; Zuo, Z.; Wang, Z.; Abudula, A.; Guan, G., Facile fabrication of CuO microcube@ Fe-Co_3O_4 nanosheet array as a high-performance electrocatalyst for the oxygen evolution reaction. *J. Mater. Chem. A* **2017,** *5* (41), 21740-21749.
25. Wang, Y.; Zhou, J.; Lv, W.; Fang, H.; Wang, W., Electrochemical reduction of CO_2 to formate catalyzed by electroplated tin coating on copper foam. *Appl. Surf. Sci.* **2016,** *362*, 394-398.
26. Lv, W.; Zhou, J.; Kong, F.; Fang, H.; Wang, W., Porous tin-based film deposited on copper foil for electrochemical reduction of carbon dioxide to formate. *Int. J. Hydrogen Energy* **2016,** *41* (3), 1585-1591.
27. Lv, W.; Zhang, R.; Gao, P.; Lei, L., Studies on the faradaic efficiency for electrochemical reduction of carbon dioxide to formate on tin electrode. *J. Power Sources* **2014,** *253*, 276-281.
28. Gu, J.; Héroguel, F.; Luterbacher, J.; Hu, X., Densely Packed, Ultra small SnO nanoparticles for enhanced activity and selectivity in electrochemical CO_2 reduction. *Angew. Chem.* **2018,** *130* (11), 2993-2997.
29. Li, F.; Chen, L.; Xue, M.; Williams, T.; Zhang, Y.; MacFarlane, D. R.; Zhang, J., Towards a better Sn: Efficient electrocatalytic reduction of CO_2 to formate by Sn/SnS_2 derived from SnS_2 nanosheets. *Nano Energy* **2017,** *31*, 270-277.
30. Chen, Y.; Kanan, M. W., Tin oxide dependence of the CO_2 reduction efficiency on tin electrodes and enhanced activity for tin/tin oxide thin-film catalysts. *J. Am. Chem. Soc.* **2012,** *134* (4), 1986-1989.
31. Cui, C.; Han, J.; Zhu, X.; Liu, X.; Wang, H.; Mei, D.; Ge, Q., Promotional effect of surface hydroxyls on electrochemical reduction of CO_2 over SnO_x/Sn electrode. *J. Catal.* **2016,** *343*, 257-265.
32. Li, X.; Du, X.; Ma, X.; Wang, Z.; Hao, X.; Abudula, A.; Yoshida, A.; Guan, G., CuO nanowire@Co_3O_4 ultrathin nanosheet core-shell arrays: An effective catalyst for oxygen evolution reaction. *Electrochim. Acta* **2017,** *250*, 77-83.
33. Luc, W.; Collins, C.; Wang, S.; Xin, H.; He, K.; Kang, Y.; Jiao, F., Ag-Sn bimetallic catalyst with a core-shell structure for CO_2 reduction. *J. Am. Chem. Soc.* **2017,** *139* (5), 1885-1893.
34. Zhang, S.; Kang, P.; Meyer, T. J., Nanostructured tin catalysts for selective electrochemical reduction of carbon dioxide to formate. *J. Am. Chem. Soc.* **2014,** *136* (5), 1734-7.
35. Wen, G.; Lee, D. U.; Ren, B.; Hassan, F. M.; Jiang, G.; Cano, Z. P.; Gostick, J.;

Croiset, E.; Bai, Z.; Yang, L.; Chen, Z., Orbital Interactions in Bi-Sn bimetallic electrocatalysts for highly selective electrochemical CO_2 reduction toward formate production. *Adv. Energy. Mater.* **2018,** *8* (31), 1802427.

36. Oviedo, J.; Gillan, M., Energetics and structure of stoichiometric SnO_2 surfaces studied by first-principles calculations. *Surf. Sci.* **2000,** *463* (2), 93-101.
37. Cheng, B.; Russell, J. M.; Shi, W.; Zhang, L.; Samulski, E. T., Large-scale, solution-phase growth of single-crystalline SnO_2 nanorods. *J. Am. Chem. Soc.* **2004,** *126* (19), 5972-5973.
38. Henrich, V. E.; Cox, P. A., The surface science of metal oxides. Cambridge university press, **1996**, pp 398-400.
39. Won da, H.; Choi, C. H.; Chung, J.; Chung, M. W.; Kim, E. H.; Woo, S. I., Rational Design of a hierarchical tin dendrite electrode for efficient electrochemical reduction of CO_2. *ChemSusChem* **2015,** *8* (18), 3092-3098.
40. Feaster, J. T.; Shi, C.; Cave, E. R.; Hatsukade, T.; Abram, D. N.; Kuhl, K. P.; Hahn, C.; Nørskov, J. K.; Jaramillo, T. F., Understanding selectivity for the electrochemical reduction of carbon dioxide to formic acid and carbon monoxide on metal electrodes. *ACS Catal.* **2017,** *7* (7), 4822-4827.
41. Liu, Y.; Zhao, J.; Cai, Q., Pyrrolic-nitrogen doped graphene: a metal-free electrocatalyst with high efficiency and selectivity for the reduction of carbon dioxide to formic acid: a computational study. *Phys. Chem. Chem. Phys.* **2016,** *18* (7), 5491-5498.
42. Díaz, R.; Díez-Pérez, I.; Gorostiza, P.; Sanz, F.; Morante, J. R., An electrochemical study of tin oxide thin film in borate buffer solutions. *J. Braz. Chem. Soc.* **2003,** *14* (4), 523-529.

Chapter 4 Bi-doped SnO nanosheets supported on Cu foam for electrochemical reduction of CO_2 to HCOOH

4.1 Introduction

In recent years, conversion of carbon dioxide (CO_2) to high-value-added chemicals has attracted widespread attention due to its important impact on the environment and energy.[1] As a method for the energy conversion and storage, the electrochemical reduction of CO_2 can not only reduce the damage to the environment by utilizing excessive emission of greenhouse effective CO_2, but also can convert unstable renewable energy such as solar and wind energies into stable chemical energy for the storage.[2] As one of the high-value-added chemicals by CO_2 electroreduction, formic acid (HCOOH) is an important product since it is widely used as the feedstock for the industrial synthesis in the fields such as dye and leather industries.[3] In addition, HCOOH can also be used as one of the centres in energy conversion and storage since it can be conveniently and efficiently converted to H_2 or CO.[4-5] Compared with the routes in the conversion of CO_2 to other high-value-added chemicals, the electrochemical reduction of CO_2 to HCOOH is a prone two-electron transfer reaction with high electron utilization efficiency, which is recognized as an economically viable way.[6]

Electrocatalyst is the core of electrochemical reduction of CO_2 to HCOOH. Nowadays, the electrocatalysts with excellent activity are mainly metal-based catalysts such as Sn,[7-9] Bi,[10-13] Pb,[14-15] In,[16-17] Pd[18-19] and so on. Following the consideration of price and environmental friendliness, Sn and Bi-based electrocatalysts are the most promising ones for the large-scale CO_2 electroreduction to HCOOH.[20] Chen *et al.* found that the Bi-Sn

alloy catalysts exhibited higher catalytic activity than the metal tin alone because of the increased adsorption ability for *OOCH intermediate due to the changes in electron states.[20] Meanwhile, Cu, as an unique electrocatalyst, has been widely used in the electroreduction of CO_2 to methane (CH_4),[21-22] ethylene (C_2H_4),[23-24] methanol (CH_3OH),[25] ethanol (C_2H_5OH)[26-27] and other high-value-added chemicals. Although it has low selectivity to HCOOH, it is widely used as either substrate[28-29] or a component[30-32] of the electrocatalysts due to its excellent conductivity and unique catalytic properties. For example, Cui *et al.* found that incorporation of Cu into Sn could facilitate the transfer of electrons from Sn to Cu, which making Sn maintain in the positive oxidation states under the operating conditions, thus favoring the formate generation.[32] These studies suggest that different metal elements could work synergistically, leading to an enhanced catalytic activity.

The study of the electrocatalytic mechanism has great significance for the design and development of catalysts. Currently, it is generally considered that surface oxides could contribute to improve the selectivity towards HCOOH for the tin-based catalysts.[33-36] Through *in-situ* attenuated total reflectance infrared spectroscopy (ATR-IR) measurements, Bocarsly *et al.* found that even under reducing potentials, a metastable oxide layer could be formed on the tin-based cathodes during the CO_2 electroreduction.[37] Sargent *et al.* prepared a sulfur-modulated tin (Sn (S)) by an atomic layer deposition method for the electrochemical reduction of CO_2 to HCOOH. X-ray absorption near-edge structure (XANES) studies revealed that the excellent catalytic performance could be attributed to the higher oxidation states of tin in Sn (S) compared with that of tin in Sn nanoparticles.[8] In our previous studies, we found that the tin oxide/tin interface had a positive impact on inhibiting hydrogen evolution, and divalent Sn^{2+} had a higher

selectivity towards HCOOH than Sn^{4+} and Sn^0 through the DFT calculation.[38] Therefore, for a tin-based catalyst, maintaining its surface tin in a positive oxidation state by suitable structural design should be an effective strategy to increase its catalytic activity and selectivity. In general, the monometallic tin based catalysts always have an unsatisfactory ability to maintain the surface positive valence at a negative reduction potential, which makes it still facing the problems of low efficiency and poor stability in the practical application. Therefore, it is an urgent demand to design high-performance catalysts by properly regulating the structure and surface state of the tin-based catalyst through the assistance of other elements. To date, the researches on the effect of doping or compounding with additional elements and the influence of the substrate on the performances are still insufficient yet. For example, most of the current researches on metal doped tin oxides focused on the SnO_2, such as Bi doped SnO_2,[39] Sb doped SnO_2,[40] and Mn doped SnO_2,[41] and only a few studies on the aspects of metal doped SnO. In addition, although Cu foam substrate was used in many studies,[28-29] the effect of the Cu substrate on the catalysis performance was not investigated.

Herein, based on the research results of the previous chapter, to further increase the selectivity and current density of HCOOH production, Bi-doped SnO nanosheets were designed and grown on Cu foam by a one-step hydrothermal synthesis method and applied for the CO_2 electroreduction to HCOOH. It was found that Bi doping increased the selectivity to HCOOH when compared to the pure SnO catalyst, and the Cu foam as a substrate also played a positive role in catalysis. Besides the common physicochemical characterizations, DFT calculations were used to understand the structure-function relationship by studying the effects of Bi doping and Cu substrate on the electrocatalytic performances.

4.2 Methods

4.2.1 Preparation of electrodes and physical characterizations

As the substrate, Cu foam (2 × 2 × 0.16 cm^3, Xiamen TOB new energy technology Co., Ltd, China) was pre-treated with ultrasound successively in hydrochloric acid (1 M HCl) and deionized water for 20 min respectively to remove the surface copper oxide. In preparations of with and without Bi doped SnO/Cu foam electrodes, the nanosheet catalysts were directly grown on the surface of the Cu foam using a one-step hydrothermal method. For the preparation of SnO/Cu foam electrode, the precursor solution was prepared by dissolving 2.0 mmol of $SnCl_2$, 12 mmol of NH_2CONH_2 and 6 mmol of NH_4F in deionized water (36 mL) at first and then, transferred into a 40 mL Teflon-lined autoclave with a piece of pre-treated Cu foam (2 × 2 cm^2) and kept at 100 °C for 8 h. For preparations of Bi-SnO/Cu foam electrodes with different Bi doping amounts, different molar percentages of $BiCl_3$ were used to replace a part of $SnCl_2$, and other conditions were consistent with those for the preparation of SnO/Cu foam electrode. Based on the preliminary experiments, the optimum molar ratio was found to be 1.8 mmol $SnCl_2$: 0.2 mmol $BiCl_3$ in the precursor solution. Unless otherwise stated, the Bi-SnO/Cu foam mentioned in the experimental part represents the Bi (0.10)-SnO/Cu foam, where the numbers in parentheses represent the ratio of Bi to the total moles of Sn and Bi in the hydrothermal reaction. After the hydrothermal reaction, the electrode was taken out and washed repeatedly with deionized water and ethanol and then dried overnight at 80 °C. For the performance test, the obtained electrodes (cut to 1×1 cm^2) were immersed in the electrolyte and applied for CO_2 reduction. It is found that about 2.5 - 3.0 mg cm^{-2} electrocatalysts were grown on the Cu forms by a balance weighing.

The obtained electrodes were characterized by a scanning electron microscope (SEM)

equipped with a Horiba Scientific energy dispersive spectrometer (EDS) analyzer, a transmission electron microscope (TEM), a X-ray diffraction (XRD) machine and a X-ray photoelectron spectroscopy (XPS) instrument. The detail information on these characterizations is given in the chapter 2.

4.2.2 Electrochemical characterizations and reduction of CO_2

Linear sweep voltammetry (LSV) was carried out in a potential range of 0 to -2 V at a scan rate of 10 mV s^{-1} in N_2 or CO_2-saturated 0.1 M $KHCO_3$ solution. Electric double layer capacitance was determined by cyclic voltammetry (CV) measurement at various scan rates (40, 80, 120, 160, 200 mV s^{-1}) in N_2 -saturated 0.1 M $KHCO_3$ solution. Electrochemical impedance spectroscopy (EIS) was performed within a frequency range of 0.01 Hz - 0.1 MHz in a CO_2-saturated 0.1 M $KHCO_3$ solution at -1.2 V.

The electrochemical reduction of CO_2 was tested by constant potential method at various working potentials (i.e., -1.6, -1.7, -1.8, -1.9, -2.0 V) for 1 h. Before the working electrode used for the electrocatalysis, it was pre-reduced for 1 h at -1.6 V in 0.1 M CO_2-saturated $KHCO_3$ solution. All the gas and liquid products were collected and analyzed by gas chromatography (GC) and high performance liquid chromatography (HPLC).

4.2.3 DFT computational

To investigate the influences of Bi doping and Cu substrate on the performance of SnO-based electrocatalyst, firstly, a model of 1 × 1 × 1 SnO cells was established. The SnO cell was expanded to 2 × 2 × 2 by establishing a supercell. For Bi doped SnO, a Sn atom in the center of the model was replaced by Bi using the direct atomic replacement method commonly used in literatures.[39, 42-43] Since the catalytic reaction occurs on the catalyst surface, four surface models related to SnO (001), Bi-SnO (001), SnO (001)/Cu and Bi-

SnO (001)/Cu were established to study the specific catalytic mechanism. A vacuum layer of 15 Å was added in the Z direction to avoid the possible slab interlayer interaction.[20] Herein, the SnO (001) facet was found to have the lowest surface energy[38] and was frequently observed in the TEM images of our and others' SnO materials,[44] and meanwhile, SnO is a typical layered material with Sn-O-Sn slabs stacked along the [001] crystal direction by weak interlayer forces.[45] Therefore, the SnO (001) crystal plane should be the most easily exposed crystal facet, and it was chosen for the calculation in this study. For the models containing Cu substrate, SnO and Bi-SnO were combined with a Cu (111) crystal plane since Cu (111) facet was observed as a main peak in the XRD pattern of Cu foam and also had the lowest surface energy.[46] Based on these models, geometric optimization, adsorption energy, charge distribution, and density of state (DOS) were calculated. The detailed calculation parameters are given in the chapter 2.

4.3 Results and Discussion

4.3.1 Characterization of electrodes

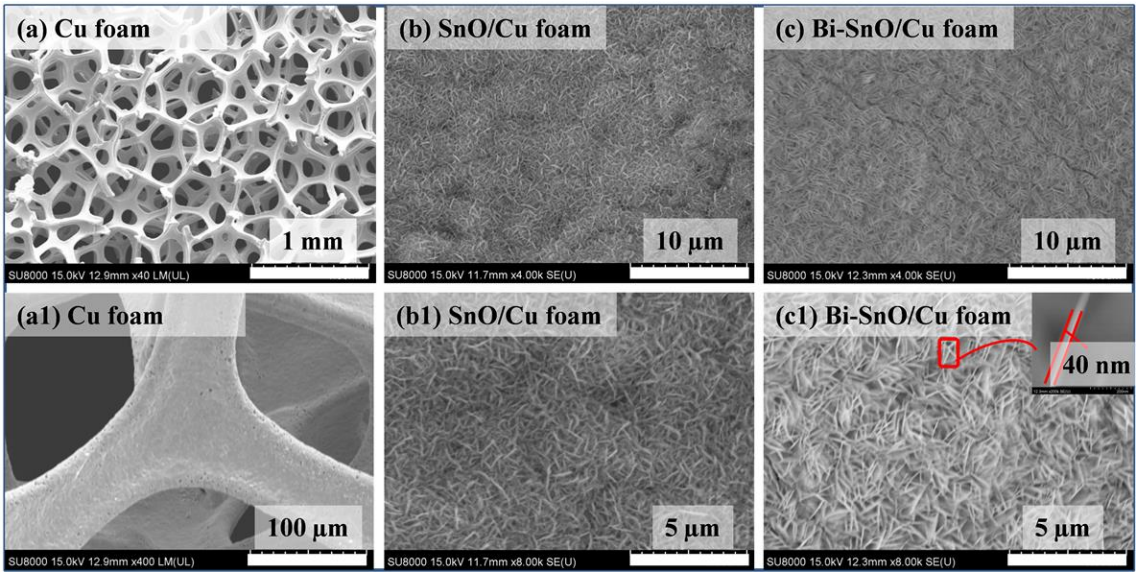

Figure 4.1 SEM images of Cu foam (a, a1), SnO/Cu foam (b, b1) and Bi-SnO/Cu foam

(c, c1) electrodes.

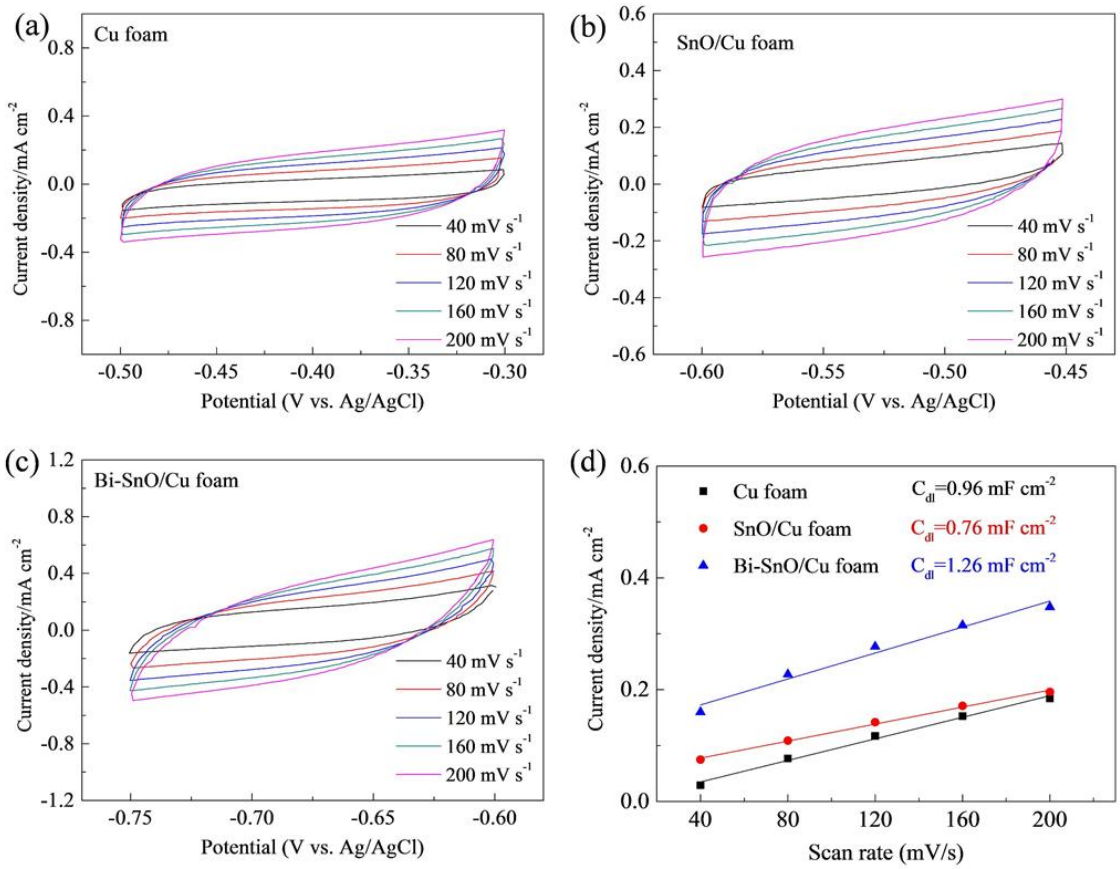

Figure 4.2. CV curves over a range of scan rates from 40-200 mV s^{-1} for the (a) Cu foam, (b) SnO/Cu foam and (c) Bi-SnO/Cu foam electrodes. (d) Determination of double layer capacitance for the three kinds of electrodes.

Figure 4.1 shows the SEM images of the three electrodes. It can be seen that the Cu foam exhibited a three-dimensional porous structure for loading more active materials and providing spaces for the diffusion of dissolved CO_2 in the solution to the electrode. In addition, its superior mechanical strength could also meet the industrial application requirements. Through the one-step hydrothermal synthesis process, it can be observed that the nanosheet electrocatalysts were uniformly grown on the surface of the Cu foam.

In the presence of Bi species, the surface morphology was changed only slightly but the nanosheet structure became more ordered. The thickness of the nanosheet was roughly measured to be 40 nm. In addition, the electrochemical double layer capacitance measurements indicated that the Bi-doped SnO catalyst had a higher electrochemically active surface area (Figure 4.2). In general, hydrothermal reaction can produce some nanostructures. However, if the substrate is not used, the morphology of the obtained powder-type catalyst is often disordered. For example, Qiao *et al.* used the similar synthesis conditions to that for this study, however, since the substrate was not used for the growth of the nanostructure, the nanosheet structure was not observed in their obtained powder-type catalyst.[44] Herein, the direct growth of electrocatalyst on the conductive substrate avoided the use of the binder (e.g., Nafion), which made it possible to show better stability in a practical application.[47]

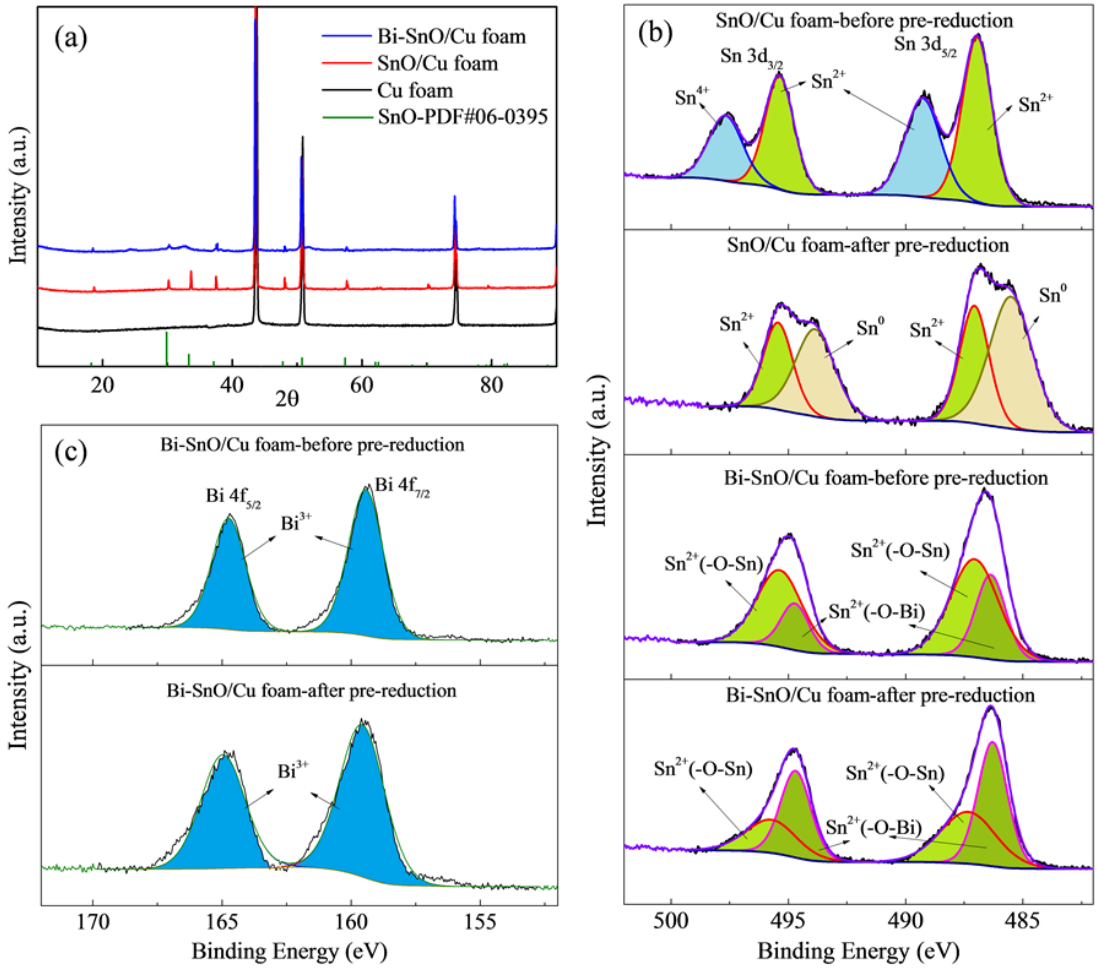

Figure 4.3. (a) XRD patterns of Cu foam, SnO/Cu foam and Bi-SnO/Cu foam electrodes. (b) High-resolution Sn 3d XPS spectra of SnO/Cu foam and Bi-SnO/Cu foam electrodes before and after pre-reduction. (c) High-resolution Bi 4f XPS spectra of Bi-SnO/Cu foam electrode before and after pre-reduction. The pre-reduction was conducted in the CO_2-saturated 0.1 M $KHCO_3$ solution at a potential of 1.6 V for 1 h.

Figure 4.3 (a) shows XRD patterns of the three electrodes. Three peaks of Cu foam at 43.8º, 50.8º, 74.4º corresponded to the Cu (111), Cu (200) and Cu (220) crystal facets, respectively (Cu: PDF#04-0836).[48] All catalysts before and after the Bi doping showed the SnO crystal structure (PDF#06-0395), which was in agreement with the results

reported by Qiao *et al.*[44], in which the main component of the catalyst synthesized at 100 ºC was SnO. It is worth noting that changing the synthesis conditions such as temperature could result in different compositions in the finally obtained catalysts. For example, the main component of the catalyst was changed to SnO_2 when the temperature was changed to 180 ºC by Chen *et al.*[20] Because the potential of electrochemical reduction of CO_2 is relatively negative, some tin oxides could be unavoidably reduced to the metal tin in the CO_2 electroreduction process.[38]

Since the electrocatalytic reaction always occurs on the surface of catalysts, the surface composition and the valence states of elements are usually investigated by XPS analysis. Many studies have demonstrated that some tin oxides still existed on the surface of electrocatalyst during the electroreduction of tin oxides to metallic tin. For example, through *in-situ* ATR-IR measurements, Bocarsly *et al.* confirmed that a metastable SnO layer always existed on the tin cathode even under reducing potentials.[37] In order to understand the effect of the reducing potential on the catalyst performance, the surface composition information of the catalyst before and after pre-reduction was examined by XPS. As shown in Figure 4.3b, the three peak groups in the Sn $3d_{3/2}$ and Sn $3d_{5/2}$ spectra corresponded to Sn^{4+} (497, 489 eV), Sn^{2+} (495, 487 eV), and Sn^0 (493, 485 eV). These values were slightly larger than those previously observed using carbon paper as the substrate,[38] which was possibly resulted from the charge transfer from the electrocatalyst to the Cu foam.[32, 49] For the SnO/Cu foam electrode, Sn^{4+} and Sn^{2+} species were present on the surface of the electrode before the pre-reduction, and they were changed to Sn^{2+} and Sn^0 species after the pre-reduction. For the Bi-SnO/Cu foam electrode before and after pre-reduction, the spectrum can be also deconvoluted to two peaks. The peak on the left corresponds to Sn^{2+}; however, the peak on the right low energy region obviously

cannot be attributed to Sn^0 since its electronic state is very close to Sn^{2+}. Herein, the Bi-doping could affect the electronic state of Sn^{2+}, resulting in the presence of two Sn^{2+} states in the Bi-SnO crystal (Sn^{2+}-O-Sn and Sn^{2+}-O-Bi, respectively). The charge distribution results obtained from DFT calculation also showed that the Bi doping slightly reduced the Sn valence state (from 0.958 to 0.938). Therefore, the left and right peaks should correspond to Sn^{2+}-O-Sn and Sn^{2+}-O-Bi, respectively. Unlike SnO, the surface valence states of Bi-SnO/Cu foam electrode before and after the pre-reduction maintained the Sn^{2+} state, which indicated that the doping of Bi stabilized the presence of Sn^{2+} species and made it not easily reduced to the metal tin. Many studies have confirmed that the surface tin oxide can improve the selectivity of CO_2 electroreduction to HCOOH.[33, 35-36, 38] Therefore, Bi doping could have a positive impact on this process.

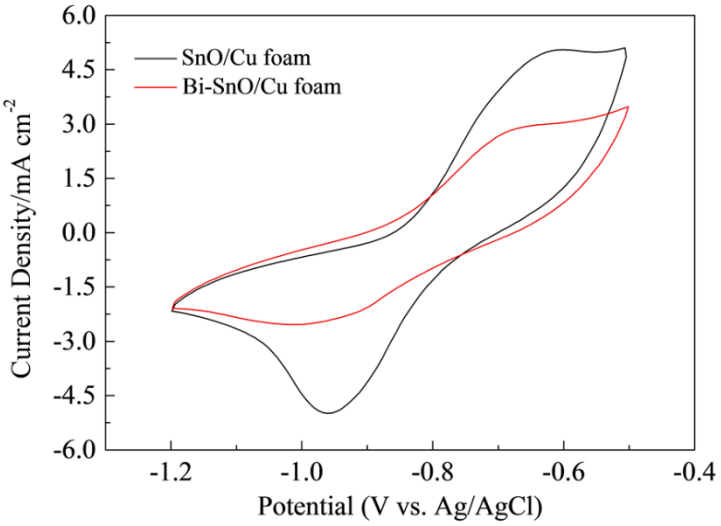

Figure 4.4 CV curves of the SnO/Cu foam and Bi-SnO/Cu foam electrodes in the N_2-saturated 0.1 M $KHCO_3$ solutions at a scan rate of 120 mV s^{-1}.

In order to verify whether the SnO electrocatalyst after Bi doping is more difficult to be reduced, the CV characteristics of the Bi doped and undoped SnO/Cu foam electrodes

were tested at a potential range of -0.5 to -1.2 V. As shown in Figure 4.4, the reduction peaks corresponded to the reduction of tin oxide.[7, 44] Obviously, the Bi doped electrode had a more negative reduction potential and a lower current density, indicating that the reduction of tin oxide became more difficult after the Bi doping.

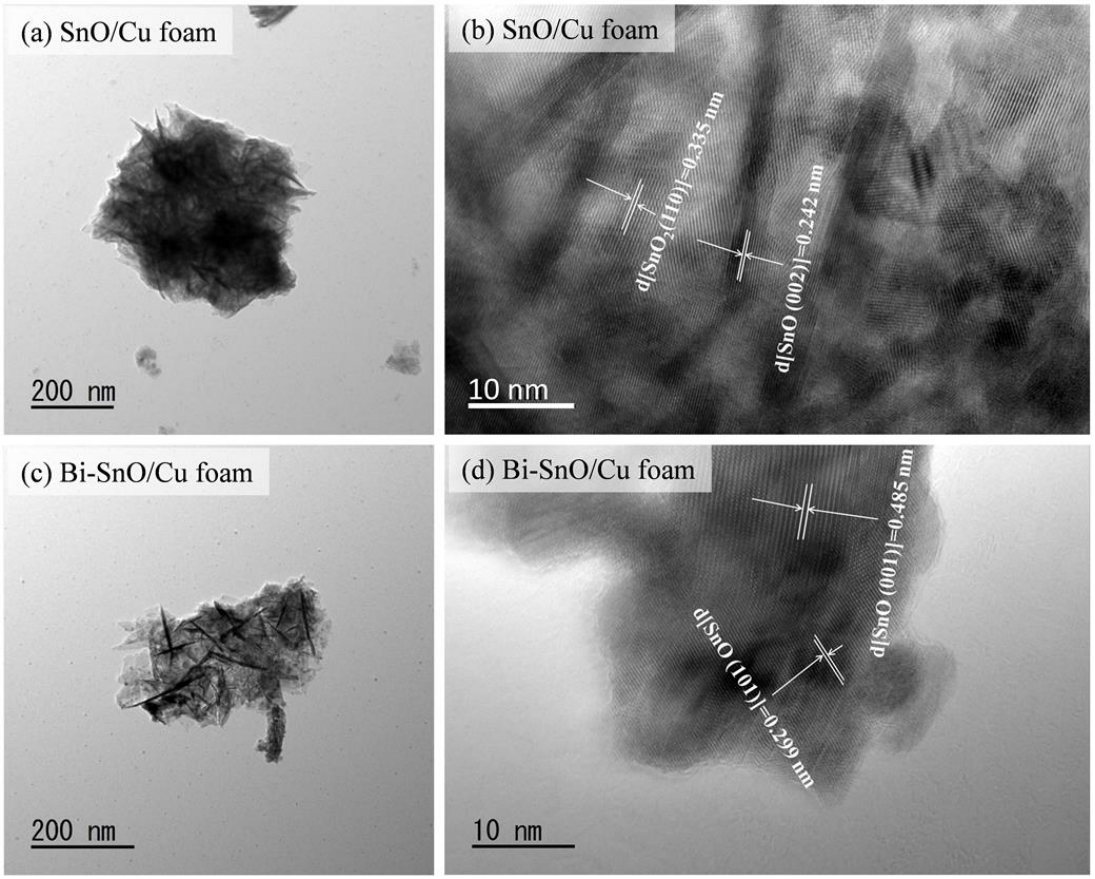

Figure 4.5. TEM and HRTEM images of the SnO (a, b) and Bi-SnO on the Cu foam (c, d) on the Cu foam.

Figure 4.5 shows TEM and HRTEM images of the SnO and Bi-SnO on the Cu foam. It can be seen from Figure 4.5a and 4.5c that some nanosheet structures existed in the catalyst. For SnO, the lattice fringes observed in Figure 4.5b with a lattice spacing of 0.24 nm corresponded to the (002) plane of SnO.[38, 44] This crystal facet was also frequently

observed as the main lattice plane in the Sn-based catalysts synthesized by Qiao *et al.*[44] Meanwhile, the crystal plane with a lattice spacing of 0.335 nm corresponded to the SnO_2 (110) crystal plane, and this crystal facet was also been reported as the most stable crystal facet with the lowest surface energy.[50-52] For Bi-SnO, the crystal planes with d-spacings of 0.485 and 0.299 nm corresponded to the SnO (001) and SnO (101) crystal planes, respectively.[38] Considering that SnO (001) is the most easily exposed crystal face[35] and has been usually observed in the TEM images, we used this crystal facet for the catalytic mechanism study in the subsequent theoretical calculations.

4.3.2 Electrochemical reduction of CO_2

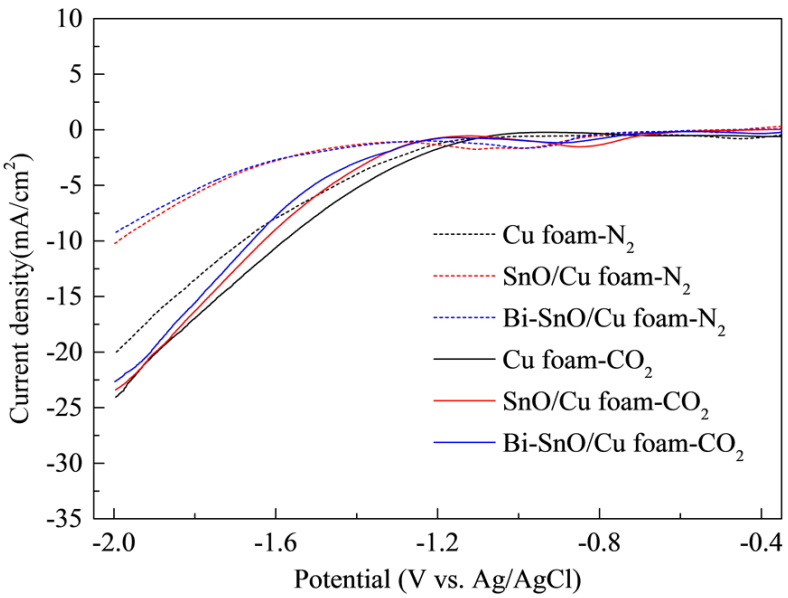

Figure 4.6. Polarization curves of the Cu foam, SnO/Cu foam and Bi-SnO/Cu foam electrodes under N_2 (dashed) and CO_2 (solid) in 0.1M $KHCO_3$ solution. Scan rate: 10 mV s^{-1}.

The LSV test was first performed to evaluate the catalytic activities of the three kinds of electrodes for CO_2 electroreduction. Comparing the current densities of the three

electrodes in N_2 with CO_2-saturated $KHCO_3$ solutions, it can be seen clearly that the three electrodes had more negative current densities under the CO_2 atmosphere, indicating that CO_2 has been reduced on them. In particular, for Cu foam, this difference was not obvious, but after the growth of the catalysts on it, the current densities of SnO/Cu foam and Bi-SnO/Cu foam electrodes under N_2 atmosphere were significantly decreased, indicating that the H_2 evolution reaction was strongly suppressed. This phenomenon is commonly observed on tin-based catalysts.[7, 20, 28, 44]

In addition, in the CO_2-saturated $KHCO_3$ solution, compared with the SnO/Cu foam electrode, the electrode with the Bi doping exhibited a slightly reduced current density, which may be due to that the Bi doping made SnO difficult to be reduced to metal tin as confirmed by XPS and CV in the previous sections. As a semiconductor, SnO has a lower electronic conductivity than metal Sn. Thus, more SnO on the electrode could make the electronic conductivity relatively low. Herein, for the Bi-SnO/Cu foam electrode, although the current density was slightly sacrificed, its selectivity to HCOOH was significantly enhanced, which made it still valuable in the practical applications. This will be discussed in details in the next section.

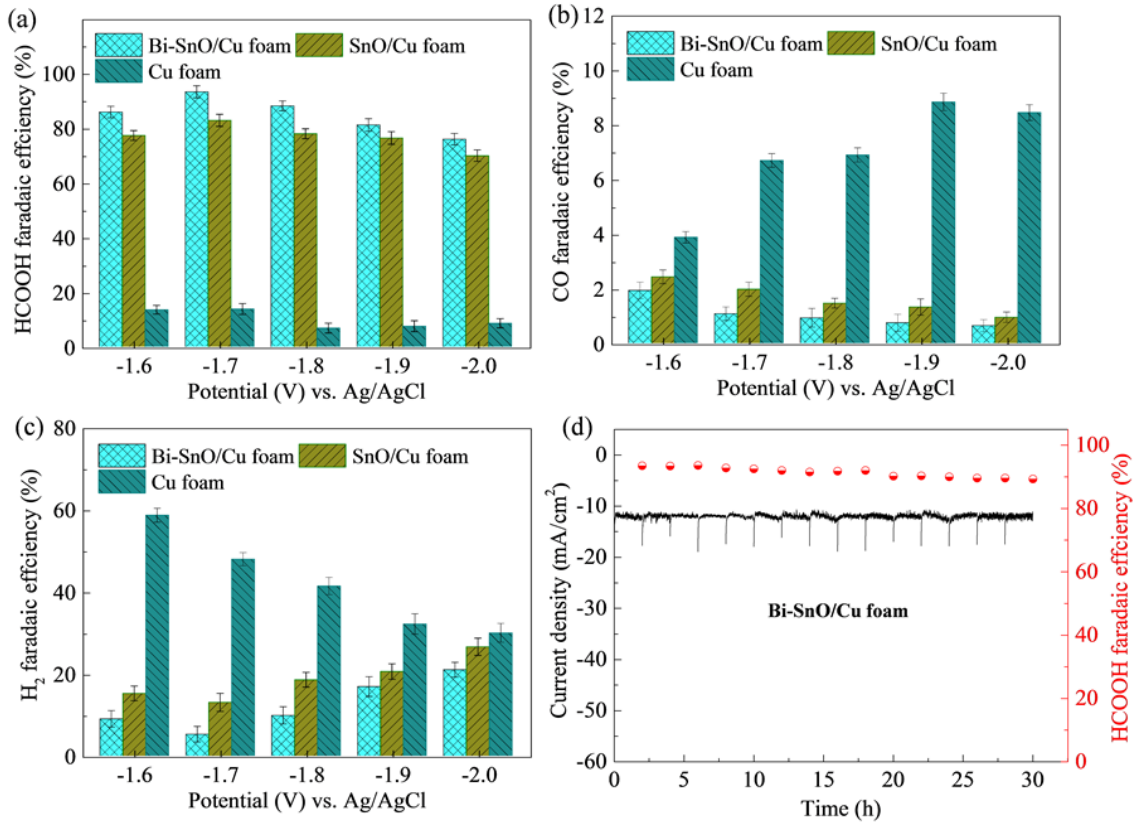

Figure 4.7. Faradaic efficiencies for HCOOH (a), CO (b) and H_2 (c) producing at different potentials on the three electrodes. (d) The long-term stability of the Bi-SnO/Cu foam electrode at -1.7 V.

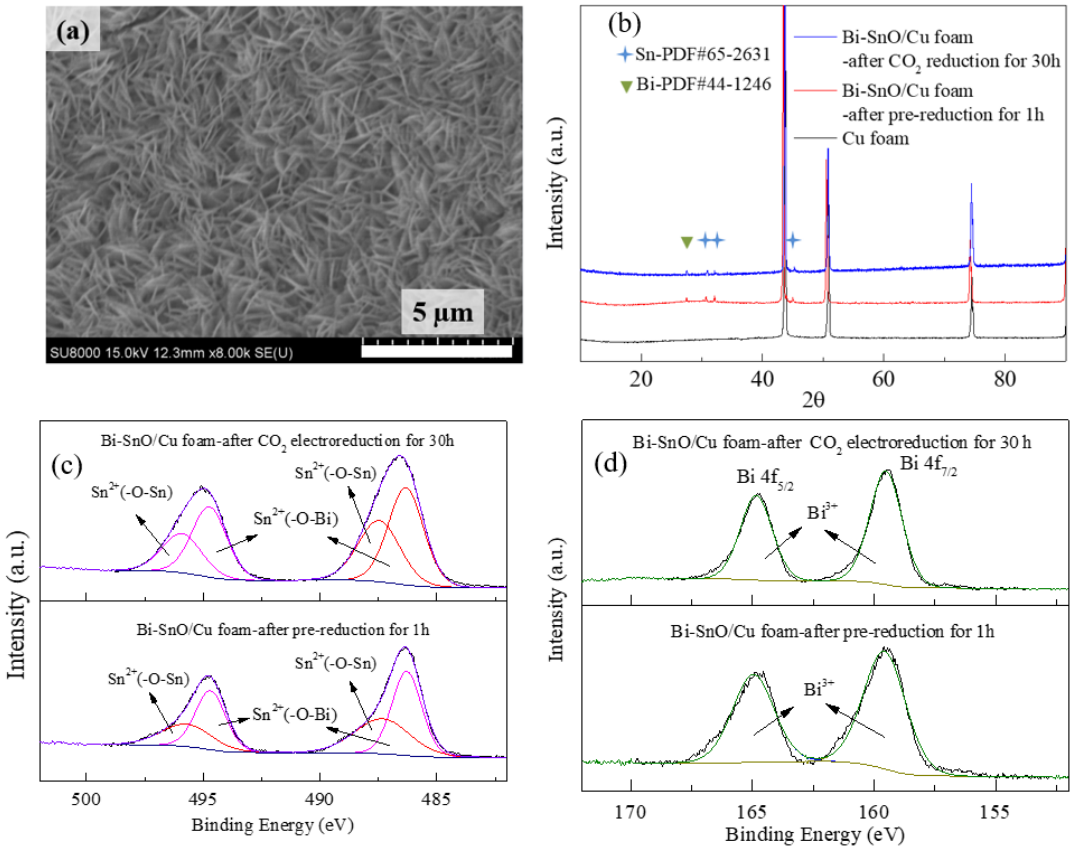

Figure 4.8. SEM images of Bi-SnO/Cu foam electrode after 30 h electrolysis operation. (b) XRD, (c) Sn 3d XPS and (d) Bi 4f XPS spectra of Bi-SnO/Cu foam electrode before and after 30 h electrolysis operation.

Further performance testing was conducted to calculate the faradaic efficiency by analyzing the gas and liquid phase products after one hour of potentiostatic electrolysis. The analysis results showed that the total faradaic efficiency of approximate 100% (HCOOH, CO and H_2) during the one hour electroreduction process indicated that no other products were formed, which was consistent with most of the tin-based catalysts.[7, 20] From Figure 4.7a, comparing the faradaic efficiency of the HCOOH produced by the three electrodes, it can be seen clearly that the Bi-SnO/Cu foam electrode had higher faradaic efficiency, especially reached a maximum of 93% at -1.7 V. From Figures 4.7b

and 4.7c, by comparing the evolution of CO and H_2, it can be found that the Bi doping inhibited the formations of CO and H_2. In conclusion, the Bi doping improved the selectivity of the catalyst towards HCOOH. In order to test the stability of the electrode, a batch potentiostatic test was performed at -1.7 V, in which the refreshing of the electrolyte and product collection analysis were performed every two hours. As shown in Figure 4.7d, the Bi-SnO/Cu foam electrode showed excellent stability. During the 30 h electrolysis operation, the current density remained basically stable, and the HCOOH faradaic efficiency remained above 90%. Also, the surface morphology and composition of the Bi-SnO/Cu foam electrode had no significant change (Figure 4.8).

4.3.3 Mechanism analysis

In order to study the effect of Bi doping and Cu foam on the catalysis performance, it is necessary to understand the reduction path of CO_2 on the electrocatalyst surface. Currently, the following reaction steps of CO_2 reduced to HCOOH and CO have been widely accepted for the tin-based electrocatalysts.[8, 38, 53]

HCOOH formation:

$$CO_2 + H^+ + e^- + * \rightarrow *OOCH \quad (4\text{-}1)$$

$$*OOCH + H^+ + e^- \rightarrow * + HCOOH \quad (4\text{-}2)$$

$$CO_2 + H^+ + e^- + * \rightarrow *COOH \quad (4\text{-}3)$$

$$*COOH + H^+ + e^- \rightarrow * + HCOOH \quad (4\text{-}4)$$

CO formation:

$$CO_2 + H^+ + e^- + * \rightarrow *COOH \quad (4\text{-}5)$$

$$*COOH + H^+ + e^- \rightarrow * + CO + H_2O \quad (4\text{-}6)$$

H_2 formation (side reactions)

$$H^+ + e^- + * \rightarrow *H \quad (4\text{-}7)$$

$$*H + H^+ + e^- \rightarrow * + H_2 \quad (4\text{-}8)$$

It can be seen from the above equations that *COOH and *OOCH are the key intermediates for the production of HCOOH, and *COOH intermediate can also result in the formation of CO. Generally, for the tin-based catalysts, the formation energy barrier of *OOCH is much lower than that of *COOH.[32, 38] Therefore, *OOCH is the most important intermediate for the production of HCOOH, and its binding energy is widely studied as a descriptor for explaining the selectivity for electroreduction of CO_2 to HCOOH.[8, 53]

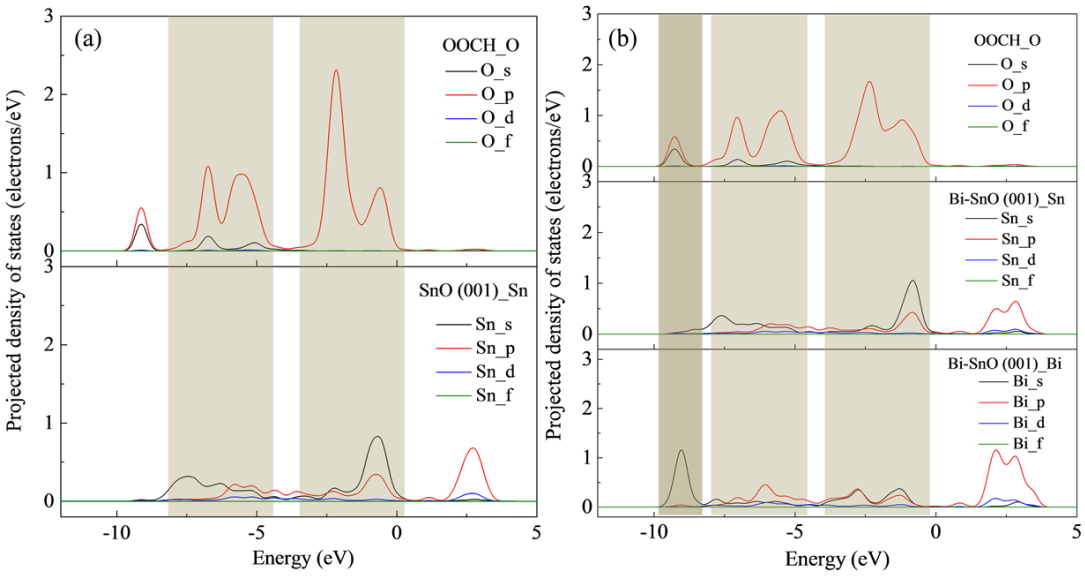

Figure 4.9. Projected density of states (PDOS) of O, Sn and Bi atoms on SnO (001) (a) and Bi-SnO (001) (b) surfaces with the adsorbed *OOCH.

In order to investigate the effect of Bi doping on the catalytic performance of SnO, we firstly calculated the binding energy of *OOCH intermediates on the SnO (001) surface before and after the Bi doping. The calculation results showed that the binding energy was changed from -2.31 to -2.65 eV after the Bi doping, which indicated that the Bi

doping enhanced the binding ability of SnO (001) surface to *OOCH. To further analyze the underlying cause of this enhancement, projected density of states (PDOS) calculations were performed to analyze the electronic interaction of the *OOCH with the catalyst surface. From the calculation result in Figure 4.9a, it can be seen that the interaction of *OOCH intermediate with the SnO (001) plane was mainly resulted from the orbital hybridization of O 2p with Sn 5s and 5p states. The hybrid regions were mainly distributed in two light-colored regions in the figure. After the Bi doping, a new hybridization region colored with dark region was formed as shown in Figure 4.9b, which was mainly composed of Bi 6s with O 2s and 2p orbital hybridization. Similar conclusions were also found in Chen *et al.*'s study of the Sn-Bi bimetallic electrocatalysts.[20] Therefore, it can be considered that this additional orbital hybridization enhanced the adsorption ability of the SnO (001) surface for the *OOCH intermediate.

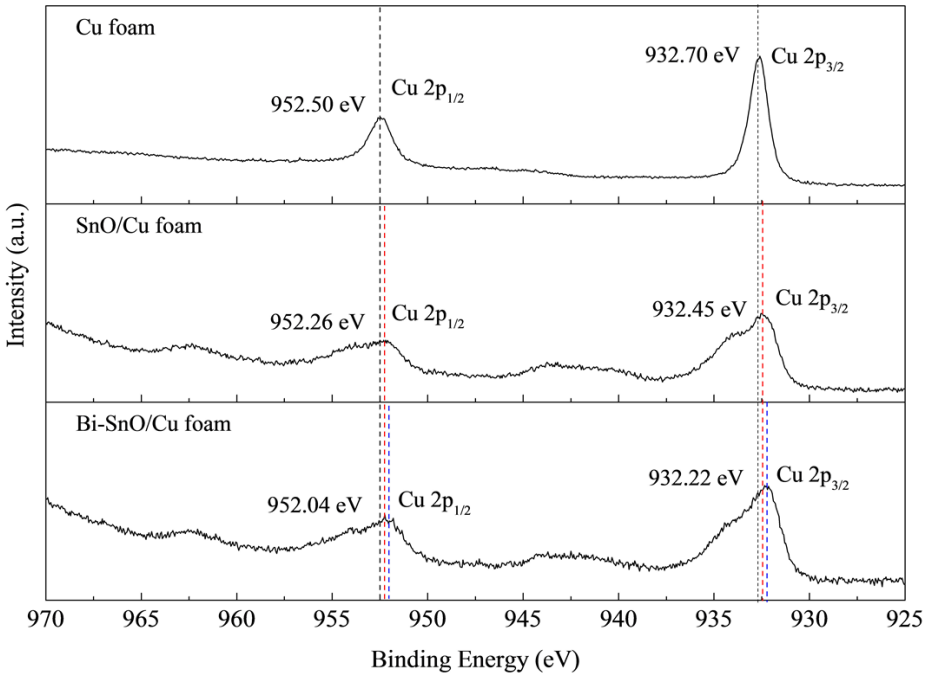

Figure 4.10. High-resolution Cu 2p XPS spectra of Cu foam, SnO/Cu foam and Bi-SnO/Cu foam electrodes.

In addition, Cu foam is often used as the substrate material due to its superior electrical conductivity and its three-dimensional porous structure. In the XPS results of Figure 4.10, Cu 2p peaks emerged at 952 and 932 eV indicated metallic Cu.[48, 54] It is found that when SnO or Bi-SnO was deposited on the Cu foam, the peaks of Cu $2p_{1/2}$ and Cu $2p_{3/2}$ moved slightly to the low energy region, and the degree of movement after the Bi doping was more obvious. This indicated that the electrons of SnO and Bi-SnO were transferred to Cu foam. Cui *et al.* also found that in $CuSn_3$, electrons of Sn were transferred to Cu, thereby maintaining Sn under the positive oxidation states under the operating conditions, which had a positive effect on enhancing the selectivity of HCOOH.[32]

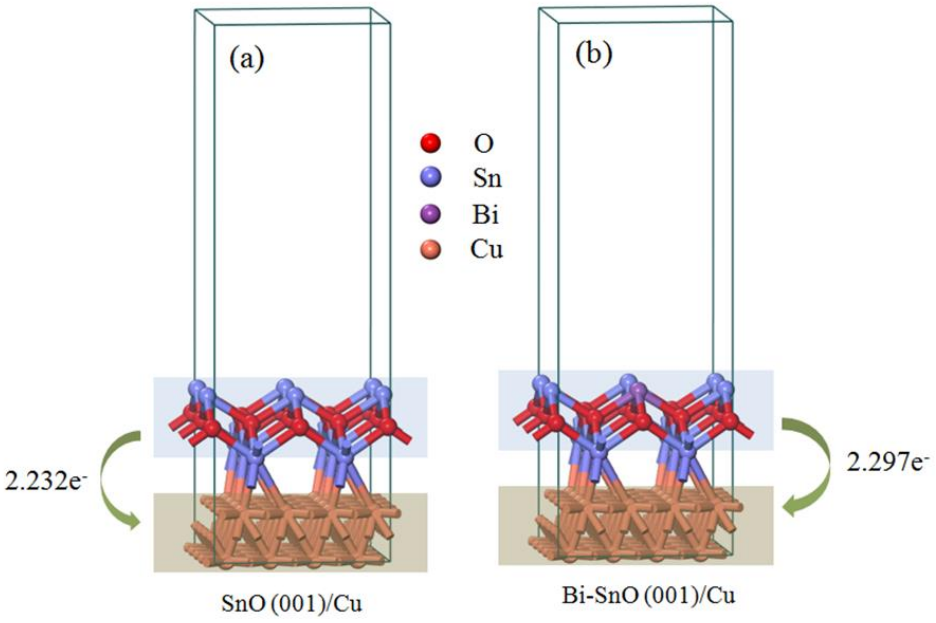

Figure 4.11 The electronic transfer diagrams of the SnO (001)/Cu (a) and Bi-SnO (001)/Cu.

In order to verify whether this phenomenon also existed in our catalyst, we established a catalyst model containing a Cu substrate and performed the Mulliken charge distribution calculation. The calculation results indicated that 2.232 electrons of SnO were transferred

to the Cu substrate; and in contrast, the number of transferred electrons became 2.297 after the Bi doping (Figure 4.11). This electron transfer led to further enhancement of adsorption ability of Bi-SnO to the *OOCH intermediate (Binding energy was -2.78 eV). Therefore, using Cu foam as the substrate may further enhance the HCOOH selectivity of the Bi doped SnO electrocatalyst.

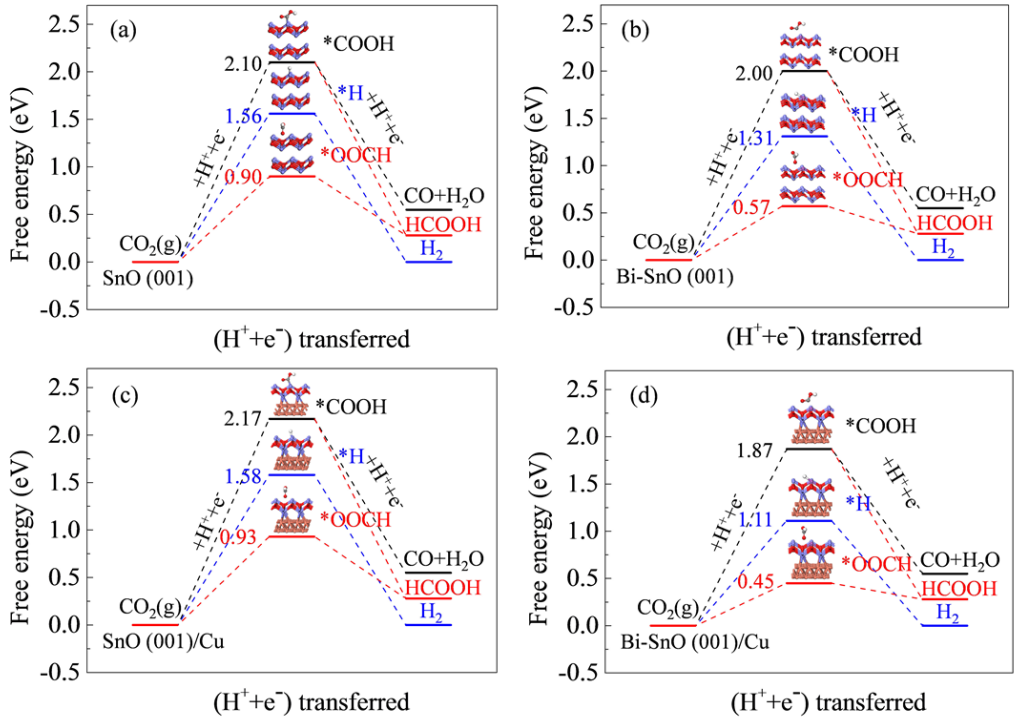

Figure 4.12 Free energy diagrams of CO_2 reduced to HCOOH, CO and H_2 on SnO (001) (a), Bi-SnO (001) (b), SnO (001)/Cu (c) and Bi-SnO (001)/Cu (d) surfaces.

During the electrocatalytic process, besides the formation of HCOOH, CO and H_2 were also produced. In order to comprehensively evaluate the influences of Bi doping and Cu substrate, according to the equations of 5-12, the free energy diagrams for reducing CO_2 to HCOOH, CO and H_2 on SnO (001), Bi-SnO (001), SnO (001)/Cu and Bi-SnO (001)/Cu were obtained. For the four models, the order of formation energy barrier of three

intermediates was *COOH > *H > *OOCH. This indicated that the selectivity of the catalyst towards CO_2 reduction products was HCOOH > H_2 > CO, which is consistent with the selectivity sequence shown in the experiments. Comparing Figures 4.12a and 4.12b, it can be seen that after the Bi doping, the energy barriers for forming three intermediates were dropped to some extent, but the energy barrier of *OOCH was reduced mostly. Since the selectivity of the products can be estimated by the thermodynamic formula of exp[-(ΔG/RT)],[55] it confirmed that the Bi doping enhanced the selectivity towards HCOOH. Comparing Figures 4.12a and 4.12c, it can be found that the effect of adding the Cu substrate on the free energy barrier was extremely slight in the absence of Bi doping. However, comparing Figures 9b and 9d, it can be seen that the adding of the Cu substrate reduced the energy barrier of the three intermediates to some different extents. In addition, compared to the pure SnO (001) surface, the formation energy barrier of *OOCH still had the greatest reduction. Therefore, it can be concluded that the Bi doping and the use of Cu foam substrate improved the HCOOH selectivity.

Herein, it should be pointed out that the XPS characterization used in this work was *ex-situ*, which cannot indicate the valence states of Sn under working condition. In this study, DFT calculations were applied to explore the effect of oxidized tin on catalytic performance. However, more *in-situ* characterization works are still needed to verify these conclusions. Thus, based on the current research, it can conclude that the Sn in positive oxidation state should be a site with higher catalytic activity for the electroreduction of CO_2 to HCOOH compared to metallic tin site.

4.4 Conclusions

In summary, the SnO and Bi-doped SnO nanosheets were uniformly grown on the Cu foam substrate by a facile hydrothermal synthesis method. As an electrocatalyst for

electrochemical reduction of CO_2, the Bi-SnO/Cu foam exhibited higher HCOOH selectivity than the SnO/Cu foam, and the highest faradaic efficiency reached 93%. Also, the Bi-SnO/Cu foam electrode exhibited excellent long-term stability in 30 h of operation. The physicochemical characterization indicated that the Bi doping stabilizes the existence of divalent tin (Sn^{2+}) on the surface of the electrocatalyst, making it not easy to be reduced to metallic tin (Sn^0). Meanwhile, the DTF calculation revealed that the Bi doping enhanced the adsorption ability of SnO (001) facet for *OOCH intermediates by the electron orbital hybridization, thereby increasing the selectivity to HCOOH. In addition, the influence of Cu foam as the substrate on the catalysis was also investigated. It is found that when the Bi-SnO was grown on the Cu foam, the electron transfer from the electrocatalyst to the Cu foam promoted the maintenance of tin under positive oxidation state, favored the adsorption of *OOCH intermediates. Finally, this work analyzed the relationship between catalyst structure and catalytic performance from the electronic structure level, and deepened the understanding of the catalytic mechanism of CO_2 electrochemical reduction, which is expected to provide important guiding for the design and synthesis of electrocatalyst.

References

1. Vasileff, A.; Zheng, Y.; Qiao, S. Z., Carbon solving carbon's problems: recent progress of nanostructured carbon-based catalysts for the electrochemical reduction of CO_2. *Adv. Energy. Mater.* **2017,** *7* (21), 1700759.
2. Zhang, W.; Hu, Y.; Ma, L.; Zhu, G.; Wang, Y.; Xue, X.; Chen, R.; Yang, S.; Jin, Z., Progress and perspective of electrocatalytic CO_2 reduction for renewable carbonaceous fuels and chemicals. *Adv. Sci.* **2018,** *5* (1), 1700275.
3. Leitner, W., Carbon dioxide as a raw material: the synthesis of formic acid and its derivatives from CO_2. *Angew. Chem. Int. Ed.* **1995,** *34* (20), 2207-2221.
4. Wang, J.; Li, X.; Zheng, J.; Cao, J.; Hao, X.; Wang, Z.; Abudula, A.; Guan, G., Non-precious molybdenum-based catalyst derived from biomass: CO-free hydrogen production from formic acid at low temperature. *Energy Convers. Manage.* **2018,**

164, 122-131.

5. Lee, H. J.; Kang, D. C.; Pyen, S. H.; Shin, M.; Suh, Y. W.; Han, H.; Shin, C. H., Production of H_2-free co by decomposition of formic acid over ZrO_2 catalysts. *Appl. Catal. A-Gen.* **2017,** *531*, 13-20.
6. Verma, S.; Kim, B.; Jhong, H. R. M.; Ma, S.; Kenis, P. J., A gross-margin model for defining technoeconomic benchmarks in the electroreduction of CO_2. *ChemSusChem* **2016,** *9* (15), 1972-1979.
7. Fan, L.; Xia, Z.; Xu, M.; Lu, Y.; Li, Z., 1D SnO_2 with wire-in-tube architectures for highly selective electrochemical reduction of CO_2 to C1 products. *Adv. Funct. Mater.* **2018,** *28* (17), 1706289.
8. Zheng, X.; De Luna, P.; García de Arquer, F. P.; Zhang, B.; Becknell, N.; Ross, M. B.; Li, Y.; Banis, M. N.; Li, Y.; Liu, M.; Voznyy, O.; Dinh, C. T.; Zhuang, T.; Stadler, P.; Cui, Y.; Du, X.; Yang, P.; Sargent, E. H., Sulfur-modulated tin sites enable highly selective electrochemical reduction of CO_2 to formate. *Joule* **2017,** *1* (4), 794-805.
9. Liu, S.; Xiao, J.; Lu, X. F.; Wang, J.; Wang, X.; Lou, X. W., Efficient electrochemical reduction of CO_2 to HCOOH over Sub-2 nm SnO_2 quantum wires with exposed grain boundaries. *Angew. Chem. Int. Ed.* **2019,** *58* (25), 8499-8503.
10. Su, P.; Xu, W.; Qiu, Y.; Zhang, T.; Li, X.; Zhang, H., Ultrathin bismuth nanosheets as highly efficient electrocatalyst for CO_2 reduction. *ChemSusChem* **2018,** *11* (5), 848-853.
11. Lee, C. W.; Hong, J. S.; Yang, K. D.; Jin, K.; Lee, J. H.; Ahn, H. Y.; Seo, H.; Sung, N. E.; Nam, K. T., Selective electrochemical production of formate from carbon dioxide with bismuth-based catalysts in an aqueous electrolyte. *ACS Catal.* **2018,** *8* (2), 931-937.
12. Chen, Z.; Mou, K.; Wang, X.; Liu, L., Nitrogen-doped graphene quantum dots enhance the activity of Bi_2O_3 nanosheets for electrochemical reduction of CO_2 in a wide negative potential region. *Angew. Chem. Int. Ed.* **2018,** *57* (39), 12790-12794.
13. Liu, S.; Lu, X. F.; Xiao, J.; Wang, X.; Lou, X. W., Bi_2O_3 nanosheets grown on multi-channel carbon matrix to catalyze efficient CO_2 electroreduction to HCOOH. *Angew. Chem. Int. Ed.* **2019,** *58* (39), 13828-13833.
14. Fan, M.; Garbarino, S.; Botton, G. A.; Tavares, A. C.; Guay, D., Selective electroreduction of CO_2 to formate on 3D[100] Pb dendrites with nanometer-sized needle-like tips. *J. Mater. Chem. A* **2017,** *5* (39), 20747-20756.
15. García, J.; Jiménez, C.; Martínez, F.; Camarillo, R.; Rincón, J., Electrochemical reduction of CO_2 using Pb catalysts synthesized in supercritical medium. *J. Catal.* **2018,** *367*, 72-80.

16. Hori, Y.; Wakebe, H.; Tsukamoto, T.; Koga, O., Electrocatalytic process of CO selectivity in electrochemical reduction of CO_2 at metal electrodes in aqueous media. *Electrochim. Acta* **1994,** *39* (11-12), 1833-1839.
17. Mizuno, T.; Ohta, K.; Sasaki, A.; Akai, T.; Hirano, M.; Kawabe, A., Effect of temperature on electrochemical reduction of high-pressure CO_2 with In, Sn, and Pb electrodes. *Energy Sources* **1995,** *17* (5), 503-508.
18. Jiang, B.; Zhang, X. G.; Jiang, K.; Wu, D. Y.; Cai, W. B., Boosting Formate production in electrocatalytic CO_2 reduction over wide potential window on Pd surfaces. *J. Am. Chem. Soc.* **2018,** *140* (8), 2880-2889.
19. Zhu, W.; Zhang, L.; Yang, P.; Chang, X.; Dong, H.; Li, A.; Hu, C.; Huang, Z.; Zhao, Z. J.; Gong, J., Morphological and compositional design of Pd-Cu bimetallic nanocatalysts with controllable product selectivity toward CO_2 electroreduction. *Small* **2017,** *14* (7), 1703314.
20. Wen, G.; Lee, D. U.; Ren, B.; Hassan, F. M.; Jiang, G.; Cano, Z. P.; Gostick, J.; Croiset, E.; Bai, Z.; Yang, L.; Chen, Z., Orbital interactions in Bi-Sn bimetallic electrocatalysts for highly selective electrochemical CO_2 reduction toward formate production. *Adv. Energy. Mater.* **2018,** *8* (31), 1802427.
21. Qiu, Y. L.; Zhong, H. X.; Zhang, T. T.; Xu, W.-B.; Su, P.-P.; Li, X. F.; Zhang, H. M., Selective electrochemical reduction of carbon dioxide using Cu based metal organic framework for CO_2 capture. *ACS Appl. Mater. Interfaces* **2018,** *10* (3), 2480-2489.
22. Kaneco, S.; Katsumata, H.; Suzuki, T.; Ohta, K., Electrochemical reduction of CO_2 to methane at the Cu electrode in methanol with sodium supporting salts and its comparison with other alkaline salts. *Energy Fuels* **2006,** *20* (1), 409-414.
23. Huo, Y.; Peng, X.; Liu, X.; Li, H.; Luo, J., High selectivity toward C_2H_4 production over Cu particles supported by butterfly-wing-derived carbon frameworks. *ACS Appl. Mater. Interfaces* **2018,** *10* (15), 12618-12625.
24. Wang, J.; Li, Z.; Dong, C.; Feng, Y.; Yang, J.; Liu, H.; Du, X., Silver/copper interface for relay electroreduction of carbon dioxide to ethylene. *ACS Appl. Mater. Interfaces* **2019,** *11* (3), 2763-2767.
25. Lu, L.; Sun, X. F.; Ma, J.; Yang, D. X.; Wu, H. H.; Zhang, B. X.; Zhang, J. L.; Han, B. X., Highly efficient electroreduction of CO_2 to methanol on palladium-copper bimetallic aerogels. *Angew. Chem. Int. Ed.* **2018,** *57* (43), 14149-14153.
26. Song, Y.; Peng, R.; Hensley, D. K.; Bonnesen, P. V.; Liang, L.; Wu, Z.; Meyer, H. M.; Chi, M.; Ma, C.; Sumpter, B. G.; Rondinone, A. J., High-selectivity electrochemical conversion of CO_2 to ethanol using a copper nanoparticle/N-doped graphene electrode. *ChemistrySelect* **2016,** *1* (19), 6055-6061.

27. Zhao, K.; Liu, Y.; Quan, X.; Chen, S.; Yu, H., CO_2 electroreduction at low overpotential on oxide-derived Cu/carbons fabricated from metal organic framework. *ACS Appl. Mater. Interfaces* **2017,** *9* (6), 5302-5311.
28. Wang, Y.; Zhou, J.; Lv, W.; Fang, H.; Wang, W., Electrochemical reduction of CO_2 to formate catalyzed by electroplated tin coating on copper foam. *Appl. Surf. Sci.* **2016,** *362*, 394-398.
29. Lv, W.; Zhou, J.; Kong, F.; Fang, H.; Wang, W., Porous tin-based film deposited on copper foil for electrochemical reduction of carbon dioxide to formate. *Int. J. Hydrogen Energy* **2016,** *41* (3), 1585-1591.
30. Deng, Y.; Huang, Y.; Ren, D.; Handoko, A. D.; Seh, Z. W.; Hirunsit, P.; Yeo, B. S., on the role of sulfur for the selective electrochemical reduction of CO_2 to formate on CuSx catalysts. *ACS Appl. Mater. Interfaces* **2018,** *10* (34), 28572-28581.
31. Wang, Y.; Hu, H.; Sun, Y.; Tang, Y.; Dai, L.; Hu, Q.; Fisher, A.; Yang, X. J., Facile synthesis of nanostructural high-performance Cu-Pb Electrocatalysts for CO_2 reduction. *Adv. Mater. Interfaces* **2019,** *6* (2), 1801200.
32. Zheng, X.; Ji, Y.; Tang, J.; Wang, J.; Liu, B.; Steinrück, H. G.; Lim, K.; Li, Y.; Toney, M. F.; Chan, K.; Cui, Y., Theory-guided Sn/Cu alloying for efficient CO_2 electroreduction at low overpotentials. *Nat. Catal.* **2019,** *5*, 55-61.
33. Won da, H.; Choi, C. H.; Chung, J.; Chung, M. W.; Kim, E. H.; Woo, S. I., Rational design of a hierarchical tin dendrite electrode for efficient electrochemical reduction of CO_2. *ChemSusChem* **2015,** *8* (18), 3092-3098.
34. Chen, Y.; Kanan, M. W., Tin oxide dependence of the CO_2 reduction efficiency on tin electrodes and enhanced activity for tin/tin oxide thin-film catalysts. *J. Am. Chem. Soc.* **2012,** *134* (4), 1986-1989.
35. Cui, C.; Han, J.; Zhu, X.; Liu, X.; Wang, H.; Mei, D.; Ge, Q., Promotional effect of surface hydroxyls on electrochemical reduction of CO_2 over SnO_x/Sn electrode. *J. Catal.* **2016,** *343*, 257-265.
36. Zhang, R.; Lv, W.; Lei, L., Role of the oxide layer on Sn electrode in electrochemical reduction of CO_2 to formate. *Appl. Surf. Sci.* **2015,** *356*, 24-29.
37. Baruch, M. F.; Pander, J. E.; White, J. L.; Bocarsly, A. B., Mechanistic insights into the reduction of CO_2 on tin electrodes using in situ ATR-IR spectroscopy. *ACS Catal.* **2015,** *5* (5), 3148-3156.
38. An, X.; Li, S.; Yoshida, A.; Wang, Z.; Hao, X.; Abudula, A.; Guan, G., Electrodeposition of tin-based electrocatalysts with different surface tin species distributions for electrochemical reduction of CO_2 to HCOOH. *ACS Sustain. Chem. Eng.* **2019,** *7* (10), 9360-9368.

39. Dong, W.; Xie, X.; Jia, J.; Du, H.; Zhong, L.; Liang, Z.; Han, P., Theoretical calculation and experimental study on the conductivity and stability of Bi-doped SnO_2 electrode. *Electrochim. Acta* **2014,** *132*, 307-314.
40. Kim, H.; Pique, A., Transparent conducting Sb-doped SnO_2 thin films grown by pulsed-laser deposition. *Appl. Phys. Lett.* **2004,** *84* (2), 218-220.
41. Wei, Y.; Liu, J.; Cheng, F.; Chen, J., Mn-doped atomic SnO_2 layers for highly efficient CO_2 electrochemical reduction. *J. Mater. Chem. A* **2019,** *7* (34), 19651-19656.
42. Lu, X. F.; Yu, L.; Lou, X. W., Highly crystalline Ni-doped FeP/carbon hollow nanorods as all-pH efficient and durable hydrogen evolving electrocatalysts. *Sci. Adv.* **2019,** *5* (2), eaav6009.
43. Stashans, A.; Puchaicela, P.; Rivera, R., DFT study of chromium-doped SnO_2 materials. *J. Mater. Sci.* **2014,** *49* (7), 2904-2911.
44. Li, Y.; Qiao, J.; Zhang, X.; Lei, T.; Girma, A.; Liu, Y.; Zhang, J., Rational design and synthesis of SnO_x electrocatalysts with coralline structure for highly improved aqueous CO_2 reduction to formate. *ChemElectroChem* **2016,** *3* (10), 1618-1628.
45. Zhou, W.; Umezawa, N., Band gap engineering of bulk and nanosheet SnO: an insight into the interlayer Sn-Sn lone pair interactions. *Phys. Chem. Chem. Phys.* **2015,** *17* (27), 17816-17820.
46. Wen, Y.-N.; Zhang, J. M., Surface energy calculation of the fcc metals by using the MAEAM. *Solid State Commun.* **2007,** *144* (3), 163-167.
47. Li, S.; Sirisomboonchai, S.; Yoshida, A.; An, X.; Hao, X.; Abudula, A.; Guan, G., Bifunctional CoNi/$CoFe_2O_4$/Ni foam electrodes for efficient overall water splitting at a high current density. *J. Mater. Chem. A* **2018,** *6* (39), 19221-19230.
48. Chung, J.; Koh, J.; Kim, E.-H.; Woo, S. I., Hierarchical Cu pillar electrodes for electrochemical CO_2 reduction to formic acid with low overpotential. *Phys. Chem. Chem. Phys.* **2016,** *18* (8), 6252-6258.
49. Li, Q.; Fu, J.; Zhu, W.; Chen, Z.; Shen, B.; Wu, L.; Xi, Z.; Wang, T.; Lu, G.; Zhu, J. J.; Sun, S., Tuning Sn-catalysis for electrochemical reduction of CO_2 to CO via the core/shell Cu/SnO_2 structure. *J. Am. Chem. Soc.* **2017,** *139* (12), 4290-4293.
50. Oviedo, J.; Gillan, M., Energetics and structure of stoichiometric SnO_2 surfaces studied by first-principles calculations. *Surf. Sci.* **2000,** *463* (2), 93-101.
51. Cheng, B.; Russell, J. M.; Shi, W.; Zhang, L.; Samulski, E. T., Large-scale, solution-phase growth of single-crystalline SnO_2 nanorods. *J. Am. Chem. Soc.* **2004,** *126* (19), 5972-5973.
52. Henrich, V. E.; Cox, P. A., *The surface science of metal oxides*. Cambridge university

press, **1996**.

53. Feaster, J. T.; Shi, C.; Cave, E. R.; Hatsukade, T.; Abram, D. N.; Kuhl, K. P.; Hahn, C.; Nørskov, J. K.; Jaramillo, T. F., Understanding selectivity for the electrochemical reduction of carbon dioxide to formic acid and carbon monoxide on metal electrodes. *ACS Catal.* **2017,** *7* (7), 4822-4827.
54. Duan, Y. X.; Meng, F. L.; Liu, K. H.; Yi, S. S.; Li, S. J.; Yan, J. M.; Jiang, Q., Amorphizing of Cu nanoparticles toward highly efficient and robust electrocatalyst for CO_2 reduction to liquid fuels with high faradaic efficiencies. *Adv. Mater.* **2018,** *30* (14), 1706194.
55. Liu, Y.; Zhao, J.; Cai, Q., Pyrrolic-nitrogen doped graphene: a metal-free electrocatalyst with high efficiency and selectivity for the reduction of carbon dioxide to formic acid: a computational study. *Phys. Chem. Chem. Phys.* **2016,** *18* (7), 5491-5498.

Chapter 5 *In-situ* morphology transformation of bismuth-based catalysts for effective electroreduction of carbon dioxide

5.1 Introduction

Carbon dioxide (CO_2) has been considered as a kind of greenhouse gas with excessive emission, which has caused harmful effect on the earth's ecological environment. However, CO_2 can be also used as an important carbon resource.[1] Among many CO_2 utilization methods, electrocatalysis stands out because of the advantages of easy control, cleanliness, and sustainability.[2] Renewable resources such as solar energy and wind energy can be first converted into electrical energy and then coupled into a large-scale utilization of electrochemical reduction of CO_2 system to achieve energy conversion and storage.[3] Depends on different types of electrocatalysts and catalytic conditions, CO_2 can be reduced to a variety of hydrocarbons, such as methane (CH_4),[4-5], formic acid (HCOOH),[6-7] methanol (CH_3OH),[8-9] ethylene (C_2H_4),[10-11] ethanol (C_2H_5OH).[12-13] Among them, HCOOH is widely used in a variety of industrial synthesis processes as a common feedstock.[6] In addition, it can be used for direct HCOOH fuel cells or as a high energy density hydrogen storage chemical.[14] Because it is relatively easy to be obtained from CO_2 reduction and has a nearly 100% electron utilization efficiency under the action of some high-efficiency electrocatalysts, it is considered as an economically viable route for the CO_2 utilization.[15]

To date, various metal-based electrocatalysts such as Sn,[16] Bi,[17] In,[18] Pb,[19] and Co[20] have been widely used for the electrochemical reduction of CO_2 to HCOOH. Among them, Sn and Bi, as the two most popular catalysts, have been deeply studied. Generally, Bi-

based catalyst has a lower HCOOH formation overpotential and higher faradaic efficiency than Sn-based ones,[21] which is deemed to be the most promising electrocatalysts for practical industrial applications.[22] Therefore, various Bi-based catalysts such as Bi_2O_3-derived Bi,[23] Bi_2S_3-derived Bi,[24] BiOCl-derived Bi[25] and nitrogen-doped graphene quantum dots compound Bi_2O_3 nanosheets have been developed to catalyze the reduction of CO_2 to HCOOH.[26] It is found that the particle size,[27] lattice misalignment,[28] defect[29] and other physicochemical properties of the Bi-based catalyst have significant impacts on the catalytic performances by analyzing the relationship between the structure and properties.

In the previous studies, some researchers believed that the main active site of Bi-based catalysts was metal Bi^0 since the bismuth oxide-based electrocatalysts would be reduced to metal Bi^0 during CO_2 reduction.[30-32] However, with the deepening of research, many researchers have found that some metastable oxides exist in some metal-based catalysts even at a negative reduction potential during the electrochemical reduction of CO_2. For example, by using *in-situ* attenuated total reflectance infrared spectroscopy (ATR-IR), Bocarsly *et al.* confirmed such metastable oxides on the surface of Sn-based catalysts.[33] Our previous studies also found that the Sn site in the positive oxidation state had better catalytic performance.[34-35] Recently, some researchers have found the similar phenomena for the Bi-based catalysts. For instance, by using the *in-situ* X-ray absorption near edge structure (XANES) analysis, Nam *et al.* observed that 16.6% of Bi^{3+} was present on the BiO_x/C catalyst surface even at -1.51 V (vs Ag/AgCl).[17] Deng *et al.* found that the bismuth-oxygen structure of bismuth oxides should be beneficial for the adsorption of CO_2 to generate intermediates with a lower free energy in CO_2 electroreduction.[36] Therefore, the design and synthesis of electrocatalysts containing high-valence state of

Bi and maintaining them in a positive oxidation state as well as possible during the CO_2 electroreduction process may be an effective strategy to increase the catalytic activity.

In addition, some studies on the catalytic processes and mechanisms indicated that the carbonate (*CO_3H) adsorbed on the surface of the catalyst should be a probable intermediate that can be further reduced to *OOCH and *COOH intermediates.[17, 22, 33, 37] Therefore, the design and synthesis of the electrocatalyst containing carbonate species in itself may improve the electrocatalysis performance due to its presence in a similar imprinting effect by enhancing the initial intermediate adsorption. In view of this, bismuth subcarbonate ($Bi_2O_2CO_3$) was proposed as an electrocatalyst for CO_2 reduction by Lv *et al*. They synthesized the $Bi_2O_2CO_3$ nanosheets by hydrothermal method and then coated them on a glassy carbon electrode for the CO_2 reduction and found that it exhibited better catalytic activity at low overpotentials.[38] Besides, Bond *et al.* also used the electrochemical exfoliation method at a potential up to 10 V to prepare $Bi_2O_2CO_3$ nanosheets with few layers and then coated them on a carbon paper for the electrochemical reduction of CO_2.[39] However, both of these methods for the utilization of $Bi_2O_2CO_3$ electrocatalysts are too complicated and a binder (nafion) had to be used, making it less conducive to the industrial applications.[40] In addition, to the best our knowledge, the catalytic mechanism on electrochemical reduction of CO_2 over $Bi_2O_2CO_3$ is still unclear, and more researches on theoretical analysis are still necessary.

In this study, to further reduce the overpotential of CO_2RR, a bulk-structured Bi-based catalyst was synthesized using an electrodeposition method at first, but after a facile *in-situ* treatment process, it is observed that a significant surface morphology change from bulk-structure to petal-shaped nanostructure occurred. After careful characterization, it is found that a stable $Bi_2O_2CO_3$ species was spontaneously formed on the surface, which

resulted in the catalytic performance greatly improved. Subsequently, a comprehensive density functional theory (DFT) calculation was applied to compare and analyze the electrocatalytic properties of Bi and $Bi_2O_2CO_3$ species in order to understand the electrocatalytic mechanisms.

5.2 Methods

5.2.1 Preparation of electrodes and characterizations

Bi coated Cu foam electrode (Bi/Cu foam) was prepared by the potentiostatic deposition method in a 0.05 mol/L $BiCl_3$ (dissolved in 1M HCl) solution. In detail, the potential of -0.2 V was applied to a Cu foam support immersed in the $BiCl_3$/HCl solution for 10 minutes. Subsequently, the electrode was taken out and repeatedly washed with distilled water and dried in the air at 60 ^{o}C overnight. For the pretreatment of Bi/Cu foam electrode (named as Bi/Cu foam-*in-situ* treated*)*, the dried Bi/Cu foam electrode was first electrochemically treated by potentiostatic method at -1.6 V in a CO_2-saturated 0.1 M $KHCO_3$ solution for 2 h and then dried again in the air at 60 ^{o}C for 12 h.

Surface morphology and composition of the obtained electrode were charaterized by a scanning electron microscope (SEM) with an energy dispersive spectrometer (EDS), a X-ray diffractometer (XRD), a X-ray photoelectron spectroscopy (XPS), and a transmission electron microscope (TEM) instrument. Detail characterization information is given in the chapter 2.

5.2.2 Electrochemical reduction of CO_2

Electrochemical performance was evaluated by using a two-compartment electrochemical cell separated by a Nafion 117 membrane, which was continuously purged with a CO_2 gas flow of 10 cm^3 min^{-1} during the reaction. Reactor temperature was

controlled at 20±2 °C through a circulating water jacket connected to a temperature controller (UA-10S). A three-electrode system controlled by an electrochemical workstation (RST, 5090F) was used to evaluate the electrochemical performance of electrodes. An Ag/AgCl electrode saturated with KCl and a platinum (Pt) wire were applied as the reference and counter electrodes, respectively. Unless stated otherwise, all potentials present in this study were versus Ag/AgCl saturated KCl and current densities were normalized to the geometric surface (1×1 cm^2) of the electrode immersed in the electrolyte. The electrochemical reductions of CO_2 were performed by a constant potential method at various working potentials (i.e., -1.3, -1.4, -1.5, -1.6, -1.7, -1.8 V) for 1 h. All gas and electrolytes were collected and analyzed by a gas chromatography (GC) and a high performance liquid chromatography (HPLC) respectively to calculate faradaic efficiency.

5.2.3 DFT computational

In order to compare the electrocatalytic CO_2 reduction activities of Bi and $Bi_2O_2CO_3$ species, the crystalline structures of Bi and $Bi_2O_2CO_3$ were built firstly. Then, the Bi(012) and $Bi_2O_2CO_3$(001) crystal planes were cleaved from the corresponding unit cells to investigate the catalytic activity. The reason for the selecting of the Bi(012) crystal plane is that this crystal plane was observed in the TEM results. Besides, the Bi(012) crystal plane has been confirmed by most literatures that it exhibits the most favorable ability to adsorb *OOCH intermediate, thereby exhibiting better catalytic performance.[41-42] For $Bi_2O_2CO_3$, the (001) plane was chosen because it was alsoobserved as the main exposed crystal plane in the TEM results. Furthermore, the $Bi_2O_2CO_3$(001) plane is particularly easy to expose due to its largest lattice spacing (6.8 Å), which was also confirmed by a variety of reported $Bi_2O_2CO_3$ nanomaterials.[43-44] For the surface model, a 15 Å vacuum

space was built to avoid possible interactions in the Z direction. Subsequently, the CO_2 electroreduction mechanism was studied by optimizing the reactants, intermediates and product structures.

5.3 Results and discussion

5.3.1 Characterizations of electrodes

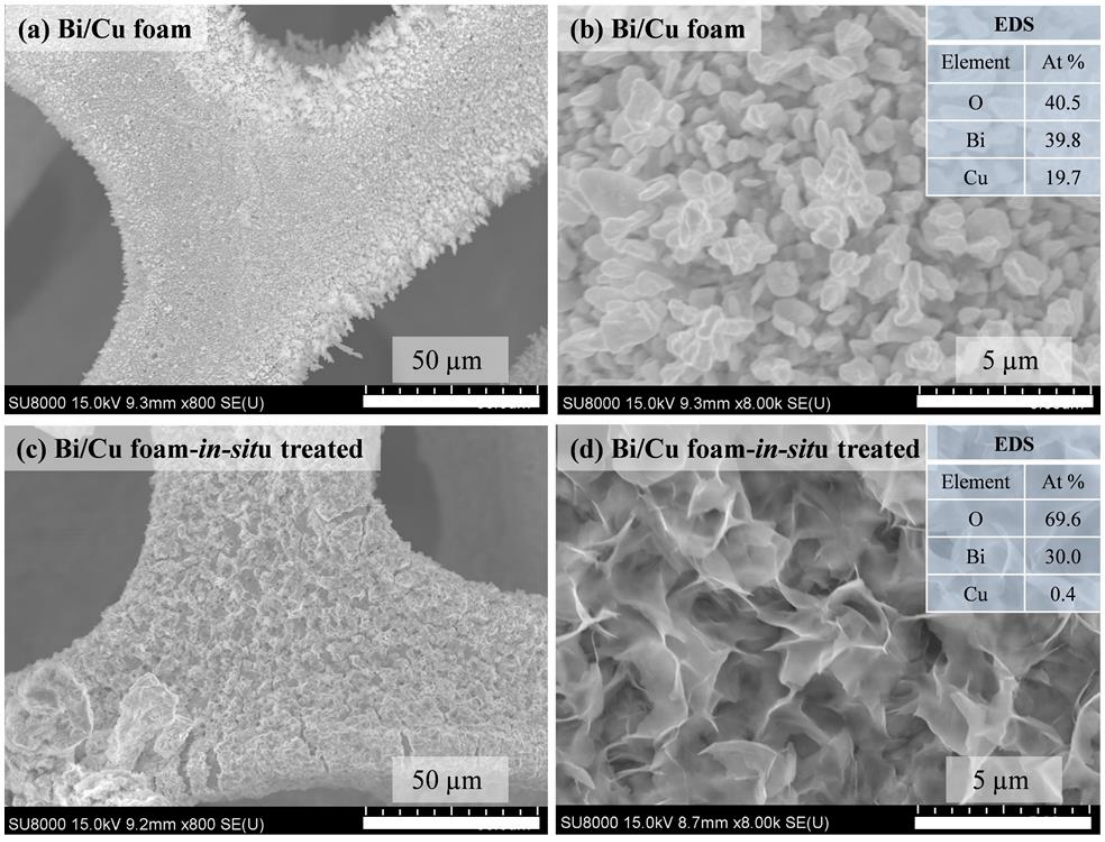

Figure 5.1 SEM images of (a, b) Bi/Cu foam and (c, d) Bi/Cu foam-*in-situ* treated electrodes with different scales. The upper right corners of the Figures b and d are the EDS results.

Cu foam was selected as the substrate due to its three-dimensional (3D) porous structure, which can provide sufficient specific surface area for the catalyst and simultaneously provide sufficient spaces for the electrocatalytic reaction. As can be seen

from Figure 5.1a and b, the granular catalyst particles were uniformly deposited on the surface of the Cu foam by the electrodeposition method. However, as can be seen from Figure 5.1c and d, the surface morphology of the electrocatalyst was changed from granular to petal-shaped nanosheet structure after the *in-situ* treatment. In general, such a petal-shaped nanosheet structure is rich in edges or unsaturated sites, which could effectively improve the electrocatalytic efficiency.[40] Lv *et al.*[38] and Bond *et al.*[39] *also had* synthesized the $Bi_2O_2CO_3$ nanosheets by hydrothermal and electrochemical exfoliation methods respectively. However, they obtained powder material had to be coated on a substrate with a nafion binder, and the electrochemical exfoliation method requires a potential up to 10 V. These complex and energy-consuming preparation methods limit its practical application.

The upper right corners of Figures 5.1b and d are the EDS results. Comparing the contents of O and Bi on the electrode surface before and after the *in-situ* treatment, it can be noted that the relative content of O increased from 40.5 to 69.6%. These results indicated that the nanosheet structural surface contained more O content. Other studies on Sn-based catalysts confirmed that such surface oxides had great contribution to the electrochemical reduction of CO_2[45-46] and a metastable oxide layer could be present on the catalyst surface even at relatively negative potentials.[33] Similarly, for the Bi-based catalysts, such surface oxides could also be benefit for the CO_2 reduction. The reasons for the morphology transformation and the increase in surface O content will be discussed in details in the following sections by combining XRD, XPS and TEM characterizations.

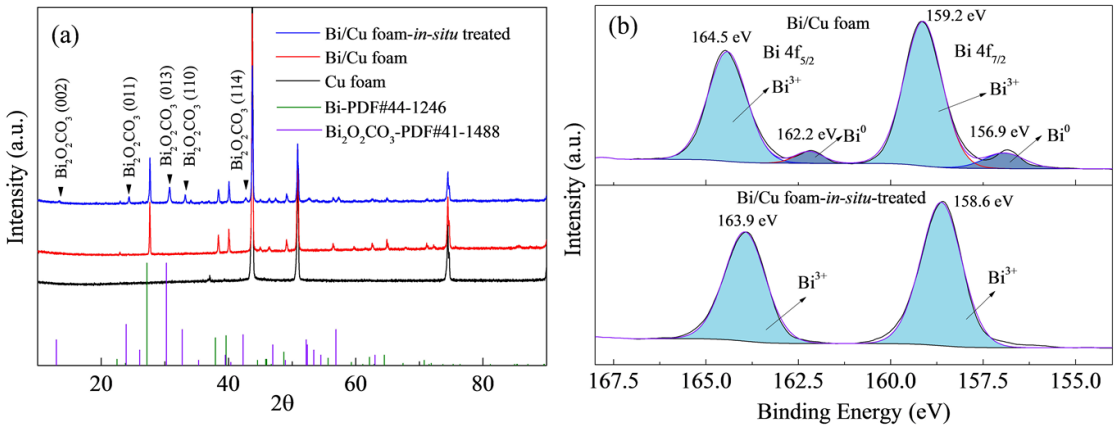

Figure 5.2 (a) XRD patterns and (b) high-resolution Bi 4f XPS spectra of Bi/Cu foam and Bi/Cu foam-*in-situ* treated electrodes.

To further analyze the cause of the morphology transformation, XRD and XPS analyses were carried out to characterize the crystalline structure, composition and surface elemental valence states of the catalyst. It can be seen from the XRD spectra in Figure 5.2a that except the Cu foam peaks, the remaining peaks of Bi/Cu foam electrode corresponded to the standard PDF card (no. 44-1246) of the metal Bi. However, after the *in-situ* treatment, some new peaks appeared in the spectrum, corresponding to $Bi_2O_2CO_3$, e.g., (002), (011), (013), (110) and (114) facets. In a previous report, Zhang *et al.* used BiOCl nanosheets-derived Bi-based catalyst for the electrochemical reduction of CO_2, and two new peaks in the XRD pattern also appeared after the electrocatalysis.[25] After careful comparison, we found that these two peaks also corresponded to the $Bi_2O_2CO_3$ species, however, they did not give a corresponding explanation. Recently, Lou *et al.* also observed the presence of the $Bi_2O_2CO_3$ species from the XRD analysis result after the electrocatalytic CO_2 reduction using Bi_2O_3 nanosheets grown on multi-channel carbon matrix catalyst.[47] However, the specific impact of this species on the electrocatalytic process was not fully discussed by them. Besides, from the XRD results we can see that

a large amount of metal Bi still present in the electrode after in-situ treatment, it should be noted that the presence of metal Bi in $Bi_2O_2CO_3$ should be conducive to electronic conductivity compared with $Bi_2O_2CO_3$ alone.

For the XPS spectra before and after the *in-situ* treatment (Figure 5.2b), the two groups of peaks in the Bi 4f spectrum belonged to Bi $4f_{5/2}$ and Bi $4f_{7/2}$, respectively. For the Bi/Cu foam electrode, the peaks at the high energy level peak positions of 164.5 and 159.2 eV corresponded to Bi^{3+} (in Bi_2O_3),[48] whereas the peaks at the low energy level peak positions of 162.2 and 156.9 eV corresponded to the metallic Bi^0.[49] However, after the *in-situ* treatment, the Bi^0 on the surface of the catalyst was no longer detected, and only Bi^{3+} species was observed. The inconsistencies in the analyses of XRD and XPS should be resulted from the two different analysis techniques, which focus on bulk and surface testing respectively. In addition, by comparing the positions of the Bi^{3+} peaks before and after the electrochemical treatment, it can be found that the position of the peaks had a significant shift. The shifted peaks to 163.9 and 158.6 eV just corresponded to the Bi^{3+} in $Bi_2O_2CO_3$, which is consistent with the reported result.[44] Therefore, from the XRD and XPS analysis results, it can be concluded that $Bi_2O_2CO_3$ species were formed on the electrode surface after the *in-situ* treatment. Because $Bi_2O_2CO_3$ has a higher O content than Bi_2O_3, the surface O content will be greatly increased after the *in-situ* treatment.

In order to understand the mechanism of $Bi_2O_2CO_3$ formation, a series of parallel experiments were performed to explore the conditions of morphology transformation. The results showed that the electrochemical treatment and drying in air were two necessary steps for the forming of such petal-shaped $Bi_2O_2CO_3$ nanosheets. Combined the above analysis results, it can be inferred that the following processes may exist during the *in-situ* treatment process.

$$CO_2 + H_2O + 2e^- \rightleftharpoons HCOO^- + OH^- \quad (5\text{-}1)$$

$$CO_2 + H_2O + 2e^- \rightleftharpoons CO + 2OH^- \quad (5\text{-}2)$$

$$2H_2O + 4e^- \rightleftharpoons H_2 + 2OH^- \quad (5\text{-}3)$$

$$Bi^{3+} + OH^- \rightleftharpoons Bi(OH)_3 \quad (5\text{-}4)$$

$$2Bi(OH)_3 + CO_2 \rightleftharpoons Bi_2O_2CO_3 + 3H_2O \quad (5\text{-}5)$$

$$4Bi + 3O_2 + 2H_2O \rightleftharpoons 4BiO^+ + 4OH^- \quad (5\text{-}6)$$

$$2BiO^+ + CO_3^{2-} \rightleftharpoons Bi_2O_2CO_3 \quad (5\text{-}7)$$

Firstly, the metal Bi exposed to air easily results in the formation of a surface oxide layer (Bi^{3+}), which was also confirmed by the above XPS analysis results. Usually, such an oxide layer could be present even at a negative potential during the CO_2 reduction.[17, 33, 37] Thereafter, in the process of electrochemical reduction of CO_2, it is reported that some reactions as shown in equations of 1-3 may occur on the surface of the cathode, thereby accumulating a large amount of OH^- on the surface of the cathode, resulting in local alkalinity.[50] As such, in this situation, the OH^- reacting with the Bi^{3+} could occur on the surface of the electrode to form $Bi(OH)_3$. However, $Bi(OH)_3$ is always unstable, which easily reacts with CO_2 to form $Bi_2O_2CO_3$ as shown in the equations of 4-5. Besides, it is also reported that the metal Bi exposed to the air can also be oxidized to BiO^+ and further reacted with CO_3^{2-} to form $Bi_2O_2CO_3$ species as shown in equations of 6-7.[39] Since the $Bi_2O_2CO_3$ is a layer structure material,[51] the morphology of the electrocatalyst was also changed after the *in-situ* treatment.

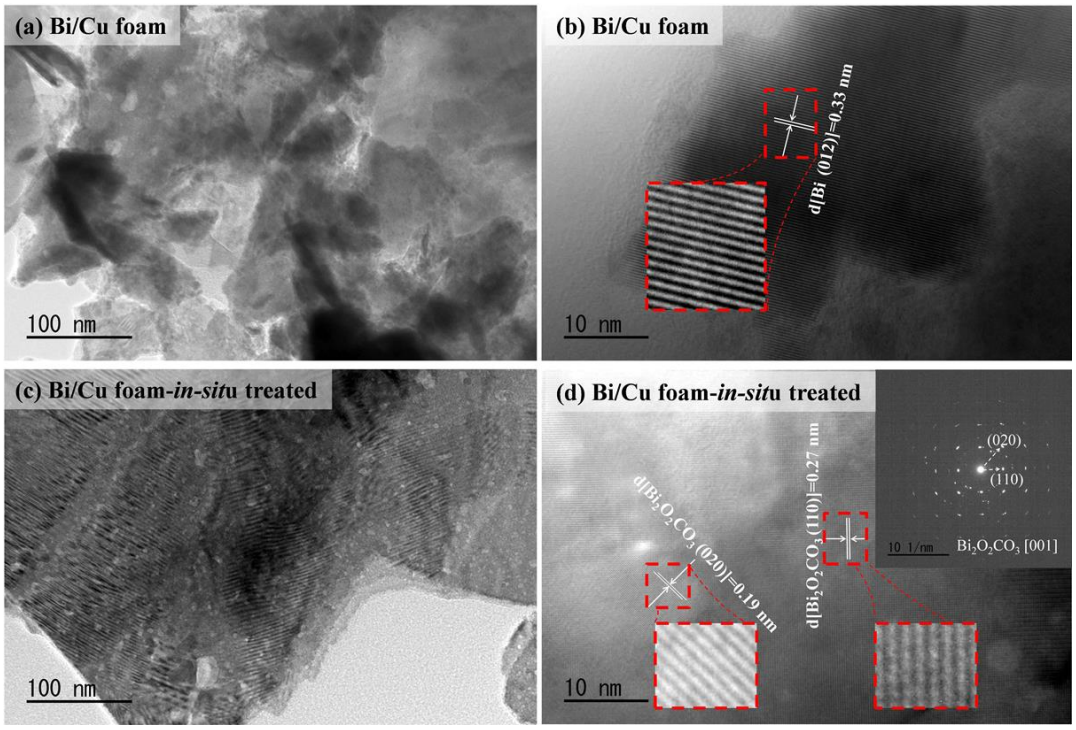

Figure 5.3 TEM and selected area electron diffraction (SAED) pattern (inset d) images of the (a, b) Bi/ Cu foam and (c, d) Bi/Cu foam-*in-situ* treated electrodes.

TEM measurement was used to reconfirm the composition of the electrocatalyst surface before and after the *in-situ* treatment. Comparing Figure 5.3a with 3c, it is found that a layered structure was formed on the surface of the catalyst after the *in-situ* treatment, which is consistent with the forementioned $Bi_2O_2CO_3$ species with a layered structure. For Bi/Cu foam electrode, it can also be seen from Figure 5.3b that before the *in-situ* treatment, the lattice fringe with a spacing of 0.33 nm corresponded to Bi(012) crystal plane, which was also observed as the main peak in the XRD spectrum. Some researches also indicated that the high-index crystal of Bi metal played a major role in CO_2 electroreduction, especially the Bi(012) crystal plane exhibited the most favorable ability to adsorb *OOCH intermediate.[41-42] For the electrode after the *in-situ* treatment as shown in Figure 5.3d, the lattice fringe with the spacing of 0.19 nm belonged to the

$Bi_2O_2CO_3$(020) crystal plane, and the lattice fringe with the spacing of 0.27 nm was the $Bi_2O_2CO_3$(110) crystal plane. The inserted SADE image in Figure 5.3d indicated that the $Bi_2O_2CO_3$(001) crystal plane was mainly exposed on the surface of the electrocatalyst after the *in-situ* treatment.[43] Therefore, TEM analysis reconfirmed the formation of $Bi_2O_2CO_3$ species on the surface after the *in-situ* electrochemical treatment.

5.3.2 Electrochemical reduction of CO_2

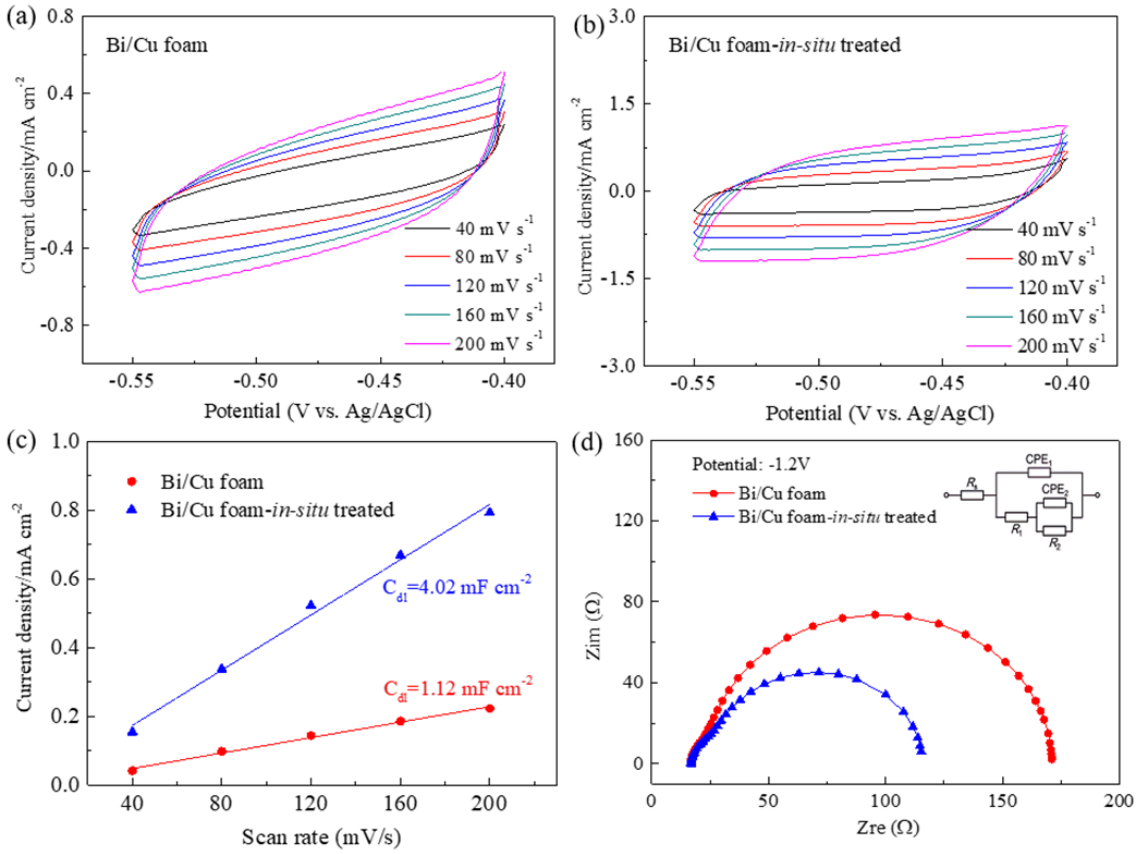

Figure 5.4 (a, b and c) Determination of electrochemical double layer capacitance and (d) electrochemical impedance spectroscopy (EIS) tests for Bi/Cu foam and Bi/Cu foam-in-situ treated electrodes.

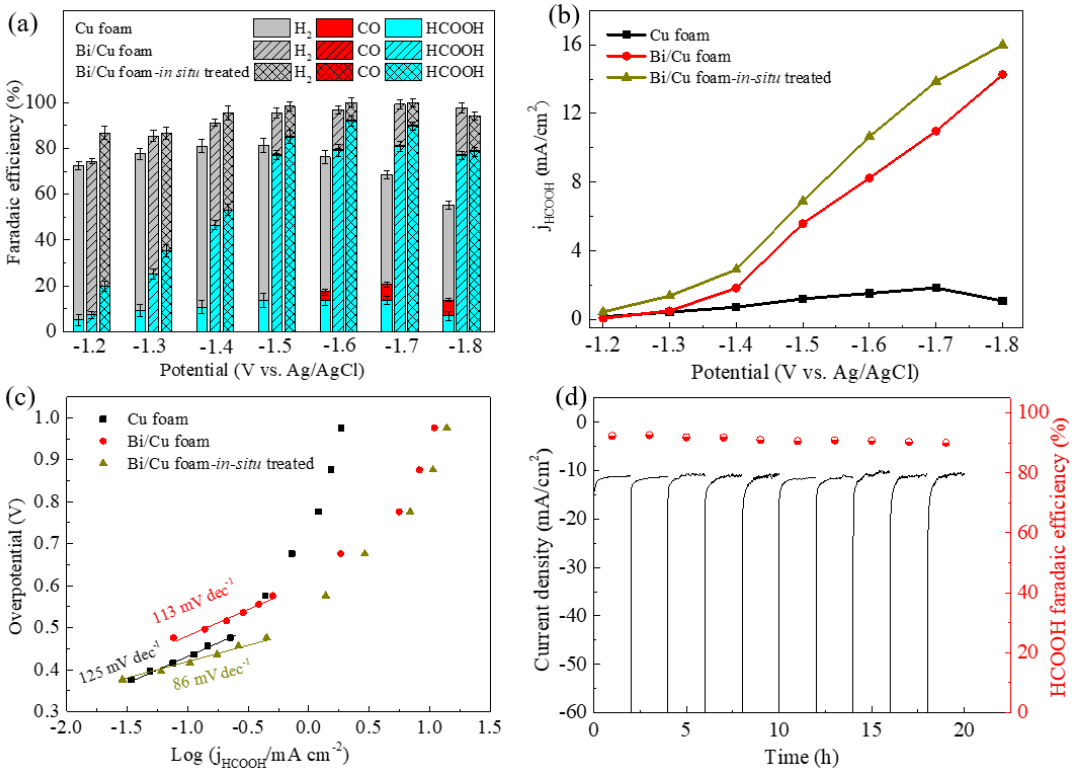

Figure 5.5 (a) Faradaic efficiencies of HCOOH, CO and H_2, (b) HCOOH partial current densities and (c) Tafel plots of Cu foam, Bi/Cu foam and Bi/Cu foam-*in-situ* treated electrodes. (d) Periodic operation for a long-term stability test of the Bi/Cu foam-*in-situ* treated electrode.

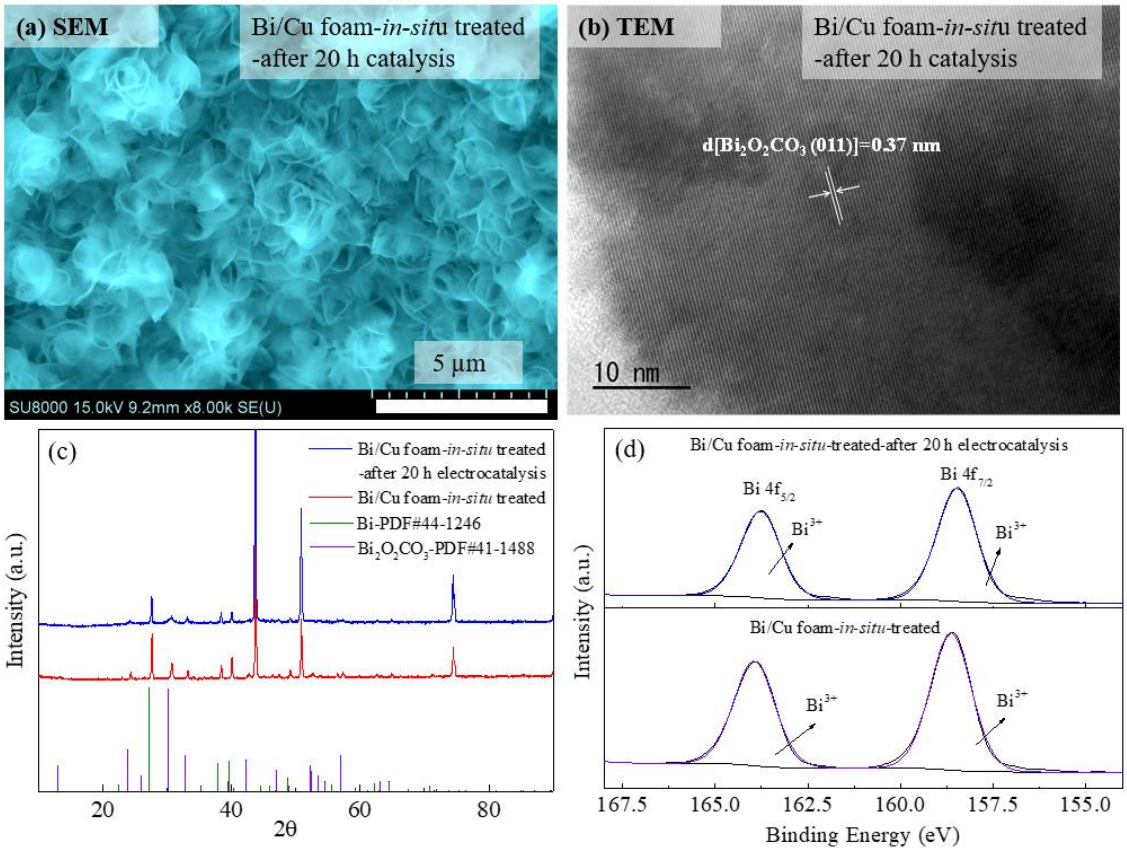

Figure 5.6 (a) SEM and (b) TEM images of Bi/Cu foam-in-situ treated electrode after 20 h electrocatalysis. (c) XRD patterns and (d) high-resolution Bi 4f XPS spectra of Bi/Cu foam-in-situ treated electrode before and after 20 h electrocatalysis.

As mentioned above, we obtained the electrocatalyst riched in $Bi_2O_2CO_3$ species by a simple *in-situ* treatment. In order to investigate the electrochemical activity of the electrode, the electrochemical double layer capacitance and electrochemical impedance spectroscopy (EIS) were firstly measured. It is found that the electrode after the *in-situ* treatment had a larger double layer capacity but a smaller charge transfer resistance (Figure 5.4), which should be beneficial for the electrocatalytic process.

In order to further compare the catalytic performances of the two electrodes for electrocatalytic CO_2 reduction, potentiostatic tests were performed at a series of different

potentials to calculate the faradaic efficiency. The liquid and gas phase products were collected after the electrolysis for one hour in a CO_2 saturated 0.1 M $KHCO_3$ solution continuously with CO_2 gas flow. In addition, the electrocatalytic activity of Cu foam substrate was also tested. As shown in Figure 5.5a, the Cu foam exhibited no more than 20% HCOOH faradaic efficiency. In contrast, after the surface was coated by Bi species, the electrocatalytic reduction of CO_2 to HCOOH was obviously enhanced with a total faradaic efficiency of HCOOH, H_2 and CO close to 100%, which is consistent with the most reported Bi-based catalysts.[17, 41] From the comparison of the faradaic efficiencies before and after the *in-situ* treatment in Figure 5.5a, it can be seen that the *in-situ* treatment obviously improved the faradaic efficiency of HCOOH, up to 92% at -1.6 V. The partial current density of the HCOOH showed in Figure 5.5b also indicated that the electrode after the *in-situ* treatment had a higher current density, suggesting that the rate of electrocatalytic reduction of CO_2 to HCOOH was improved.

Since the reduction of CO_2 to HCOOH or CO is a two-electron transfer reaction, two electrons are generally considered to be transferred in steps.[52] The first electron transfer step can activate CO_2 to form a *COOH or *OOCH intermediate, and then the second electron transfer step further reduces the intermediate to product.[53-54] Generally, the information of the reaction kinetics can be obtained by the Tafel plot analysis. Therefore, the potentiostatic electrolysis was performed at the low overpotential region where the reaction was kinetically controlled to obtain the Tafel slope as shown in Figure 5.5c. One can see that the Tafel slope of Cu foam was 125 mV dec^{-1}, which indicated that the first electron transfer step in the CO_2 reduction process was the rate-limiting step in this case.[52] After it was coated with Bi, the Tafel slope only decreased slightly to 113 mV dec^{-1}. However, after the *in-situ* treatment, the electrode showed a Tafel slope as low as 86 mV

dec^{-1}, which is close to that of pure $Bi_2O_2CO_3$ species reported by Lv *et al.*[38] Generally, the smaller Tafel slope indicates that the electrocatalyst has a lower rate-limiting activation energy barrier, which is advantageous for practical applications.[55] Also, as reported in the literature, the lower Tafel slope for the *in-situ* treated electrode indicated that the rate-limiting step of the catalytic process over it may be changed to the second electron transfer step.[28, 52] Finally, the stability of the Bi/Cu foam *in-situ* treated electrode by refreshing the electrolyte and performing the product analysis every two hours. As shown in Figure 5.5d, the current density was basically stable whereas the HCOOH faradaic efficiency remained above 90% during 20 hours. After the stability test, the electrode was re-characterized by SEM, TEM, XRD and XPS, and it is found that the electrode surface morphology and composition remained almost unchanged (Figure 5.6).

5.3.3 Mechanism analysis

As observed above, the electrode with the *in-situ* formed $Bi_2O_2CO_3$ species exhibited better performance. Lv *et al.*[38] and Zhang *et al.*[39] also found that the $Bi_2O_2CO_3$ species had better electrocatalytic CO_2 reduction performance than the metal Bi. However, up to now, no DFT calculations were performed to explain this phenomenon, and understand the mechanism. Herein, the DFT calculations were used to compare the electrocatalytic properties of the Bi and $Bi_2O_2CO_3$ species. According to our previous researches[34-35] and most reported results [29, 42, 56], during the electrochemical reduction of CO_2 to HCOOH or CO, *COOH and *OOCH intermediates species will be formed and adsorbed on the surface of the catalyst before being further reduced as shown in the following equations of 8-9.

$$CO_2 + H^+ + e^- + * \rightarrow *COOH \qquad (5\text{-}8)$$

$$CO_2 + H^+ + e^- + * \rightarrow *OOCH \quad (5\text{-}9)$$

Here, the *OOCH is the main intermediate for producing HCOOH whereas the *COOH is the main intermediate for producing CO.[53] Especially, the *OOCH is more likely to form on the surfaces of Sn, Pb and Bi since these metals have strong binding ability with O in the *OOCH, thus exhibiting high HCOOH selectivity. In comparison, *COOH is more likely to form on the surface of Au, Ag, and Zn, showing high selectivity of CO since these metals can interacted with C of *COOH. Therefore, the binding energy of the catalyst surface to the *COOH or *OOCH intermediate is usually used as a descriptor to explain the electrocatalytic performance. Generally, such a descriptor has a volcanic trend with an optimal value, neither too large nor too small. Too weak adsorption could lead to the difficulty in the formation and stabilizing the intermediates, whereas too strong adsorption could cause the intermediate difficult to be further reduced and desorbed, thus affecting its catalytic performance.[54]

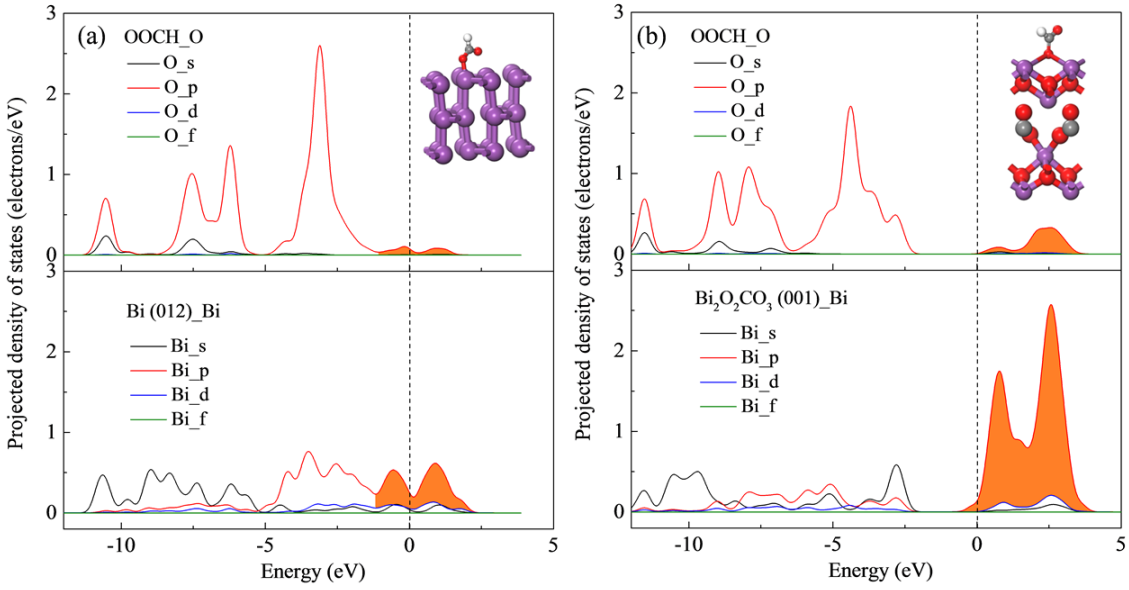

Figure 5.7 Projected density of states (PDOS) of O of *OOCH intermediate and Bi atoms on the (a) Bi(012) and (b) $Bi_2O_2CO_3$(001) facets. The Fermi level is denoted with a

dashed line.

In order to understand the higher catalytic activity of $Bi_2O_2CO_3$ species, the binding energies of Bi(012) and $Bi_2O_2CO_3$(001) facets to *COOH and *OOCH species were calculated firstly. The binding energies of Bi(012) facet to *COOH and *OOCH were -1.41 and -2.33eV, respectively, which were much lower than those of $Bi_2O_2CO_3$(001) facet to *COOH and *OOCH with values of -1.77 and -3.41eV, respectively, indicating that the binding ability of $Bi_2O_2CO_3$(001) facet to *COOH and *OOCH was higher than that of Bi(012) facet. Furthermore, the projected density of states (PDOS) of *COOH and *OOCH adsorbed on Bi(012) and $Bi_2O_2CO_3$(001) facets were calculated in order to analyze this stronger binding ability. Figure 5.7 shows the results for the *OOCH on the two crystal faces, in which the stronger orbital hybridization of O 2p with Bi 6p states was observed near the Fermi level for the *OOCH intermediate adsorbed on $Bi_2O_2CO_3$(001). This stronger orbital hybridization should be the source of the stronger binding ability of the $Bi_2O_2CO_3$(001) facet to the *OOCH intermediate species. However, as mentioned above, the strong binding ability for the intermediate does not necessarily mean the good catalytic performance since it could also prevent further reduction. Therefore, the Gibbs free energy was further calculated to reflect the free energy change in the CO_2 electroreduction process. Herein, the formation free energy barrier of the intermediate was calculated according to equations of 8-9, and then for the further reduction of the intermediate to the HCOOH and CO, the free energy barrier was calculated according to equations of 10-12.

$$*COOH + H^+ + e^- \rightarrow * + HCOOH \quad (5\text{-}10)$$

$$*OOCH + H^+ + e^- \rightarrow * + HCOOH \quad (5\text{-}11)$$

$$*COOH + H^+ + e^- \rightarrow * + CO + H_2O \quad (5\text{-}12)$$

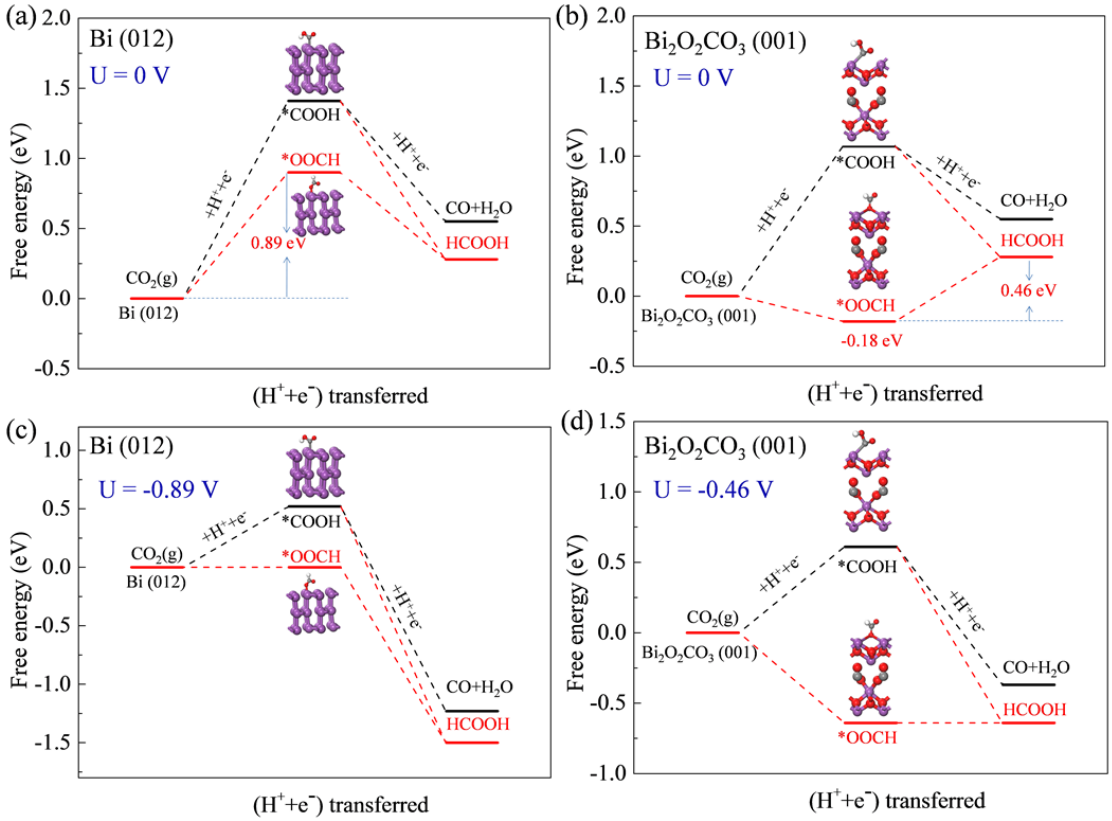

Figure 5.8 Calculated free energy diagrams without (a, b) and with applied potential (c, d) for the electroreduction of CO_2 to HCOOH and CO on Bi (012) and $Bi_2O_2CO_3$ (001) facets.

Figure 5.8 shows the changes in free energy for the reductions of CO_2 to HCOOH and CO on the Bi(012) and $Bi_2O_2CO_3$ (001) facets, respectively. It can be seen from Figure 5.8a that the *OOCH had a lower formation energy barrier (0.89 eV) than the formation of the *COOH intermediate for the Bi (012) facet, making it more easily form HCOOH, even compared to the formation energy barrier of the *H intermediate for H_2 evolution (0.93 eV), which is similar to the trend reported in the literature.[41-42] In contrast, for the $Bi_2O_2CO_3$ (001) facet, it can be seen from Figure 5.8b that due to its strong binding ability

to the *OOCH intermediate, the *OOCH species were extremely easily formed on the surface. Herein, the change of free energy was -0.18V, and the negative value indicates that this step is an exergonic step. This strong binding ability to the *OOCH intermediate also causes the rate-limiting step for forming HCOOH to be the second electron transfer step (Energy barrier: 0.46 eV) as shown in Figure 5.8b, which is in agreement with the Tafel slope analysis. This may be the main reason why $Bi_2O_2CO_3$ species exhibited higher catalytic activity.

In addition, since the CO_2 electroreduction reaction occurs under a certain potential, in order to investigate the effect of electrode potential on the free energy, a negative electrode potential was applied for eliminating the energy barriers of the rate-limiting step according to the method developed by Nørskov and co-workers.[57] That is, the negative electrode potentials of -0.89 and -0.47 V (vs. normal hydrogen electrode, NHE) were applied to the Bi(012) and $Bi_2O_2CO_3$(001) facets, respectively. The calculation results shown in Figures 5.8c and d indicated that each step of the pathway for producing HCOOH became exergonic at the specified potential. However, the pathway for producing CO was still endergonic, which means that under such an onset electrode potential, only HCOOH was the product of CO_2 electroreduction. In the experiments, HCOOH was also detected at a lower overpotential, but CO was only detected at a higher overpotential, which is consistent with the calculation results.

5.4 Conclusions

In summary, when a bulk-structure Bi-based catalyst prepared by the potentiostatic electrodeposition method in a $BiCl_3$/HCl system was applied it for the electrocatalytic CO_2 reduction, it is surprising that the surface morphology of this catalyst changed to petal-shaped nanosheet structure after a facile *in-situ* treatment process. The

physicochemical characterizations by SEM, TEM, EDS, XRD and XPS indicated that the change in morphology was due to the formation of $Bi_2O_2CO_3$ nanosheets on the surface of Bi coated electrode after the *in-situ* treatment. Electrochemical characterization showed that Bi coated electrode with the formed $Bi_2O_2CO_3$ species had higher electrochemically active surface area and lower charge transfer resistance. The electrocatalytic performance tests showed that the Bi-based catalyst after the morphology transformation had better electrocatalytic activity for the CO_2 reduction to HCOOH. The highest HCOOH faradaic efficiency reached to 92% at -1.6 V at a current density of 10 mA cm^{-2} with a long-term stability in 20 h operation.

Subsequently, DFT calculations were performed to compare the electrocatalytic CO_2 reduction performances of the Bi and $Bi_2O_2CO_3$ species. PDOS analyses revealed that the stronger orbital hybridization of O 2p with Bi 6p states near the Fermi level for *OOCH intermediate adsorbed on $Bi_2O_2CO_3$ (001) resulted in stronger adsorption of *OOCH intermediate. The rate-limiting step of reducing CO_2 to HCOOH became to the second-step electron transfer step due to this strong adsorption, which was consistent with the Tafel slope analysis results. All in all, this work provided a facile method for the *in-situ* preparation of petal-shaped $Bi_2O_2CO_3$ nanosheets based catalyst, and systematically analyzed the $Bi_2O_2CO_3$ formation mechanism and catalytic mechanism, which is expected to give a meaningful reference for the electrocatalytic CO_2 reduction.

References

1. Zhang, W.; Hu, Y.; Ma, L.; Zhu, G.; Wang, Y.; Xue, X.; Chen, R.; Yang, S.; Jin, Z., Progress and perspective of electrocatalytic CO_2 reduction for renewable carbonaceous fuels and chemicals. *Adv. Sci.* **2018,** *5* (1), 1700275.
2. Jin, H.; Guo, C.; Liu, X.; Liu, J.; Vasileff, A.; Jiao, Y.; Zheng, Y.; Qiao, S. Z., Emerging two-dimensional nanomaterials for electrocatalysis. *Chem. Rev.* **2018,** *118* (13), 6337-6408.

3. Daiyan, R.; Lu, X.; Ng, Y. H.; Amal, R., Liquid hydrocarbon production from CO_2: recent development in metal-based electrocatalysis. *ChemSusChem* **2017,** *10* (22), 4342-4358.
4. Liu, X.; Yang, H.; He, J.; Liu, H.; Song, L.; Li, L.; Luo, J., Highly active, durable ultrathin $MoTe_2$ layers for the electroreduction of CO_2 to CH_4. *Small* **2018,** *14* (16), 1704049.
5. Sun, X.; Kang, X.; Zhu, Q.; Ma, J.; Yang, G.; Liu, Z.; Han, B., Very highly efficient reduction of CO_2 to CH_4 using metal-free N-doped carbon electrodes. *Chem. Sci.* **2016,** *7* (4), 2883-2887.
6. Zheng, X.; De Luna, P.; García de Arquer, F. P.; Zhang, B.; Becknell, N.; Ross, M. B.; Li, Y.; Banis, M. N.; Li, Y.; Liu, M.; Voznyy, O.; Dinh, C. T.; Zhuang, T.; Stadler, P.; Cui, Y.; Du, X.; Yang, P.; Sargent, E. H., Sulfur-modulated tin sites enable highly selective electrochemical reduction of CO_2 to formate. *Joule* **2017,** *1* (4), 794-805.
7. Gao, S.; Sun, Z.; Liu, W.; Jiao, X.; Zu, X.; Hu, Q.; Sun, Y.; Yao, T.; Zhang, W.; Wei, S.; Xie, Y., Atomic layer confined vacancies for atomic-level insights into carbon dioxide electroreduction. *Nat. Commun.* **2017,** *8*, 14503.
8. Sun, X.; Zhu, Q.; Kang, X.; Liu, H.; Qian, Q.; Zhang, Z.; Han, B., Molybdenum-bismuth bimetallic chalcogenide nanosheets for highly efficient electrocatalytic reduction of carbon dioxide to methanol. *Angew. Chem. Int. Ed.* **2016,** *55* (23), 6771-6775.
9. Lu, L.; Sun, X. F.; Ma, J.; Yang, D. X.; Wu, H. H.; Zhang, B. X.; Zhang, J. L.; Han, B. X., Highly efficient electroreduction of CO_2 to methanol on palladium-copper bimetallic aerogels. *Angew. Chem. Int. Ed.* **2018,** *57* (43), 14149-14153.
10. Ma, M.; Djanashvili, K.; Smith, W. A., Controllable hydrocarbon formation from the electrochemical reduction of CO_2 over Cu nanowire arrays. *Angew. Chem. Int. Ed. Engl.* **2016,** *55* (23), 6680-4.
11. Ning, H.; Mao, Q.; Wang, W.; Yang, Z.; Wang, X.; Zhao, Q.; Song, Y.; Wu, M., N-doped reduced graphene oxide supported Cu_2O nanocubes as high active catalyst for CO_2 electroreduction to C_2H_4. *J. Alloys Compd.* **2019,** *785*, 7-12.
12. Liu, Y.; Zhang, Y.; Cheng, K.; Quan, X.; Fan, X.; Su, Y.; Chen, S.; Zhao, H.; Zhang, Y.; Yu, H.; Hoffmann, M. R., Selective electrochemical reduction of carbon dioxide to ethanol on a boron- and nitrogen-Co-doped nanodiamond. *Angew. Chem. Int. Ed. Engl.* **2017,** *56* (49), 15607-15611.
13. Song, Y.; Peng, R.; Hensley, D. K.; Bonnesen, P. V.; Liang, L.; Wu, Z.; Meyer, H. M.; Chi, M.; Ma, C.; Sumpter, B. G.; Rondinone, A. J., High-selectivity electrochemical conversion of CO_2 to ethanol using a copper nanoparticle/N-doped

graphene electrode. *ChemistrySelect* **2016,** *1* (19), 6055-6061.

14. Wang, J.; Li, X.; Zheng, J.; Cao, J.; Hao, X.; Wang, Z.; Abudula, A.; Guan, G., Non-precious molybdenum-based catalyst derived from biomass: CO-Free hydrogen production from formic acid at low temperature. *Energy Convers. Manage.* **2018,** *164*, 122-131.
15. Verma, S.; Kim, B.; Jhong, H. R. M.; Ma, S.; Kenis, P. J., A gross-margin model for defining technoeconomic benchmarks in the electroreduction of CO_2. *ChemSusChem* **2016,** *9* (15), 1972-1979.
16. Irtem, E.; Andreu, T.; Parra, A.; Hernández-Alonso, M. D.; García-Rodríguez, S.; Riesco-García, J. M.; Penelas-Pérez, G.; Morante, J. R., Low-energy formate production from CO_2 electroreduction using electrodeposited tin on GDE. *J. Mater. Chem. A* **2016,** *4* (35), 13582-13588.
17. Lee, C. W.; Hong, J. S.; Yang, K. D.; Jin, K.; Lee, J. H.; Ahn, H.-Y.; Seo, H.; Sung, N.-E.; Nam, K. T., Selective electrochemical production of formate from carbon dioxide with bismuth-based catalysts in an aqueous electrolyte. *ACS Catal.* **2018,** *8* (2), 931-937.
18. Zhang, Z.; Ahmad, F.; Zhao, W.; Yan, W.; Zhang, W.; Huang, H.; Ma, C.; Zeng, J., Enhanced electrocatalytic reduction of CO_2 via chemical coupling between indium oxide and reduced graphene oxide. *Nano Lett.* **2019,** *19* (6), 4029-4034.
19. Fan, M.; Garbarino, S.; Botton, G. A.; Tavares, A. C.; Guay, D., Selective electroreduction of CO_2 to formate on 3D[100] Pb dendrites with nanometer-sized needle-like tips. *J. Mater. Chem. A* **2017,** *5* (39), 20747-20756.
20. Gao, S.; Lin, Y.; Jiao, X.; Sun, Y.; Luo, Q.; Zhang, W.; Li, D.; Yang, J.; Xie, Y., Partially oxidized atomic cobalt layers for carbon dioxide electroreduction to liquid fuel. *Nature* **2016,** *529* (7584), 68-71.
21. Lv, W.; Zhou, J.; Bei, J.; Zhang, R.; Wang, L.; Xu, Q.; Wang, W., Electrodeposition of nano-sized bismuth on copper foil as electrocatalyst for reduction of CO_2 to formate. *Appl. Surf. Sci.* **2017,** *393*, 191-196.
22. Wen, G.; Lee, D. U.; Ren, B.; Hassan, F. M.; Jiang, G.; Cano, Z. P.; Gostick, J.; Croiset, E.; Bai, Z.; Yang, L.; Chen, Z., Orbital interactions in Bi-Sn bimetallic electrocatalysts for highly selective electrochemical CO_2 reduction toward formate production. *Adv. Energy. Mater.* **2018,** *8* (31), 1802427.
23. Bertin, E.; Garbarino, S.; Roy, C.; Kazemi, S.; Guay, D., Selective electroreduction of CO_2 to formate on Bi and oxide-derived Bi films. *J. CO_2 Util.* **2017,** *19*, 276-283.
24. Zhang, Y.; Li, F.; Zhang, X.; Williams, T.; Easton, C. D.; Bond, A. M.; Zhang, J., Electrochemical reduction of CO_2 on defect-rich Bi derived from Bi_2S_3 with

enhanced formate selectivity. *J. Mater. Chem. A* **2018,** *6* (11), 4714-4720.

25. Zhang, H.; Ma, Y.; Quan, F.; Huang, J.; Jia, F.; Zhang, L., Selective electro-reduction of CO_2 to formate on nanostructured Bi from reduction of BiOCl nanosheets. *Electrochem. Commun.* **2014,** *46*, 63-66.
26. Chen, Z.; Mou, K.; Wang, X.; Liu, L., Nitrogen-doped graphene quantum dots enhance the activity of Bi_2O_3 Nanosheets for electrochemical reduction of CO_2 in a wide negative potential region. *Angew. Chem. Int. Ed.* **2018,** *57* (39), 12790-12794.
27. Kim, S.; Dong, W. J.; Gim, S.; Sohn, W.; Park, J. Y.; Yoo, C. J.; Jang, H. W.; Lee, J.-L., Shape-controlled bismuth nanoflakes as highly selective catalysts for electrochemical carbon dioxide reduction to formate. *Nano Energy* **2017,** *39*, 44-52.
28. Zhang, X.; Sun, X.; Guo, S.-X.; Bond, A. M.; Zhang, J., Formation of lattice-dislocated bismuth nanowires on copper foam for enhanced electrocatalytic CO_2 reduction at low overpotential. *Energy Environ. Sci.* **2019,** *12* (4), 1334-1340.
29. Gong, Q.; Ding, P.; Xu, M.; Zhu, X.; Wang, M.; Deng, J.; Ma, Q.; Han, N.; Zhu, Y.; Lu, J.; Feng, Z.; Li, Y.; Zhou, W.; Li, Y., Structural defects on converted bismuth oxide nanotubes enable highly active electrocatalysis of carbon dioxide reduction. *Nat. Commun.* **2019,** *10* (1), 2807.
30. He, S.; Ni, F.; Ji, Y.; Wang, L.; Wen, Y.; Bai, H.; Liu, G.; Zhang, Y.; Li, Y.; Zhang, B.; Peng, H., The p-Orbital delocalization of main-group metals to boost CO_2 electroreduction. *Angew. Chem. Int. Ed. Engl.* **2018,** *57* (49), 16114-16119.
31. Su, P.; Xu, W.; Qiu, Y.; Zhang, T.; Li, X.; Zhang, H., Ultrathin bismuth nanosheets as highly efficient electrocatalyst for CO_2 reduction. *ChemSusChem* **2018,** *11* (5), 848-853.
32. Qiu, Y.; Du, J.; Dong, W.; Dai, C.; Tao, C., Selective conversion of CO_2 to formate on a size tunable nano-Bi electrocatalyst. *J. CO_2 Util.* **2017,** *20*, 328-335.
33. Baruch, M. F.; Pander, J. E.; White, J. L.; Bocarsly, A. B., Mechanistic insights into the reduction of CO_2 on tin electrodes using in situ ATR-IR spectroscopy. *ACS Catal.* **2015,** *5* (5), 3148-3156.
34. An, X.; Li, S.; Yoshida, A.; Wang, Z.; Hao, X.; Abudula, A.; Guan, G., Electrodeposition of tin-based electrocatalysts with different surface tin species distributions for electrochemical reduction of CO_2 to HCOOH. *ACS Sustain. Chem. Eng.* **2019,** *7* (10), 9360-9368.
35. An, X.; Li, S.; Yoshida, A.; Yu, T.; Wang, Z.; Hao, X.; Abudula, A.; Guan, G., Bi-doped SnO nanosheets supported on Cu foam for electrochemical reduction of CO_2 to HCOOH. *ACS Appl. Mater. Interfaces* **2019,** *11* (45), 42114-42122.
36. Deng, P.; Wang, H.; Qi, R.; Zhu, J.; Chen, S.; Yang, F.; Zhou, L.; Qi, K.; Liu, H.;

Xia, B. Y., Bismuth oxides with enhanced bismuth-oxygen structure for efficient electrochemical reduction of carbon dioxide to formate. *ACS Catal.* **2020,** *10* (1), 743-750.

37. Cui, C.; Han, J.; Zhu, X.; Liu, X.; Wang, H.; Mei, D.; Ge, Q., Promotional effect of surface hydroxyls on electrochemical reduction of CO_2 over SnO_x/Sn electrode. *J. Catal.* **2016,** *343*, 257-265.
38. Lv, W.; Bei, J.; Zhang, R.; Wang, W.; Kong, F.; Wang, L.; Wang, W., $Bi_2O_2CO_3$ nanosheets as electrocatalysts for selective reduction of CO_2 to formate at low overpotential. *ACS Omega* **2017,** *2* (6), 2561-2567.
39. Zhang, Y.; Zhang, X.; Ling, Y.; Li, F.; Bond, A. M.; Zhang, J., Controllable synthesis of few-layer bismuth subcarbonate by electrochemical exfoliation for enhanced CO_2 reduction Performance. *Angew. Chem. Int. Ed.* **2018,** *57* (40), 13283-13287.
40. Li, S.; Sirisomboonchai, S.; Yoshida, A.; An, X.; Hao, X.; Abudula, A.; Guan, G., Bifunctional CoNi/$CoFe_2O_4$ /Ni foam electrodes for efficient overall water splitting at a high current density. *J. Mater. Chem. A* **2018,** *6* (39), 19221-19230.
41. Koh, J. H.; Won, D. H.; Eom, T.; Kim, N.-K.; Jung, K. D.; Kim, H.; Hwang, Y. J.; Min, B. K., Facile CO_2 electro-reduction to formate via oxygen bidentate intermediate stabilized by high-index planes of bi dendrite catalyst. *ACS Catal.* **2017,** *7* (8), 5071-5077.
42. Lu, P.; Gao, D.; He, H.; Wang, Q.; Liu, Z.; Dipazir, S.; Yuan, M.; Zu, W.; Zhang, G., Facile synthesis of a bismuth nanostructure with enhanced selectivity for electrochemical conversion of CO_2 to formate. *Nanoscale* **2019,** *11* (16), 7805-7812.
43. Hu, D.; Zhang, K.; Yang, Q.; Wang, M.; Xi, Y.; Hu, C., Super-high photocatalytic activity of Fe_2O_3 nanoparticles anchored on $Bi_2O_2CO_3$ nanosheets with exposed {001} active facets. *Appl. Surf. Sci.* **2014,** *316*, 93-101.
44. Zhang, Y.; Zhu, G.; Hojamberdiev, M.; Gao, J.; Hao, J.; Zhou, J.; Liu, P., Synergistic effect of oxygen vacancy and nitrogen doping on enhancing the photocatalytic activity of $Bi_2O_2CO_3$ nanosheets with exposed {0 0 1} facets for the degradation of organic pollutants. *Appl. Surf. Sci.* **2016,** *371*, 231-241.
45. Zhang, R.; Lv, W.; Lei, L., Role of the oxide layer on Sn electrode in electrochemical reduction of CO_2 to formate. *Appl. Surf. Sci.* **2015,** *356*, 24-29.
46. Won da, H.; Choi, C. H.; Chung, J.; Chung, M. W.; Kim, E. H.; Woo, S. I., Rational design of a hierarchical tin dendrite electrode for efficient electrochemical reduction of CO_2. *ChemSusChem* **2015,** *8* (18), 3092-3098.
47. Liu, S.; Lu, X. F.; Xiao, J.; Wang, X.; Lou, X. W., Bi_2O_3 nanosheets grown on multi-channel carbon matrix to catalyze efficient CO_2 electroreduction to HCOOH. *Angew.*

Chem. Int. Ed. **2019,** *58* (39), 13828-13833.

48. Sang, Y.; Cao, X.; Dai, G.; Wang, L.; Peng, Y.; Geng, B., Facile one-pot synthesis of novel hierarchical Bi_2O_3/Bi_2S_3 nanoflower photocatalyst with intrinsic p-n junction for efficient photocatalytic removals of RhB and Cr(VI). *J. Hazard. Mater.* **2020,** *381*, 120942.
49. Wu, X. F.; Wang, Y. J.; Song, L. J.; Su, J. Z.; Zhang, J. R.; Jia, Y. N.; Shang, J. L.; Nian, X. W.; Zhang, C.-Y.; Sun, X. G., A yolk shell Bi@ void@ SnO_2 photocatalyst with enhanced tetracycline degradation. *J. Mater. Sci-Mater. El.* **2019,** *30* (16), 14987-14994.
50. Zhang, F.; Co, A. C., Direct evidence of local pH change and the role of alkali cation during CO_2 electroreduction in aqueous media. *Angew. Chem. Int. Ed.* **2020,** *59* (4), 1674-1681.
51. Liu, Y.; Wang, Z.; Huang, B.; Yang, K.; Zhang, X.; Qin, X.; Dai, Y., Preparation, electronic structure, and photocatalytic properties of $Bi_2O_2CO_3$ nanosheet. *Appl. Surf. Sci.* **2010,** *257* (1), 172-175.
52. Dunwell, M.; Luc, W.; Yan, Y.; Jiao, F.; Xu, B., Understanding surface-mediated electrochemical reactions: CO_2 reduction and beyond. *ACS Catal.* **2018,** *8* (9), 8121-8129.
53. Feaster, J. T.; Shi, C.; Cave, E. R.; Hatsukade, T.; Abram, D. N.; Kuhl, K. P.; Hahn, C.; Nørskov, J. K.; Jaramillo, T. F., Understanding selectivity for the electrochemical reduction of carbon dioxide to formic acid and carbon monoxide on metal electrodes. *ACS Catal.* **2017,** *7* (7), 4822-4827.
54. Liu, Y.; Zhao, J.; Cai, Q., Pyrrolic-nitrogen doped graphene: a metal-free electrocatalyst with high efficiency and selectivity for the reduction of carbon dioxide to formic acid: a computational study. *Phys. Chem. Chem. Phys.* **2016,** *18* (7), 5491-5498.
55. Lei, F.; Liu, W.; Sun, Y.; Xu, J.; Liu, K.; Liang, L.; Yao, T.; Pan, B.; Wei, S.; Xie, Y., Metallic tin quantum sheets confined in graphene toward high-efficiency carbon dioxide electroreduction. *Nature communications* **2016,** *7*, 12697.
56. Han, N.; Wang, Y.; Yang, H.; Deng, J.; Wu, J.; Li, Y.; Li, Y., Ultrathin bismuth nanosheets from in situ topotactic transformation for selective electrocatalytic CO_2 reduction to formate. *Nat. Commun.* **2018,** *9* (1), 1320.
57. Nørskov, J. K.; Rossmeisl, J.; Logadottir, A.; Lindqvist, L.; Kitchin, J. R.; Bligaard, T.; Jonsson, H., Origin of the overpotential for oxygen reduction at a fuel-cell cathode. *J. Phys. Chem. B* **2004,** *108* (46), 17886-17892.

Chapter 6 Conclusions and outlook

6.1 Conclusions

In this work, we focus on the Sn- and Bi-based electrocatalysts for electrochemical reduction of CO_2 to HCOOH due to their unique advantages. Firstly, we reviewed several commonly used strategies for improving the electrocatalytic performances of Sn- and Bi-based catalysts in recent years, including morphology control, making defects, grain boundaries and dislocations, adjusting composition dislocations. Subsequently, we prepared 3 kinds of novel Sn- or Bi-based electrocatalysts for electrochemical CO_2RR to HCOOH. The performances were summarized in the Table 6-1 below.

Table 6.1 Summary of the performances of three Sn- or Bi-based electrocatalysts for the CO_2 electroreduction to HCOOH.

Electrodes	Potential (V vs Ag/AgCl)	Current density (mA/cm^2)	HCOOH faradaic efficiency	Stability
Sn/CP-UPED	-1.7	6	89%	10 h
Bi-SnO/Cu foam	-1.7	12	93%	30 h
Bi/Cu foam-*in-situ* treated	-1.6	10	92%	20 h

As shown in Table 6.1, first of all, we prepared Sn/CP-UPED electrode, which showed a faradaic efficiency of 89% and a current density of 6 mA/cm^2, and found that the surface oxides can improve the selectivity of HCOOH. Therefore, in the next step, we directly prepared the Bi-doped SnO catalyst, and replaced the carbon paper substrate with porous Cu foam to further increase the current density. The results showed that this electrode

exhibited a faradaic efficiency as high as 93% and a current density twice higher than that of the Sn/CP-UPED electrode. Finally, after the faradaic efficiency and current density reached a satisfactory level, in order to further reduce the overpotential to save energy, we prepared a Bi-based electrocatalyst for CO_2RR. After careful physical and electrochemical characterization, performance testing, and mechanism analysis, the following results were obtained:

- For the Sn-based electrocatalysts introduced in chapter 3, it is found that the electrode prepared with the UPED method exhibited better catalytic performance than the other two. Physical and electrochemical characterizations indicated that the Sn/CP-UPED electrocatalyst composed of smaller and more uniform particles with larger electrochemically active surface area, smaller charge transfer resistance and proper ratio of surface oxides species. Furthermore, by DFT calculations, it is found that the presence of Sn^{4+} can effectively reduce the overpotential of CO_2 reduction while the presence of Sn^{2+} can improve the selectivity towards HCOOH formation. In addition, the formation of SnO_x/Sn interface can suppress the side reactions (i.e., generation of H_2), thereby improving the catalytic efficiency in the CO_2 reduction. Based on our experimental and DFT calculation results, it can be concluded that the actual CO_2 reduction catalytic process is synergistically controlled by the complex surface oxides species, which plays a key role in the electroreduction of CO_2 process.

- For the SnO and Bi-doped SnO nanosheets electrocatalysts introduced in chapter 4, it is found that the Bi-SnO/Cu foam exhibited higher HCOOH selectivity than the SnO/Cu foam, and the highest faradaic efficiency reached 93%. Also, the Bi-SnO/Cu foam electrode exhibited excellent long-term stability in 30 h of operation. The physicochemical characterization indicated that the Bi doping stabilizes the existence

of divalent tin (Sn^{2+}) on the surface of the electrocatalyst, making it not easy to be reduced to metallic tin (Sn^0). Meanwhile, the DTF calculation revealed that the Bi doping enhanced the adsorption ability of SnO (001) facet for *OOCH intermediates by the electron orbital hybridization, thereby increasing the selectivity to HCOOH. In addition, it is found that when the Bi-SnO was grown on the Cu foam, the electron transfer from the electrocatalyst to the Cu foam promoted the maintenance of tin under positive oxidation state, favored the adsorption of *OOCH intermediates.

- For the Bi-based electrocatalysts introduced in chapter 5, it is found that when a bulk-structure Bi-based catalyst was applied it for the electrocatalytic CO_2 reduction, the surface morphology of this catalyst changed to petal-shaped nanosheet structure after a facile *in-situ* treatment process. The physicochemical characterizations by SEM, TEM, EDS, XRD and XPS indicated that the change in morphology was due to the formation of $Bi_2O_2CO_3$ nanosheets on the surface. Electrochemical characterization showed that Bi coated electrode with the formed $Bi_2O_2CO_3$ species had higher electrochemically active surface area and lower charge transfer resistance, which showed the highest HCOOH faradaic efficiency of 92% at -1.6 V and a current density of 10 mA cm^{-2} with a long-term stability in 20 h operation. The PDOS analyses obtained by DFT calculations revealed that the stronger orbital hybridization of O 2p with Bi 6p states near the Fermi level for *OOCH intermediate adsorbed on $Bi_2O_2CO_3$ (001) resulted in stronger adsorption of *OOCH intermediate. The rate-limiting step of reducing CO_2 to HCOOH became to the second-step electron transfer step due to this strong adsorption, which was consistent with the Tafel slope analysis results.

6.2 Outlook

Although we obtained several excellent Sn- and Bi-based electrocatalysts in this study, some improvements still need to be made to face the demand of commercial applications of large-scale CO_2 electrochemical reduction. In addition, from the perspective of scientific research, more in-depth mechanisms should still be explored to provide guidance for the design of electrocatalysts. In detail, these works should be done in the future as mentioned in the following：

- In our study, all catalyst stability tests took less than 50 hours. However, to meet industrial applications, hundreds of hours of continuous operation may be required. Besides, how to activate the catalyst after deactivation is also an important issue, so more researches on improving catalyst life-time should be made in the future.
- As a basic research, the reactor used in our experiment is a traditional H-type electrolytic cell, which can conveniently and quickly evaluate the performance of the electrocatalyst. However, owing to the very low solubility of CO_2 in aqueous solution at the atmospheric pressure (around 30 mM at 1 atm and ambient temperature) and low mass transfer ability, the rate of electrochemical reduction of CO_2 in this case is always low. Therefore, the gas diffusion electrode should also be used to evaluate its performance in future work.
- The characterization techniques used in this study are traditional *ex-situ* characterizations. However, the surface state of the electrodes may change during the actual electrocatalysis process. Therefore, using *in-situ* characterization in combination with theoretical calculation to study the catalytic mechanism is needed in future work.

Chapter 7 List of publications, presentations and awards

Publications

① ***Xiaowei An***, Shasha Li, Akihiro Yoshida, Zhongde Wang, Xiaogang Hao, Abuliti Abudula and Guoqing Guan. "Electrodeposition of tin-based electrocatalysts with different surface tin species distributions for electrochemical reduction of CO_2 to HCOOH." ***ACS Sustainable Chemistry & Engineering****,* 2019, 7(10), 9360-9368.

② ***Xiaowei An,*** Shasha Li, Akihiro Yoshida, Tao Yu, Zhongde Wang, Xiaogang Hao, Abuliti Abudula and Guoqing Guan. "Bi-doped SnO nanosheets supported on Cu foam for electrochemical reduction of CO_2 to HCOOH." ***ACS Applied Materials & Interfaces,*** 2019, 11(45), 42114-42122.

③ ***Xiaowei An***, Shasha Li, Xiaoqiong Hao, Xiao Du, Tao Yu, Zhongde Wang, Xiaogang Hao, Abuliti Abudula and Guoqing Guan. " In-situ morphology transformation of bismuth-based catalysts for effective electroreduction of carbon dioxide." ***Sustainable Energy & Fuels****,* 2020, 4, 2831-2840.

④ ***Xiaowei An***, Akihiro Yoshida, Abuliti Abudula and Guoqing Guan. Conversion of carbon dioxide using lead/composite/oxide electrode into formate/formic acid. ***Conversion of Carbon Dioxide into Hydrocarbons Vol. 1 Catalysis***, Springer, 2020, 25-42. (**Book chapter**)

⑤ Zhengkun Xie, Zhijun Wu, ***Xiaowei An***, Xiyan Yue, Pairuzha Xiaokaiti, Akihiro Yoshida, Abuliti Abudula and Guoqing Guan. "A sandwich-type composite polymer electrolyte for all-solid-state lithium metal batteries with high areal capacity and cycling stability." ***Journal of Membrane Science****,* 2020, 596, 117739.

⑥ Zhengkun Xie, Zhijun Wu, ***Xiaowei An***, Xiyan Yue, Akihiro Yoshida, Xiao Du,

Xiaogang Hao, Abuliti Abudula and Guoqing Guan. "2-Fluoropyridine: a novel electrolyte additive for lithium metal batteries with high areal capacity as well as high cycling stability." ***Chemical Engineering Journal,*** 2020, 393, 124789.

⑦ Zhengkun Xie, Zhijun Wu, ***Xiaowei An***, Akihiro Yoshida, Zhongde Wang, Xiaogang Hao, Abuliti Abudula and Guoqing Guan. "Bifunctional ionic liquid and conducting ceramic co-assisted solid polymer electrolyte membrane for quasi-solid-state lithium metal batteries." ***Journal of Membrane Science,*** 2019, 586, 122-129.

⑧ Shasha Li, Suchada Sirisomboonchai, ***Xiaowei An***, Xuli Ma, Peng Li, Lixia Ling, Xiaogang Hao, Abuliti Abudula and Guoqing Guan. "Engineering interfacial structures to accelerate hydrogen evolution efficiency of MoS_2 over a wide pH range." ***Nanoscale,*** 2020.

⑨ Shasha Li, Suchada Sirisomboonchai, Akihiro Yoshida, ***Xiaowei An***, Xiaogang Hao, Abuliti Abudula and Guoqing Guan. "Bifunctional CoNi/$CoFe_2O_4$/Ni foam electrodes for efficient overall water splitting at a high current density." ***Journal of Materials Chemistry A*** 2018, 6(39), 19221-19230.

⑩ Zhijun Wu, Zhengkun Xie, Akihiro Yoshida, ***Xiaowei An***, Zhongde Wang, Xiaogang Hao, Abuliti Abudula and Guoqing Guan. "Novel SeS_2 doped Li_2S-P_2S_5 solid electrolyte with high ionic conductivity for all-solid-state lithium sulfur batteries." ***Chemical Engineering Journal,*** 2020, 380, 122419.

International presentations

① ***Xiaowei An***, Akihiro Yoshida, Tao Yu, Suwadee Kongparakul, Chanatip Samart, Katsuki Kusakabe, Abuliti Abudula, and Guoqing Guan, “In situ morphology transformation to form $Bi_2O_2CO_3$/Bi electrocatalyst for CO_2 reduction,” The 32nd International Symposium on Chemical Engineering (ISChE2019), Chungnam National University, Daejeon, Korea, December 6-8, 2019.

Domestic presentations

① ***安 小偉***, シリソンブーンチャイ スチャダ, 楊 言言, ショケイティ パイルザ, 吉田 暁弘，于 涛，阿布 里提，官 国清, “二酸化炭素電解還元のためのビスマス系触媒の in-situ モルフォロジー変換,” 2019 電気化学会秋季大会，山梨大学，甲府，2019 年 9 月 5- 6 日.

② ***安 小偉***，吉田 暁弘，阿布 里提，官 国清，“Electrochemical reduction of CO_2 to HCOOH on Bismuth doped Tin catalysts，” 化学工学会第 84 年会，芝浦工業大学，2019 年 3 月 13-15 日.

③ ***Xiaowei An***, Akihiro Yoshida, Tao Yu, Abuliti Abudula, Guoqing Guan, "Electrochemical reduction of CO_2 to HCOOH on Tin based electrocatalysts," 第 122 回触媒討論会，北海道教育大学，函館，2018 年 9 月 26-28 日.

④ Zhongliang Yu, Irwan Kurnia, ***Xiaowei An***, Akihiro Yoshida, Abuliti Abudula, Guoqing Guan, " Selective dehydration of formic acid with Mo_2N catalysts at low temperatures, " 第 122 回触媒討論会，北海道教育大学，函館，2018 年 9 月 26-28 日.

⑤ 余鐘亮、吉田暁弘、Kurnia Irwan、***安小偉***、阿布里提、官国清、“Mo_2N 触媒によるギ酸分解反応における脱水素・脱水選択性制御，” 第 124 回触媒討論会，長崎大学，文教キャンパス，2019 年 9 月 18-20 日.

⑥ PATIL AMAR，岳喜岩，***安小偉***，シリソンブーンチャイスチャダ，于涛，吉田暁弘，阿布里提,官国清，“Graphene oxide based nanostructured V_2O_5@RuO_2 hybrid positive electrode for high performance pseudocapacitor,” 電気化学会第 87 回大会, 名古屋工業大学, 2020 年 3 月 17−19 日.

Awards

① ***安小偉***，弘前大学表彰, 2020年3月6日.